Bachelor Thesis

Dennis Lucht

Numerical and Analytical Takeoff Field Length Calculations for Jet Aircraft

Fakultät Technik und Informatik

Department Fahrzeugtechnik und Flugzeugbau

Faculty of Engineering and Computer Science

Department of Automotive and Aeronautical Engineering

Dennis Lucht

Numerical and Analytical Takeoff Field Length Calculations for Jet Aircraft

Bachelor thesis submitted as part of the bachelor examination

Degree program: Aeronautical Engineering
Department of Automotive and Aeronautical Engineering
Faculty of Engineering and Computer Science
Hamburg University of Applied Sciences

First examiner, supervisor: Prof. Dr.-Ing. Dieter Scholz, MSME
Second examiner: Prof. Dr.-Ing. Jens Baaran

Submitted: 15.06.2022

DOI:
https://doi.org/10.15488/xxxxx

URN:
https://nbn-resolving.org/urn:nbn:de:gbv:18302-aero2022-06-15.018
Associated URLs:
https://nbn-resolving.org/html/urn:nbn:de:gbv:18302-aero2022-06-15.018

Any further request may be directed to:
Prof. Dr.-Ing. Dieter Scholz, MSME
E-Mail see: http://www.ProfScholz.de

This work is part of:
Digital Library - Projects & Theses - Prof. Dr. Scholz
http://library.ProfScholz.de

Published by
Aircraft Design and Systems Group (AERO)
Department of Automotive and Aeronautical Engineering
Hamburg University of Applied Science

This report is deposited and archived:

- Deutsche Nationalbiliothek (https://www.dnb.de)
- Repository of Leibniz University Hannover (https://www.repo.uni-hannover.de)
- Internet Archive (https://archive.org)
  Item: Item: https://archive.org/details/TextLuchtBachelor.pdf

This report has associated published data in Harvard Dataverse:
https://doi.org/10.7910/DVN/QX3MAH

Name of student

Dennis Lucht

Title of the report

Numerical and Analytical Takeoff Field Length Calculations for Jet Aircraft

Keywords

Aeronautics, Aerodynamics, Aeroplanes, Airplanes--Take-off, Aviation safety, Aircraft safety measures, Jet transports, Jet engines, Jet planes, [Balanced Field Length, Decision speed, Engine failure, Flight mechanics, Ground roll distance, Safety speed, Takeoff Field Length].

Abstract

Purpose – The greater of two distances (Balanced Field Length or Takeoff Distance +15%) results in the Takeoff Field Length (TOFL). The TOFL is a takeoff distance with safety margins according to Certification Standards for Large Aeroplanes by EASA (CS-25) and FAA (FAR Part 25). Simple analytical approximations for the TOFL are checked against more demanding numerical simulations to determine the validity of the simple solutions and to implement adjustments for them as necessary. The analyses are focused exclusively on jet aircraft with two and four engines.
Methodology – The differential equation of the aircraft's acceleration is solved in MATLAB together with varying engine failure speeds. Analytical calculations of the Balanced Field Length by Torenbeek, Kundu, and Loftin are investigated. This includes the evaluation of statistical data.
Findings – Analytical approximations deviate by 0.1% to 28.2% from the numerical solution. The most accurate analytical approximation is the simple method proposed by Loftin based on statistics. It shows deviations of less than 5.4%. The results confirm that the TOFL for jets with four engines is determined by the Takeoff Distance +15%, while for jets with two engines, the Balanced Field Length is decisive for TOFL.
Research limitations – Simplifying assumptions had to be made e.g. regarding rotation time and speed, flap geometry, and asymmetric drag. While ground distances were solved numerically from acceleration and deceleration, air distance and rotation distance had to be determined analytically.
Practical implications – A reliable and tested analytical procedure is useful for quick aircraft performance estimates and to include an inverse TOFL method into aircraft preliminary sizing.
Originality – This seems to be the first report to provide a systematic check of available analytical approximations for the TOFL in comparison with a numerical solution.

Name des Studierenden

Dennis Lucht

Thema der Bachelorarbeit

Numerical and Analytical Takeoff Field Length Calculations for Jet Aircraft

Stichworte

Luftfahrt, Flugmechanik, Flugzeugaerodynamik, Flugleistung, Auftrieb, Luftwiderstand, Flugzeuge, Tragflügel, Leitwerk, Flugtriebwerk, Startbahn, [Balanced Field Length, Strahlflugzeug, Startrollstrecke, Rotationsstrecke, Sicherheitsgeschwindigkeit, Entscheidungsgeschwindigkeit, Triebwerksausfall, Startsicherheitsstartstrecke].

Kurzreferat

Zweck - Der größere von zwei Abständen (Balanced Field Length oder Takeoff Distance +15 %) ergibt die Takeoff Field Length (TOFL). Die TOFL ist eine Startstrecke mit Sicherheitszuschlägen gemäß den Zertifizierungsstandards für Großflugzeuge der EASA (CS- 25) und der FAA (FAR Part 25). Einfache analytische Näherungen für den TOFL werden mit numerischen Simulationen verglichen, um die Gültigkeit der einfachen Lösungen zu ermitteln und gegebenenfalls Anpassungen vorzunehmen. Die Analysen konzentrieren sich ausschließlich auf Strahlflugzeuge mit zwei und vier Triebwerken.
Methodik - Die Differentialgleichung der Flugzeugbeschleunigung wird in MATLAB zusammen mit unterschiedlichen Triebwerksausfallgeschwindigkeiten gelöst. Analytische Berechnungen der Balanced Field Length von Torenbeek, Kundu und Loftin werden untersucht. Dazu gehört auch die Auswertung statistischer Daten.
Ergebnisse - Die analytischen Näherungen weichen um 0,1% bis 28,2% von der numerischen Lösung ab. Die genaueste analytische Annäherung ist die von Loftin vorgeschlagene einfache Methode auf der Grundlage von Statistiken. Sie zeigt Abweichungen von weniger als 5,4 %. Die Ergebnisse bestätigen, dass die TOFL bei Jets mit vier Triebwerken durch die Startstrecke +15 % bestimmt wird, während bei Jets mit zwei Triebwerken die Balanced Field Length für die TOFL entscheidend ist.
Limitationen- Es werden vereinfachende Annahmen getroffen werden, z.B. bezüglich der Rotationszeit und -geschwindigkeit, der Klappengeometrie und des asymmetrischen Widerstands. Während die Strecken am Boden numerisch aus Beschleunigung, respektive Entschleunigung gelöst wurden, mußten die Strecke nach dem Abheben sowie die Rotationsstrecke analytisch bestimmt werden.
Bedeutung für die Praxis - Ein zuverlässiges und erprobtes analytisches Verfahren ist nützlich für schnelle Leistungsabschätzungen von Flugzeugen und für die Einbeziehung einer inversen TOFL-Methode in die vorläufige Auslegung von Flugzeugen.
Originalität - Dies scheint der erste Bericht zu sein, der eine systematische Überprüfung der verfügbaren analytischen Näherungen für den TOFL im Vergleich zu einer numerischen Lösung bietet.

DEPARTMENT OF AUTOMOTIVE AND AERONAUTICAL ENGINEERING

Numerical and Analytical Takeoff Field Length Calculations for Jet Aircraft

Task for a Bachelor Thesis

Background

The Takeoff Field Length (TOFL) is the takeoff distance of an aircraft including some margin of safety. The TOFL is the greater of the Balanced Field Length (BFL) and 115% of the all-engines-operative takeoff distance. The BFL is determined by the condition that the distance to continue a takeoff following a failure of an engine at a critical engine failure recognition speed (go case) is equal to the distance required to abort it (stop case). It represents the worst-case scenario, since a failure at a lower speed requires less distance to abort, whilst a failure at a higher speed requires less distance to continue the takeoff. $V1$ during takeoff is the maximum speed at which the pilot is able to take the first action to stop the airplane (apply brakes) within the accelerate-stop distance and at the same time the minimum speed at which the takeoff can be continued to achieve the required height above the takeoff surface within the takeoff distance. $V1$ is called Critical Engine Failure Recognition Speed or Takeoff Decision Speed. The BFL is usually the distance that determines the TOFL for aircraft with two engines. With some precision, BFL and $V1$ can only be determined numerically with a calculation / simulation based on the integration of the differential equation describing the aircraft motion under BFL conditions. This has been done by a student at HAW Hamburg before, however, the software was written for a special purpose and cannot be used here. Simple analytical equations exist that could possibly be used to approximate a BFL calculation. Textbooks (Torenbeek, Raymer) for aircraft design claim to have such an equation. An SAE-Paper (https://doi.org/10.4271/2013-01-2324) claims to have an algorithmic approach. An approximate function derived in flight mechanics for the distance to lift-off could be used with a correction factor from aircraft statistics to determine the TOFL. This is reported by Loftin and Scholz.

Task

Set up a calculation / simulation based on the integration of the differential equation describing the aircraft motion under BFL conditions to output the BFL and V1. Compare with 115% of the all-engines-operative takeoff distance to arrive at the TOFL. Provide this software for general use. Check analytical functions that approximate BFL and TOFL and report about their accuracy. You may try to increase the accuracy. The following sub-tasks should be considered when working on this Bachelor Thesis.

- Present very briefly the fundamental principles from flight mechanics used in this thesis.
- Summarize the most relevant regulations regarding Takeoff Field Length (TOFL) and Balanced Field Length (BFL).
- Present all equations and concepts necessary to calculate the individual distance components from which the TOFL / BFL is finally determined.
- Perform a systematic review to find analytical equations for the approximation of the TOFL / BFL. Include also all three above mentioned approximations. Calculate the correction factor included in the approximation from Loftin.
- Set up a small aircraft statistic to check and improve the correction factor in Loftin's approximation.
- Set up a numerical software to calculate / simulate TOFL / BFL.
- Use the software to determine the TOFL / BFL for a jet aircraft with two engines and a jet aircraft with four engines. Comment on your findings from these numerical simulations.
- Compare the results from the numerical simulation with the analytical approximations and comment on the usefulness of the approximations pure from literature and with own improvements added.

The report has to be written in English based on German or international standards on report writing

Table of Contents

Page
List of Figures 11
List of Tables 13
List of Symbols 15
List of Abbreviations 21
List of Definitions 22

1 Introduction 25
1.1 Motivation 25
1.2 Title Terminology 25
1.3 Objectives 31
1.4 Main Literature 32
1.5 Structure of the Report 33

2 General Theoretical Principles 34
2.1 Atmosphere 34
2.2 Speed Conversion 36
2.3 Lift Coefficients 40
2.4 Oswald Span Efficiency Factor 43
2.5 Drag Coefficients 45
2.5.1 Landing Gear Drag 46
2.5.2 Asymmetric Drag 47
2.5.3 Windmill Drag 54
2.5.4 Spillage Drag 56
2.6 Maximum Lift Coefficient at Takeoff 57
2.7 Influence of High Lift Devices 58
2.7.1 Geometric Definitions 58
2.7.2 Lift Increment 60
2.7.3 Lift Curve Slope Correction 63
2.7.4 Drag Increment 64
2.7.5 Span Efficiency Factor 65
2.8 Speed Dependent Thrust 66

3 *V*-Speed 69
3.1 Stall Speed 69
3.1.1 Airbus A320-200 69
3.1.2 Airbus A340-300 72

3.2 Safety Speed 74
3.3 Rotation Speed 74
3.4 Lift-Off Speed 75

4 Regulations 76
4.1 Summary CS-25 76
4.2 Speed Limits 77

5 Performance 79
5.1 Distance Overview 79
5.2 Ground Roll Distance 81
5.2.1 Derivation of the Analytical Equation 81
5.2.2 Analytical with Average Thrust and variable Drag and Lift 85
5.2.3 Analytical with Depending Forces 87
5.2.4 Numerical Integration 89
5.3 Rotation Distance 95
5.4 Air Distance 99
5.5 Stop Distance 102
5.5.1 Time intervals 102
5.5.2 Numerical Solution 104
5.6 Accelerate Stop Distance 106

6 Balanced Field Length 108
6.1 Numerical Solution 108
6.2 Analytical Solution from Torenbeek 109
6.2.1 Derivation of the Decision Speed 110
6.2.2 Derivation of the Balanced Field Length 113
6.3 Analytical Solution from Kundu 115

7 Takeoff Field Length 116
7.1 Numerical 116
7.2 Analytical from Loftin 117
7.3 Analytical from Kroo 119
7.4 Modified Analytical Solution from Loftin 120

8 Sample Aircraft Parameters 122
8.1 Geometry of the Flaps 123
8.2 Geometry of the Vertical Tailplane 124
8.3 General Aircraft Parameter 125
8.4 Flap Dependent Coefficients 126
8.5 Lift Slope Coefficient 128
8.6 Engine Parameter 129

8.7 Maximum Lift Coefficient.......129

9 Simulation Results.......130
9.1 Height Variation.......131
9.1.1 Two-Engine Jet.......131
9.1.2 Four-Engine Jet.......132
9.2 Thrust to Weight Ratio Variation.......133
9.2.1 Two-Engine Jet.......133
9.2.2 Four-Engine Jet.......134
9.3 Distance Breakdown (BFL).......135
9.3.1 Two-Engine Jet.......135
9.3.2 Four-Engine Jet.......136
9.4 Summary of the Results.......137

1 0 Summary.......138

1 1 Conclusions and Recommendations.......139

References.......141

List of Figures

Figure 1.1	All-Engines-Operating Takeoff Distance (based on Young 2018)	25
Figure 1.2	Accelerate Go Distance $sAGD$ / Takeoff Distance $sTOD$ (Young 2018)	26
Figure 1.3	Accelerate Go Distance (based on Young 2018)	27
Figure 1.4	BFL distance vs speed (Young 2018)	28
Figure 1.5	BFL speed vs distance (based on Nicolai 2010)	28
Figure 1.6	V1, V2, VR at PFD & MCDU, Airbus A321	29
Figure 1.7	Stall speed Vs1g => CLmax (Airbus 2002)	30
Figure 1.8	Wind influence	30
Figure 2.1	$T(H)$ / $\rho(H)$ / $p(H)$ (based on McClamroch 2011)	36
Figure 2.2	Speed dependencies (based on Scheiderer 2008, p.67)	37
Figure 2.3	Speed conversion (KCAS to KTAS)	39
Figure 2.4	Dependencies for the lift coefficient	42
Figure 2.5	Optimal (elliptical) lift distribution (Frenslich 2022)	43
Figure 2.6	Oswald efficiency variation (Paape 2011)	44
Figure 2.7	Landing gear drag coefficient (Nicolai 2010)	46
Figure 2.8	Asymmetric thrust condition (OEI), (Young 2018)	48
Figure 2.9	CFM56 (based on Air Team Images 2010)	48
Figure 2.10	VTP parameters	49
Figure 2.11	Drag breakdown (engine failure A320 with, $vEF = 140$ knots)	52
Figure 2.12	Asymmetric drag coefficient increment, A320 ($vEF = 140$ knots)	52
Figure 2.13	Drag coefficient breakdown (A320 with, $vEF = 140$ knots)	53
Figure 2.14	Asymmetric drag increment, A320	53
Figure 2.15	Windmill drag coefficient as a function of the relative speed	55
Figure 2.16	Windmill drag, A320	55
Figure 2.17	Windmill drag, comparison	56
Figure 2.18	Marked (blue) reference wing areas	58
Figure 2.19	Flap parameter, (Scholz 2015)	58
Figure 2.20	Effect of flaps on lift (Torenbeek 1982)	60
Figure 2.21	Lift effectiveness η, chord extension ratio $\Delta c/$cf (Torenbeek 1982)	62
Figure 2.22	Relative flap angle Θf (Torenbeek 1982)	62
Figure 2.23	Chord extension estimate (left) / Lift effectiveness η (right)	63
Figure 2.24	(Fowler) flap factors K_b and K_c	63
Figure 2.25	Lift increment factors for single slotted fowler flaps (Nicolai 2010)	64
Figure 2.26	Increase in "Oswald Factor" due to flap deflection (Obert 2009)	65
Figure 2.27	Thrust as a function of speed with varying bypass ratios (1…12)	66
Figure 2.28	Gas generator factor (Bartel 2008)	67
Figure 2.29	Thrust (A320) as a function of Mach number and altitude	68
Figure 3.1	Stall speeds, vs1g, Airbus A320 (Airbus 2005a)	69
Figure 3.2	Stall speeds, vs1g, Airbus A320 (Excel)	70

Figure 3.3 Stall speed check, vs1g, Airbus A320 (Excel) 71
Figure 3.4 Stall speed vs1g, Airbus A340 (Airbus 2005b) 72
Figure 3.5 Stall speeds, vs1g-takeoff configurations, Airbus A340 (Excel) 73
Figure 4.1 Speed Limits (based on Scholz 1998) 77
Figure 4.2 Engine Failure Effects with, $vEF = 140$ knots 78
Figure 5.1 Force diagram (Scheiderer 2008) 81
Figure 5.2 Ground roll distance (A320): MATLAB diagram (distance vs. time) 93
Figure 5.3 Ground roll distance (A320, 78 t, 117.9 kN) 93
Figure 5.4 Ground roll distance (A320): Euler method (Excel), $\Delta t = 0.01$ 94
Figure 5.5 Ground roll distance (A320): Euler method (Excel), $\Delta t = 0.1$ 94
Figure 5.6 Rotation-Plots, A320 (OEI) 96
Figure 5.7 Schematic visualization of the takeoff phase. (Nicolai 2010) 99
Figure 5.8 Transition & rotation phase (Gudmundsson 2014) 100
Figure 5.9 AFM transition time 102
Figure 5.10 Deceleration: A340; $vEF = 140\ kt$ 103
Figure 5.11 Deceleration: A320; $vEF = 140\ kt$ 103
Figure 5.12 Deceleration due to spoiler (Scholz 1997) 105
Figure 5.13 ASD (2356 m), A320 with $v1 = 140$ kt 72.02ms 107
Figure 5.14 ASD (3051 m), A340 with $v1 = 140$ kt 72.02ms 107
Figure 5.15 Rejected takeoff, accelerate–stop distance, AM 25.92 (Young 2018) 107
Figure 6.1 Takeoff phases (Torenbeek 1982) 110
Figure 7.1 TOFL curves (Kroo) 119
Figure 7.2 Statistical TOFL evaluation 120
Figure 7.3 Residuals (statistical TOFL evaluation) 121
Figure 7.4 Average height dependent thrust reduction 121
Figure 8.1 VTP images (Lufthansa 2021a & 2021b, Airbus 2005c, & 2005d) 124
Figure 8.2 Landing gear drag coefficient (Excel) 126
Figure 8.3 Flap increments (A320) 127
Figure 8.4 Flap increments (A340) 127
Figure 8.5 Lift curve slope coefficients “clean” and with extended flaps 128
Figure 9.1 BFL, two engines (m= 78 t, $T0$ = 117.9 kN, confi 1+F, H = 0 ft) 135
Figure 9.2 BFL, four engines (m= 271 t, $T0$ = 138.8 kN, confi 1+F, H = 0 ft) 136

List of Tables

Table 2.1 General constants 35
Table 2.2 Constant parameter (troposphere, ISA) 35
Table 2.3 Example, speed conversion 38
Table 2.4 Fan parameter 49
Table 3.1 vs1g, Airbus A320 69
Table 3.2 vs1g, Airbus A340 72
Table 5.1 Distances, overview 80
Table 5.2 Friction coefficients (Scholz 2015) 81
Table 5.3 Parameter - MATLAB (m-file, ground roll distance) 91
Table 5.4 Parameter-descriptions (MATLAB-script, ground roll distance) 92
Table 5.5 Initial conditions, rotation, interval 1 97
Table 5.6 Initial conditions, rotation, Interval 2 97
Table 5.7 Rotation times t_R 98
Table 5.8 AFM Transition time 102
Table 5.9 Brake coefficient (Scheiderer 2018) 104
Table 5.10 Brake coefficients 104
Table 6.1 Minimum Control Speeds 108
Table 7.1 Numerical Takeoff Field Length Calculation 116
Table 8.1 Source, flap geometry (A320) 123
Table 8.2 Source, flap geometry (A340) 123
Table 8.3 Flap parameter results 123
Table 8.4 VTP / rudder parameter 124
Table 8.5 Main aircraft parameter 125
Table 8.6 Flap dependent coefficients 126
Table 8.7 Engine parameter 129
Table 8.8 CL, max, A320 (m=78 t) 129
Table 8.9 CL, max, A340 (m=271 t) 129
Table 9.1 Analytical equations 130
Table 9.2 A320 (H = 0 ft) 131
Table 9.3 A320 (H = 1000 ft) 131
Table 9.4 A320 (H = 2000 ft) 131
Table 9.5 A340 (H = 0 ft) 132
Table 9.6 A340 (H = 1000 ft) 132
Table 9.7 A340 (H = 2000 ft) 132
Table 9.8 BFL: A320, variable thrust/weight (confi 1+F, H = 0 ft) 133
Table 9.9 BFL: A320, variable thrust/weight, continued 133
Table 9.10 BFL: A340, variable T/W (confi 1+F, H = 0 ft) 134
Table 9.11 BFL: A340, variable T/W (confi 1+F, H = 0 ft), continued 134
Table 9.12 TOFL: A340, variable $T/$W (confi 1+F, H = 0 ft) 134

Table 9.13 BFL: A320, Distance breakdown (confi 1+F, H = 0 ft)............................135
Table 9.14 BFL: A340, Distance breakdown (confi 1+F, H = 0 ft)............................136
Table 9.15 Δ Min /Max (two engines) 137
Table 9.16 Δ Min /Max (four engines)..137
Table 9.17 Δ Min /Max (total) 137

List of Symbols

a	Acceleration
a	Speed of sound
A	Aspect ratio
A	Thrust factor (Bartel 2008)
a^*	Deceleration, incl. spoiler
A_N	Area of a nozzle
a_{Stop}	Mean deceleration (Torenbeek 1982)
$A_{V_{eff}}$	Effective aspect ratio, VTP
b, b_w	Wingspan
b_f	Flapped wingspan
$b_{f,i}$	Flapped wingspan, inside
$b_{f,o}$	Flapped wingspan, outside
c	Airfoil chord (clean, without flaps)
c'	Increased chord due to extended (fowler) flaps
C_D	Drag coefficient
c_f	Flap chord
$c_{f,eqv}$	Equivalent surface friction coefficient
$c_{f,m}$	Wing chord at the mid of the flapped area
$c_{f,t}$	Wing chord at the tip of the flapped area
C_L	Lift coefficient
$c_{L\alpha}$	Lift curve slope coefficient, flaps up (retracted / clean)
$c'_{L\alpha}$	Lift curve slope coefficient, flaps down (extended)
$C_{L,max}$	Maximum lift coefficient (in specific flap configuration)
c_r	Wing root chord
C_{Y_V}	Factor, asymmetric drag
D	Drag
d_a	Outer (engine) diameter
d_{fan}	Fan diameter
d_i	Engine (inlet) diameter
E	Glide Ratio L/D
e	Span efficiency factor (Oswald Factor)
e_{TO}	Oswald Factor with extended flaps (takeoff configuration)
G	Factor (Torenbeek 1982) $\gamma_{climb} - \gamma_{min}$
G	Gas generator factor (thrust model, Bartel 2008)
g	Gravitational acceleration
g_0	Gravitational constant
H	Geopotential height

h	Geometric height
h_{obst}	Screen height (Nicolai 2010)
h_p	Pressure height
h_{sc}	Screen height; 35 ft (transport Aircrafts); 50 ft (Military)
h_{TO}	Screen height (Torenbeek 1982)
h_{TR}	Height at transition from rotation to climb phase
h_w	Wing height (average)
i	Loop count variable
k	Factor k "clean" regarding induced drag coefficient
k_1, k_2	Factor regarding flap drag increment
K_1, K_2	Thrust coefficients (Scholz 1999)
k_1, k_2	Thrust coefficients (Bartel 2008)
K_a	Ratio lift curve slope 3D/2D
K_b	Flap span effectiveness factor
K_c	Ratio effectiveness parameter 3D/2D
k_E	Factor with respect to C_{D0} estimation
k_{TO}	Factor k with extended flaps (takeoff configuration)
L	Temperature gradient
L	Lift
l_V	Lever, VTP-MAC to CG
M	Mach number
m	A/C weight
N	Number of Engines
n	End of the loop (= rows of the matrix)
n	Load factor
p	Pressure
p_0	Sea level reference pressure
q, q_V	Dynamic pressure
R_L	Gas constant, air
r_{earth}	Earth radius
s	Distance
S_r	Ruder surface area
S_w	Wing surface area
$\mathrm{S_{wf}}$	Flapped wing area
$\mathrm{S_{w,fi}}$	Flapped wing area, inboard
$\mathrm{S_{w,fo}}$	Flapped wing area, outboard
S_{wet}	Wetted wing area
S_v	VTP area
T	Temperature
T	Thrust
t	Time

T_0	Static thrust (1 engine)
T_0	Reference temperature at sea level
T_{idle}	Idle thrust
v	Speed
W	Weight force
X	Thrust factor (Bartel 2008)
y_e	Lever, CG to (critical) engine position
Z	Thrust factor (Bartel 2008)

Greek Symbols

α	Angle of Attack
α_{LOF}	Angle of Attack at when the A/C becomes airborne (lift off)
$(\alpha\delta\ )C_L$	Flap effectiveness parameter 3D
$(\alpha\delta\ )c_l$	Flap effectiveness parameter 2D
α'_δ	Theoretical flap lift factor (based on extended chord c')
γ	Slope, flight path angle
γ	Isentropic exponent
δ	Pressure ratio
δ_f	Flap angle
$\delta T/\delta H$	Temperature gradient, also L
Δc	Chord increment estimation (due to extended flaps)
$\Delta C_{D0,f}$	Zero lift drag coefficient increment due to flap extension
Δe_f	Oswald Factor deviation due to flap deflection
$\Delta_f c_{l_0}$	2-dimensional lift increment due to flaps
$\Delta_f c'_{l_0}$	Lift increment based on extended chord c'
$\Delta_f C_{L_0}$	3-dimensional lift increment due to flaps, $\Delta_f C_{L_0} = \Delta C_{L0,flap}$
Δs_{TO}	Inertia distance (Torenbeek 1982)
ΔT	Difference (reference temperature - temperature at sea level)
ΔT_{OEI}	Net thrust loss (1 engine)
η_δ	Lift effectiveness
Θ'_f	Angle characterizing relative flap (based on extended chord c')
θ	Temperature ratio
λ	Taper ratio
λ_{BPR}	Bypass ratio (BPR)
μ	Friction coefficient
σ	Density ratio
ϕ	Factor: ground effect
φ	Sweep angle
$\omega, \dot{\alpha}$	Angular speed
$\dot{\omega}, \ddot{\alpha}$	Angular acceleration

Indices

Index	Description	Examples
$(\,)_0$	(ISA) Norm conditions	a_0 , p_0 , ρ_0 , T_0
$(\,)_0$	Refers to initial conditions	v_0, s_0, t_0
$(\,)_1$	Refers to the decision speed v_1	v_1
$(\,)_{1.15}$	Factorized Takeoff Distance (+ 15%)	$s_{TOD,1.15}$
$(\,)_2$	Refers to the safety speed v_2	v_2 , C_{L2}
$(\,)_a$	Aerodynamic	v_a
$(\,)_{AEO}$	All Engine Operative	$s_{g,AEO}$, $s_{R,AEO}$, $v_{R,AEO}$
$(\,)_{AIR}$	AIR (Airborne)	s_{AIR}
$(\,)_{asym}$	Asymmetric (drag)	$\Delta C_{D0,asym}$, $\mathrm{D}_{\mathrm{asym}}$
$(\,)_{av}$	Average	v_{av}, q_{av}, T_{av}, T_{av}
$(\,)_B$	Braking	F_B, μ_B
$(\,)_b$	Bottom	r_b,c_b
$(\,)_{BPR}$	Bypass ratio	λ_{BPR}
$(\,)_c$	Compressible	q_c
$(\,)_{CAS}$	Calibrated Airspeed	v_{CAS}
$(\,)_{CL}$	Climb	Θ_{CL}
$(\,)_{clean}$	Clean flap configuration, no flaps	$C_{D0,clean}$
$(\,)_D$	Drag	C_D
$(\,)_{EAS}$	Equivalent Airspeed	v_{EAS}
$(\,)_{EF}$	Engine Failure	v_{EF}
$(\,)_{excess}$	Excess (Thrust)	F_{excess}
$(\,)_f$	Flaps dependent	$\Delta C_{L0,f}$, $\Delta C_{D0,f}$
$(\,)_g$	Ground	s_g, C_{Dg}, C_{Lg}, v_g
$(\,)_{gear}$	(Landing) Gear	$C_{D0,gear}$
$(\,)_{IAS}$	Indicated Airspeed	v_{IAS}
$(\,)_k$	Kinematic	v_k
$(\,)_L$	Lift	C_L
$(\,)_{MCA}$	Minimum Control Speed Airborne	v_{MCA}
$(\,)_{MCG}$	Minimum Control Speed Ground	v_{MCG}
$(\,)_{obst}$	Obstacle (height) also: screen height	h_{obst}
$(\,)_{OEI}$	One Engine Inoperative	$s_{g,OEI}$, $s_{R,OEI}$, $v_{R,OEI}$
$(\,)_R$	Rudder	$\Delta C_{D0,R}$, D_R
$(\,)_R$	Rotation	s_R, v_R
$(\,)_p$	Pressure	h_p
$(\,)_{SC}$	Screen (height), also: $(\,)_{obst}$	h_{sc}
$(\,)_{sd}$	Speed of sound	c_{sd}

$()_{sp}$	Spillage (drag)	$\Delta C_{D0,sp}$
$()_{sym}$	Symmetric (drag)	$C_{D0,sym}$, D_{asym}
$()_{t}$	Tip, Top	r_t,c_t
$()_{TAS}$	True Airspeed	v_{TAS}
$()_{TO}$	Takeoff	$C_{L,max,TO}$
$()_{TR}$	Transition	s_{TR}
$()_{V}$	Vertical Tailplane	S_V, l_V, A_V
$()_{w}$	Wind	v_w
$()_{w}$	Wing	b_w, h_w, S_w, α_w
$()_{wm}$	Windmill (drag)	$\Delta C_{D0,wm}$
$()_{x}$	Engine failure Speed (Torenbeek 1982)	v_x

List of Abbreviations

A/C	Aircraft
AEO	All Engines Operative
AFM	Airplane Flight Manual
AGD	Acceleration Go Distance
ASD	Acceleration Stop Distance
AOA	Angle Of Attack
ASD	Acceleration Stop Distance
BFL	Balanced Field Length
BPR	Bypass Ratio
CAS	Calibrated Airspeed
DE	Differential Equation
EAS	Equivalent Airspeed
FCOM	Flight Crew Operating Manuals
FODE	First Order Differential Equation
IAS	Indicated Airspeed
ICAO	International Civil Aviation Organization
ISA	International Standard Atmosphere
MSL	Mean Sea Level
MTOW	Maximum Takeoff Weight
OEI	One Engine Inoperative b
TAS	True Airspeed; also, Aerodynamic Airspeed
TOD	Take Off Distance
TOFL	Takeoff Field Length
VTP	Vertical Tailplane

List of Definitions

Calibrated Airspeed v_{CAS}:

The Calibrated Airspeed (CAS) corresponds to the Indicated Airspeed (IAS) corrected for the instrument measurement errors resulting from the location / orientation of the measuring device. For modern jets it can be assumed that IAS $\approx$ CAS. (Scheiderer 2008)

Decision speed v_1:

> ”The take-off decision speed, V1, is the calibrated airspeed on the ground at which, as a result of engine failure or other reasons, the pilot is assumed to have made a decision to continue or discontinue the take-off. The take- off decision speed, V1, must be selected by the applicant but must not be less than VEF plus the speed gained with the critical engine inoperative during the time interval between the instant at which the critical engine is failed and the instant at which the pilot recognizes and reacts to the engine failure.” (Gudmundsson 2014)

Equivalent Airspeed v_{EAS}:

The Equivalent Airspeed (EAS) is the Calibrated Airspeed corrected by the compressibility effect that becomes relevant at high Mach numbers (for $M > 0.3$) and is decisive for the calculation of the aerodynamic forces on the aircraft. (Klußmann 2007)

Engine Failure Speed:

> “JAR/FAR 25.107 (a)(1) VEF is the calibrated airspeed at which the critical engine is assumed to fail. VEF must be selected by the applicant but may not be less than VMCG.” (Airbus 2002)

Geometric Height h:

> “Geometrie or tape line height is the vertical distance between a point and some datum level, usually sea-level. In aircraft performance work it is normally confined to the context of ground clearance and is used to define the height of, for example, buildings and mountains.” (Young 2001)

Geopotential Height H:

> "The geopotential height H is an auxiliary quantity with which the potential energy of a fluid element related to the mass can be described under consideration of the height variability of the acceleration due to gravity (...) Thus, if we use the geopotential height H instead of the actual height coordinate z, we can calculate with constant standard earth acceleration g_0." (Kümmel 2007)

Ground Roll Distance:

> “The ground roll is the distance from brake release to the initiation of the rotation, when the pilot pulls the control wheel (or stick or yoke) backward in order to raise the nose of the aircraft.” (Gudmundsson 2014)

International Standard Atmosphere (ISA):

> “The International Civil Aviation Organization (ICAO) Standard Atmosphere is a idealised model of the atmosphere, which by international agreement, is used for aircraft performance analysis and operation. This hypothetical vertical distribution of temperature, pressure and density is also called the International Standard Atmosphere (ISA). The ICAO Standard Atmosphere is identical to the U.S. Standard Atmosphere (1976 version) for heights up 32 km“ (Young 2001)

Indicated Airspeed v_{IAS}:

> "Refers to the airspeed indicated by an airspeed indicator. The airspeed is determined by the airspeed indicator indirectly by measuring the dynamic pressure. (...)" (Klußmann 2007)

The indicated airspeed is the velocity displayed on the primary flight display (PFD). (See Figure 1.6).

Minimum Control Speed v_{MC}:

> "The minimum control speed (VMC) of a multi-engine aircraft is a V-speed that specifies the calibrated airspeed below which directional or lateral control of the aircraft can no longer be maintained, after the failure of one or more engines. The VMC only applies if at least one engine is still operative, and will depend on the stage of flight" (Wikipedia 2021a)

Minimum Control speed on Ground v_{MCG}:

> *"JAR/FAR 25.149 Minimum control speed (e) VMCG, the minimum control speed on the ground, is the calibrated airspeed during the take-off run, at which, when the critical engine is suddenly made inoperative, it is possible to maintain control of the aeroplane with the use of the primary aerodynamic controls alone (without the use of nose-wheel steering) to enable the take-off to be safely continued using normal piloting skill."* (Airbus 2002)

Minimum Control Speed in the Air v_{MCA}:

Above the Minimum Control Speed in the Air $\boldsymbol{v_{MCA}}$ the aircraft can be controlled either:

• with a 5 maximum bank angle, or

• with zero yaw.

with one engine failed while the other engine remaining at Takeoff power. (Airbus 2002)

Minimum Unstick Speed v_{MU}:

Minimum Unstick speed is the lowest calibrated airspeed at and above which the aircraft can safely lift off the ground and continue the Takeoff without encountering critical conditions, The critical conditions are defined as:

- The necessary angle of attack to lift off becomes is too great and the A/C gets into the danger to hit the ground (tailstrike),
- The aircraft is too slow to maintain sufficient lateral control and a wing could hit the ground.

(Airbus 2005e)

Pressure Altitude h_p:

> "Pressure Altitude. Indicates for a measured air pressure what altitude it corresponds to in the standard atmosphere. The pressure altitude is therefore the flight altitude indicated by a barometric altimeter at QNE setting." (Klußmann 2007)

Rotation Distance:

The rotation distance (on the ground) starts with the rotation speed v_R when the pilot first pulls the stick (or yoke) and ends when the aircraft leaves the ground (lifts off at the lift-off speed v_{LOF}). (Based on Gudmundsson 2014)

Screen Height h_{sc}:
The Screen Height is the height of an imaginary obstacle which the aircraft would just clear when taking off with the landing gear extended. (CS-25.111). The screen height is also called obstacle height. (Based on Nicolai 2014 and Young 2018)

Stop Distance:
The stop distance is the distance from engine failure recognition by the pilot (at v_1) to zero speed. It needs (by definition at least) 1 second for the pilot to notice the failure and further actions (braking, idle thrust, spoiler) are executed in stepwise manner in the stop case after an engine failure. (Based on Scheiderer 2008 and Young 2018)

Takeoff Distance (TOD**)**:
The takeoff distance is the distance from releasing the brakes to reaching the screen height. (Based on Young 2018)

Takeoff Field Length (TOFL**)**:
The Takeoff Field Length is the longest of the following three distances:

1) Accelerate Stop Distance with an engine failure 1 sec before the decision speed v_1 (without reverse thrust in case of a dry runway)
2) Takeoff Distance (OEI) until the screen height (35 ft) is reached with an engine failure 1 sec before the decision speed v_1
3) Takeoff Distance with all engines operative (AEO) until the screen height (35 ft) is reached plus an additional 15% safety margin

Note: Simplified it is often assumed, that $v_{EF} \approx v_1$. (Scholz 1999)

Take of Safety Speed v_2:

> "V2 is the minimum climb speed that must be reached at a height of 35 feet above the runway surface, in case of an engine failure." (Airbus 2002)

True Airspeed v_{TAS}:
The True Airspeed (TAS) corrects the Equivalent Airspeed for density deviations from the reference density. (Based on Klußmann 2007)

1 Introduction

1.1 Motivation

In engineering, the search for calculation methods to solve a defined problem leads to a variety of (simplified) models and equations that promise results with just a few input parameters. Partially detailed derivations and reference values are missing, to be able to weigh seriously, how reliably the results can be, and/or which deviations from reality are to be expected.

In aircraft design, the required Takeoff Field Length (TOFL) represent a fundamental role with regard to determining the dimensions and thus in specifying the maximum permissible takeoff weight (MTOW). Aircraft design is an iterative process. In order to calculate initial values without unreasonable effort, practicable analytical solution methods would be valuable, which yield sufficiently accurate results with manageable effort.

1.2 Title Terminology

All-Engines-Operating Factorized Takeoff Distance

The All-Engines-Operating Factorized Takeoff Distance $TOD_{1.15}$ is defined as the distance from releasing the brakes to reaching the screen height at 35 ft plus an additional safety margin of 15% (=> factored takeoff distance $TOD_{1.15}$), which may be used to determine the required runway length if the factored takeoff distance $TOD_{1.15}$ is to be found greater than BFL (see Figure 1.1). *(*CS 25.133*)*.

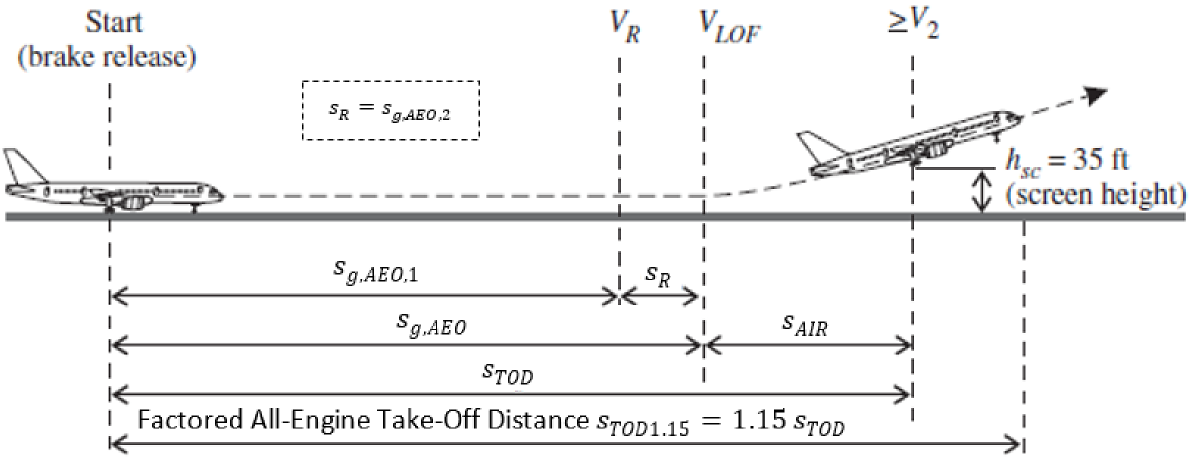

Figure 1.1 All-Engines-Operating Takeoff Distance (based on Young 2018)

h_{sc}	Screen height	[m, ft]
$s_{g,AEO,1}$	Ground Roll Distance (All Engines Operative)	""
s_R	Rotation Distance ($s_R = s_{g,AEO,2}$)	""

$s_{g,AEO}$	Total Ground Roll Distance ($s_{g,AEO,1}$ + s_R)	""
s_{AIR}	Air Distance	""
s_{TOD}	Total Takeoff Distance	""
$s_{TOD1.15}$	Factored Takeoff Distance	""
v_2	Safety Speed	[m/s, kt]
v_{LOF}	Lift - Off Speed	""
v_R	Rotation Speed	""

Accelerate Go Distance

The Accelerate Go Distance (AGD) is the distance needed to reach the screen height (35 ft) from releasing the brakes in the event of an engine failure (see Figure 1.2). Note that the ground roll distance has a section with all engines operating ($s_{g,AEO}$), followed by a portion with one engine inoperative $s_{g,OEI,1}$ (at $v = v_{EF}$). The rotation distance s_R (with one engine inoperative) is determined separately. When reaching the lift-off speed v_{LOF}, the A/C finally lifts off and reaches the obstacle height h_{sc} at $v = v_2$.

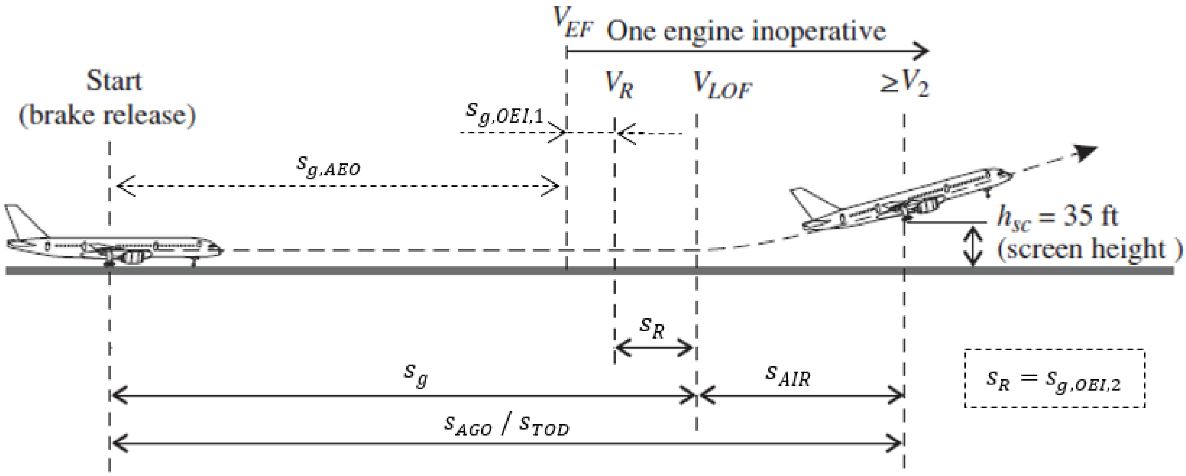

Figure 1.2 Accelerate Go Distance s_{AGD} / Takeoff Distance s_{TOD} (Young 2018)

$s_{g,AEO}$	Ground Roll Distance (All Engines Operative)	[m, ft]
$s_{g,OEI,1}$	Ground Roll Distance, with one engine inoperative (v_{EF} ... v_R)	""
$s_{g,OEI,2}$	Rotation Distance, with one engine inoperative ($s_{g,OEI,2} = s_R$)	""
s_g	Total Ground Roll Distance (v_0 ... v_{LOF})	""
s_{AGD}	Acceleration Go Distance (s_g + s_{AIR})	""
v_{EF}	Engine Failure Speed	[m/s, kt]

Accelerate–Stop Distance

The Accelerate–Stop Distance (ASD) consists of the summation of the following three parts:

1) the acceleration distance (s_{gAEO}) from brake release to the point of engine failure.
2) the distance until the pilot recognizes the engine failure s_{Rec} ($t_{min} = 1\ s$ => requirement)
3) the distance from the 1st reaction (brake actuation) until standstill s_{Stop}. (See Figure 1.3)

The pilot actions are applied in the order: brakes actuation, idle thrust, ground spoilers. For dry runways no reverse thrust is to be considered regarding the performance calculations.

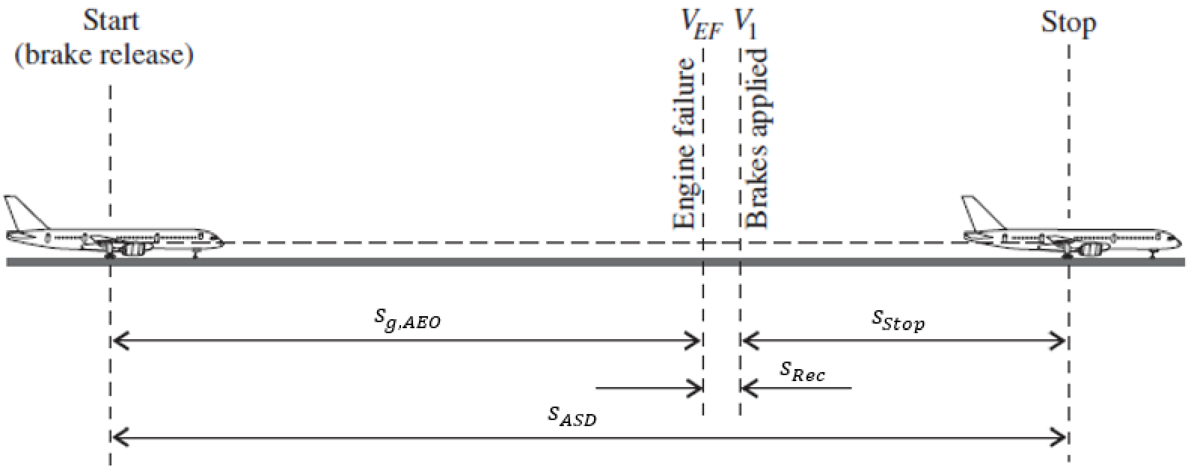

Figure 1.3 Accelerate Go Distance (based on Young 2018)

s_{Rec}	Recognition Distance	[m, ft]
s_{Stop}	Stop Distance	""
s_{ASD}	Acceleration Stop Distance	""

Air Distance

The Air Distance s_{AIR} (see Figure 1.1, Figure 1.2) is the distance from lift-off (at v_{LOF}, see Figure 1.1, Figure 1.2) when the aircraft has completely lost contact with the ground, until the obstacle height / screen height (35 ft) is reached.

Balanced Field Length

For given aircraft parameters (weight, engine thrust, flap setting), environmental conditions (temperature, altitude, wind) and runway conditions (slope, surface), the takeoff distance is no longer sufficient above a certain speed to bring the aircraft to a standstill before the end of the runway. In the named case, the takeoff must be continued, and the aircraft takes off with a failed engine. In doing so, the aircraft has to remain capable of reaching the required minimum speed v_2 (safety speed) at an altitude of 35 ft (screen height) to ensure a safe climb. The limiting speed above which a pilot is required to continue the takeoff is called decision speed v_1. If the engine fails early in the takeoff process, the required stop distance is still short. The distance required to continue takeoff until a height of 35 ft is reached, on the other hand remains long.

The distance necessary to get to the screen height will eventually become less than the stop distance with rising v_1. The Acceleration Stop Distance (ASD) results additively from the distance to accelerate to v_1 and the following stop distance to zero speed. The Take- Off Distance (TOD) or Acceleration Go Distance (AGD) is the total distance from brake release until the screen height is achieved. While the ASD rises with increasing v_1, the AGD shortens with growing v_1. The required runway length in an One-Engine-Inoperative case (OEI) represents the larger of the two distances. The distance that results when ASD and AGD are equal is called the **Balanced Field Length (BFL)** and is thus the shortest possible required runway length in case of an engine failure. In Figure 1.4 the BFL results from the intersection of the ASD and AGD curves. In Figure 1.5 the BFL is visualized as a speed vs distance diagram.

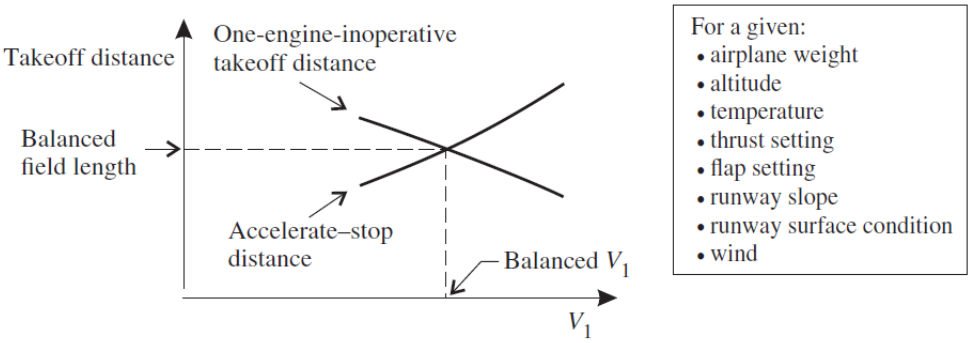

Figure 1.4 BFL distance vs speed (Young 2018)

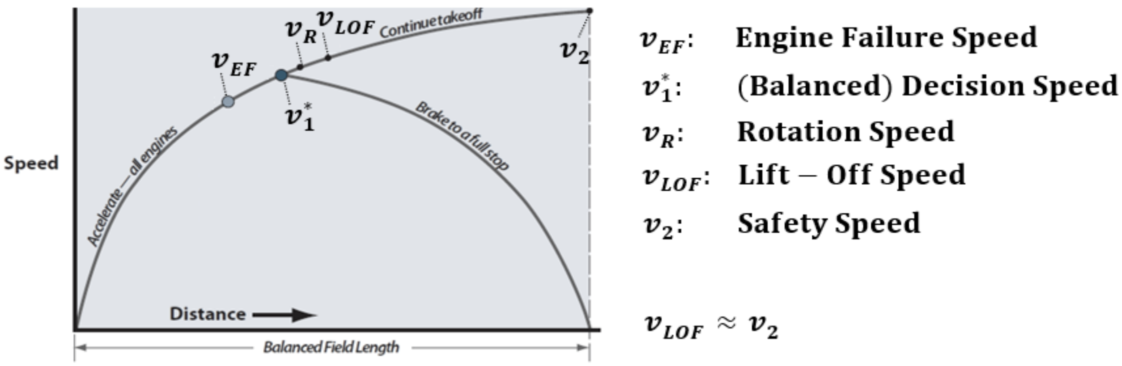

Figure 1.5 BFL speed vs distance (based on Nicolai 2010)

One-Engine-Failure Speed v_{EF}
The speed at which an engine failure occurs.

Rotation Speed v_R
During a takeoff, the pilot pulls the stick (or yoke) at a rotation speed (v_R) to rotate the aircraft until its liftoff angle of attack is reached. The v_R speed is computed such that the airplane can achieve the safety speed v_2 when reaching the screen height of 35 ft with one engine inoperative. v_2 (magenta) and v_1 (blue) are indicated on the PFD (see Figure 1.6). v_R is between v_1 and v_2 and not explicitly indicated. All 3 speeds have to be determined by the pilot based on the available runway, the environmental and runway conditions and the aircraft weight.

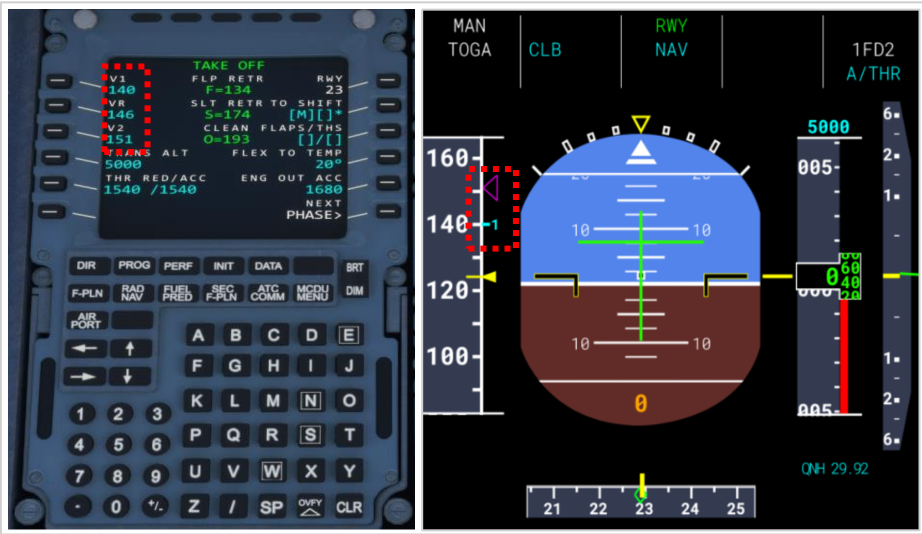

Figure 1.6 V1, V2, VR at PFD & MCDU, Airbus A321[1]

Stall Speed v_s (CS-25.103 Subpart B)
Many commercial aircraft use $v_{s,min}$ as a reference speed based on a load factor less than 1g. All operating speeds are derived from $v_{s,min}$. The low-speed protection function "alpha limit" cannot be overridden by the flight crew. Therefore, the airworthiness authorities have adapted the definitions for specific aircrafts (such as the Airbus A320 & A340 with fly-by-wire). Airworthiness authorities have agreed that a factor of 0.94 represents an adequate relationship between v_{S1g} and $v_{s,min}$ for corresponding aircrafts. This gives the following factors:

- $v_s = 0.94\ v_{s1g}$
- $v_2 = 1.2 \cdot 0.94\ v_{s1g}$

Note: The maximum lift coefficient C_{Lmax} (load factor n = 1g), results in the respective configuration at the reference stall speed $v_{SR} = v_{s1g}$, while v_s (load factor n < 1g) can no longer generate sufficient lift (due to stall) to support the aircraft weight (Figure 1.7).

[1] Screenshot: Microsoft Flight Simulator 2020, Airbus A321

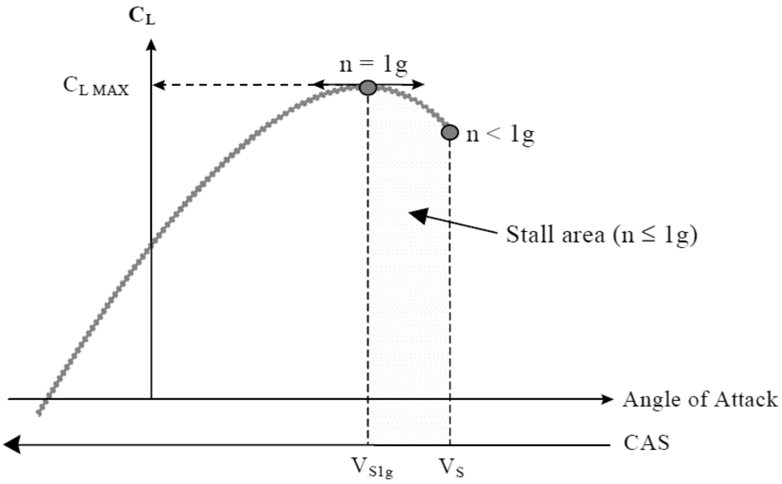

Figure 1.7 Stall speed Vs1g => CLmax (Airbus 2002)

Takeoff / Liftoff Speed v_{LOF}

The speed when the Aircraft first becomes airborne, right after the main gear wheels lose contact to the ground.

Wind Speed v_W

Regarding the aerodynamic forces, the true speed must be employed. For the distance calculation, however, the kinematic speed $\boldsymbol{v_k}$ (ground speed) is decisive and the wind speed v_W has to be considered (vectorially), where tailwind is defined negative and headwind positive according to Figure 1.8 and (2.13). 50% of the headwind component of the nominal wind speed has to be taken into account concerning the takeoff performance benefit, while 150% of the tailwind component of the nominal wind speed must be considered with respect to the takeoff performance penalty (CS-25.105).

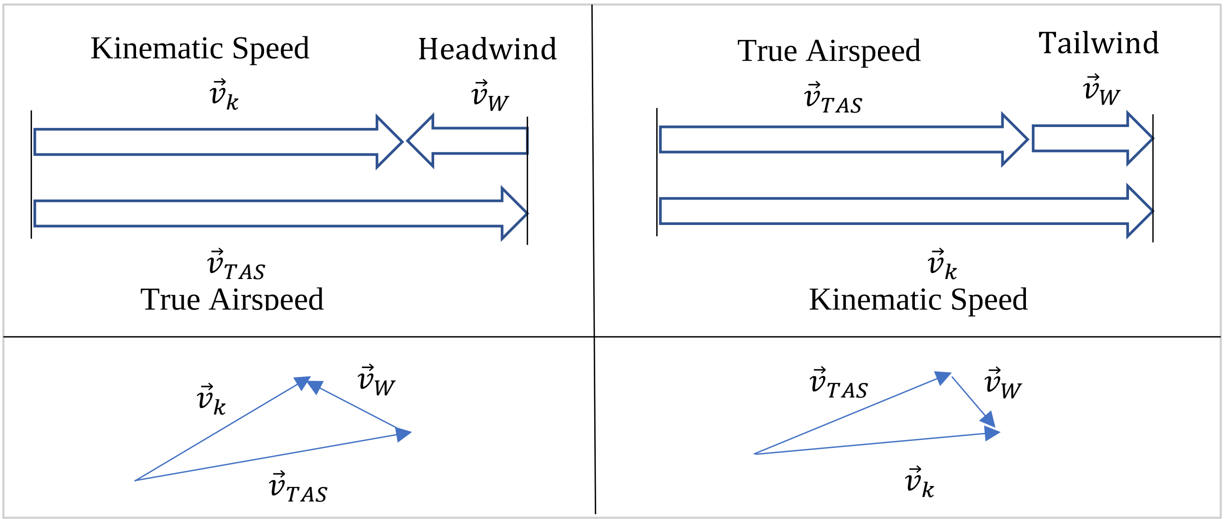

Figure 1.8 Wind influence

In the context of this thesis no wind components are applied.

1.3 Objectives

The objective of this thesis is to provide one analytical procedure each for Balanced Field Length (BFL) estimation and (factorized) Takeoff Distance (TOD) calculation. Moreover, a scope is to be defined in which these methods provide sufficiently accurate results and, if necessary, adjustments shall be made.

Both the determination of the BFL and the calculation of the TOD traditionally involve numerical calculations in which forces are evaluated as a function of velocity and which are integrated stepwise. To solve the BFL & TOD analytically, some assumptions and simplifications have been made (for example, applying an average speed to obtain a constant drag, lift and thrust).

It should be clarified with the results of this work, which accuracy is to be expected with the equations and procedures to be examined. Furthermore, it should be shown under which conditions corresponding equations and procedures can be applied.

Although the focus of this work is on the TOFL, the results should nevertheless generally show that corresponding models and equations should always be questioned at first but can deliver sufficiently exact results under certain conditions. For this purpose, the limits of applicability must be known, and the case-specific still acceptable tolerance must be defined. Thus, this work shall sensitize to a certain extent to put corresponding thoughts first before a model or an equation is used for the solution.

1.4 Main Literature

Equations for the essential flight-mechanical relationships, assumptions and parameters are mainly taken from the sources Gudmundsson 2014, Raymer 2012, Scheiderer 2008, Scholz 1998, Scholz 1999, Torenbeek 1982, Young 2018, Nicolai 2010 partially supplemented by and Young 2001 as well as Young 2005

The aircraft parameters for the sample jet were taken and / or derived based on Airbus 2005c, Airbus 2005d, Nita 2010 and Jenkinson 2001

All V-Speeds ultimately depend on vs1g, whereas vs1g of the respective model depends on the weight and is extracted from Airbus 2005a and Airbus 2005b.

The book that contributed the most content is Torenbeek 1982 and is by now available in several new editions and is still one of the most relevant sources in aircraft design. Torenbeek 1982 provided approaches for, asymmetric drag effects, analytical BFL estimation, (balanced) v1 estimation, the lift coefficient increment due to fowler flaps and a braking distance factor.

The analytical procedures for calculating the BFL and TOFL are mainly based on the sources Kundu 2010, Kroo 2001, Loftin 1980, Scholz 1998, Jenkinson 2001 and Torenbeek 1982.

The zero lift drag coefficient is estimated using a method according to Scholz 2017.

The span efficiency factors (Oswald Factor) for both the Airbus A320 and A340 are calculated on the basis of Howe 2000 and modified based on Obert 2009.

A speed-dependent thrust calculation is determined in accordance with Bartel & Young 2008.

Young 2018 is the primary source in the stop distance calculation.

The simplified and numerical ground roll calculation is made on the basis of Scholz 1998.

The air distance and the drag generated from the flaps are calculated according to Nicolai 2010.

Basic mathematical relationships were worked out with Metzinger 2010 and Papula 2015.

The calculations of all distances and most parameters were supplemented by information and notes from the script according to Scholz 1999 and Scholz 2015.

Literature apart from the sources mentioned above, had only a minor contribution to this report and are always explicitly noted at appropriate points.

1.5 Structure of the Report

The report is structured in eleven main chapters that are arranged in a consecutive order.

Chapter 2 serves the reader to introduce the general theoretical principles.

Chapter 3 describes the calculation of the V-Speeds and their dependencies to each other.

Chapter 4 outlines the most relevant regulations for this thesis.

Chapter 5 contains the analytical and numerical approaches for the determination of the individual distance components to derive the Balanced Field Length and Takeoff Distance.

Chapter 6 provides numerical and analytical procedures to determine the Balanced Field Length.

Chapter 7 represents (with Chapter 5 and 6) the most essential part of this report and presents analytical procedures to determine the Takeoff Field Length.

Chapter 8 derives and summarizes the parameters of the sample aircraft.

Chapter 9 gives an overview of the simulation results.

Chapter 10 is a summary of the contents of previous chapters.

Chapter 11 critically examines the results. This is followed by a recommendation for the application of the analytical calculation methods based on the simulation results.

2 General Theoretical Principles

2.1 Atmosphere

By transforming the Equation of state (2.1), (2.2) and inserting it into the Hydrostatic equation, the basic equation (2.3) is obtained, which by means of integration of (2.4) leads to the height-dependent pressure. In the troposphere (the takeoff process is limited to the troposphere) the temperature gradient L is approximately negative constant -6.5 K / km up to 11 km.

Equation of state:

$$\frac{p}{\rho} = R_L \cdot T \tag{2.1}$$

$$\rho_0 = \frac{p_0}{R_L \cdot T_0} \tag{2.2}$$

Hydrostatic equation:

$$\frac{dp}{dh} = -\rho \cdot g \tag{2.3}$$

This results in:

$$\int_{p0}^{p} \frac{1}{p}\, dp = -\int_{H0}^{H} \frac{g}{R_L \cdot T}\, dH \tag{2.4}$$

With the pressure, density and temperature ratio according to (2.5), (2.6) and (2.7).

$$\delta = \frac{p}{p_0} = \left(\frac{T_0 - L \cdot H}{T_0}\right)^{\frac{g}{R \cdot L}} = \left(\frac{T}{T_0}\right)^{\frac{g}{R \cdot L}} \tag{2.5}$$

$$\sigma = \frac{\rho}{\rho_0} = \left(1 - \frac{L \cdot H}{T_0}\right)^{\frac{g}{R \cdot L} - 1} = \left(\frac{T}{T_0}\right)^{\frac{g}{R \cdot L}} \tag{2.6}$$

$$\Theta = T/T_0 \tag{2.7}$$

Furthermore applies:

$$\sigma = \delta/\Theta \tag{2.8}$$

$$p = p_0 \cdot \frac{\delta}{\Theta} \tag{2.9}$$

$$\rho = \rho_0 \cdot \frac{\delta}{\Theta} \tag{2.10}$$

R_L	Gas constant, air	[K]
T_0	Reference temperature at sea level	[K]
g_0	Gravitational constant	[m/s^2]
p_0	Sea level reference pressure	[Pa]
p	Pressure at a specific altitude	[Pa]
ΔT	Difference between reference temperature and actual temperature at sea level	[K]
h	Geometric height	[m]
γ	Isentropic exponent, for air γ=1.4	[-]
H	Geopotential height	[m]
L	Temperature gradient	[K/m]
T	Temperature	[K]
g	Gravitational acceleration	[m/s^2]
δ	Pressure ratio	[-]
θ	Temperature ratio	[-]
σ	Density ratio	[-]

Converted in non-SI units. Lengths are given in feet, speed in knots.

$$1\,m\,s^{-1} = 1.94384494\,kt \tag{2.11}$$

$$1\,m\,s^{-2} = 3.280839895\,ft\,s^{-2} \tag{2.12}$$

Table 2.1 General constants

Designation	**Symbol**	**Value**	**SI- unit**
Isentropic exponent (air)	γ	1.4	
Specific gas constant (air)	R_L	287.053	$K^{-1}\,m^2\,s^{-2}$
Gravitational constant	g_0	9.80665	$m\,s^{-2}$
Earth radius	r_{earth}	$6371 \cdot 10^3$	m

Table 2.2 Constant parameter (troposphere, ISA)

Designation	**Symbol**	**Value**	**SI-unit**
(Reference) temperature (MSL)	$T_{0,ISA}$	288.15	K
(Reference) temperature (MSL)	$T_{0,ISA}$	15	C°
Temperature gradient	L	$6.5 \cdot 10^{-3}$	K m^{-1}
Speed of sound (MSL)	$a_{0,ISA}$	340.294	m s^{-1}

Table 2.1 and Table 2.2 summarize all relevant constants in SI-units, for the conversion of velocities and heights.

With (2.1) to (2.12) and the constants from Table 2.1 and Table 2.2, MATLAB produces curves corresponding to Figure 2.1 for the temperature, density and pressure as a function of altitude, whereby only the first 2000 ft are relevant for the performance calculations in the context of this thesis for the takeoff. Although there are airports that rise even further above SL. The highest airport (Dacheng Yading Airport, China) reaches 4411 m (14472 ft) above sea level, with a runway length of 4200 m (13779 ft). (International Airport Reviews 2018)

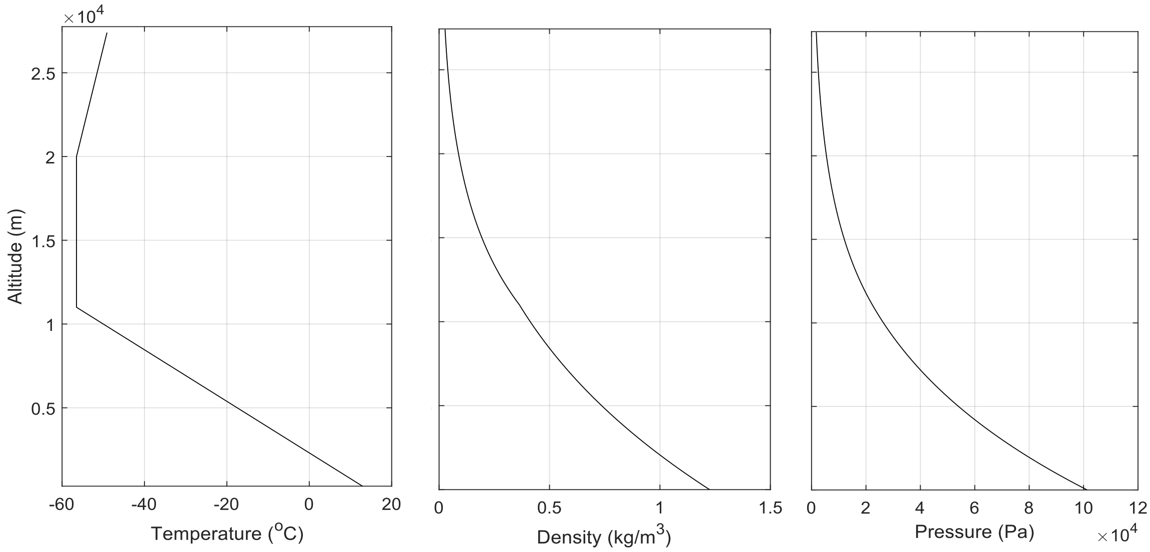

Figure 2.1 $T(H)$ / $\rho(H)$ / $p(H)$ (based on McClamroch 2011)

2.2 Speed Conversion

The kinematic speed (also called ground speed) is the determining factor for the flight distance and flight time. The kinematic speed $\vec{v}_k$ results from the aerodynamic speed $\vec{v}_a$ and wind speed $\vec{v}_w$ components:

$$\vec{v}_a = \vec{v}_k + \vec{v}_w \tag{2.13}$$

$\vec{v}_a$	Aerodynamic speed, equivalent to the True Airspeed (TAS)	[m/s], [kt]
$\vec{v}_k$	Kinematic speed, (ground speed)	""
$\vec{v}_w$	Wind speed	""

Headwind: $\vec{v}_w > 0$
Tailwind: $\vec{v}_w < 0$

The vector notation is used once with (2.13) to emphasize the vector character for the velocities. In the further course the vector arrow for the speeds is ignored.

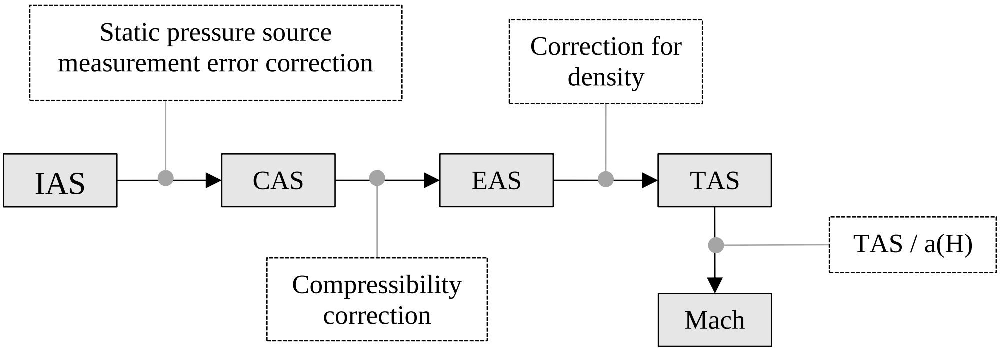

Figure 2.2 Speed dependencies (based on Scheiderer 2008, p.67)

The relationships between the speeds are visualized in Figure 2.2. The Temperature, pressure, and density change with altitude. The velocities are measured in the aircraft via pressure measuring probes, which record the difference between the dynamic and static pressure. This results in the indicated speed (IAS), the speed displayed to the pilot on the airspeed indicator. However, the displayed speed is subject to error due to static pressure source errors, alignment errors, density changes with altitude and energy differences on the aircraft fuselage due to flow processes. Therefore, the actual pressure is not accurately recorded. If the positioning errors are taken into account, the calibrated velocity (CAS) is obtained. In many modern commercial aircrafts, the differences between IAS and CAS are usually negligible.

If compressibility effects are also accounted for, the result is the equivalent airspeed (EAS). For compressible gases:

$$v_{EAS} = a \cdot \sqrt{\sigma \cdot \frac{2}{\gamma - 1} \left[\left(\frac{q_c}{p(H)} + 1 \right)^{\frac{\gamma-1}{\gamma}} - 1 \right]} \tag{2.14}$$

If, in addition, the decreasing density with increasing altitude is considered, the true airspeed (TAS) is obtained:

$$v_{TAS} = \frac{v_{EAS}}{\sqrt{\sigma}} \tag{2.15}$$

$$v_{TAS} = a \cdot \sqrt{\frac{2}{\gamma - 1} \left[\left(\frac{q_c}{p(H)} + 1 \right)^{\frac{\gamma-1}{\gamma}} - 1 \right]} \tag{2.16}$$

with dynamic pressure q_c:

$$q_c = p_0 \cdot \left(\left[\frac{(\gamma - 1)}{2} \cdot \left(\frac{v_{CAS}}{a_0} \right)^2 + 1 \right]^{\frac{\gamma}{\gamma-1}} - 1 \right) \tag{2.17}$$

Speed of sound at MSL:

$$a_0 = \sqrt{\gamma\ R\ T_0} \tag{2.18}$$

Speed of sound as a function of altitude:

$$a(H) = \sqrt{\gamma\ R\ T(H)} \tag{2.19}$$

or

$$a(H) = a_0 \cdot \sqrt{\Theta} \tag{2.20}$$

In addition to the velocities mentioned, the Mach number (at high velocities) is often decisive:

$$M = \frac{v_{TAS}}{a} \tag{2.21}$$

$a(H)$	Speed of sound as a function of altitude	[m/s], [kt]
a_0	Speed of sound at MSL	""
M	Mach number	[-]
q_c	Dynamic pressure	[Pa]

Note: For Mach numbers $M < 0.3$, the difference between EAS and CAS is marginal, and (2.22) and (2.23) could be used for conversion.

$$v_{CAS} \approx v_{EAS} \tag{2.22}$$

$$v_{TAS} = \frac{v_{CAS}}{\sqrt{\sigma}} \tag{2.23}$$

Table 2.3 Example, speed conversion

Designation	***Sign***	**Value**		
Height	*H*	20000 ft	6096.00 m	6.10 km
Calibrated Airspeed	v_{CAS}	250.00 kt	128.61 m/s	463.00 km / h
Equivalent Airspeed	v_{EAS}	245.22 kt	126.14 m/s	454.12 km / h
True Airspeed	v_{TAS}	335.95 kt	171.80 m/s	618.48 km / h
Speed of Sound	$a(H)$	614.37 kt	316.03 m/s	1137.72 km / h
Mach Number	M	0.54681		

The above example from Table 2.3 is visualized in Figure 2.3.

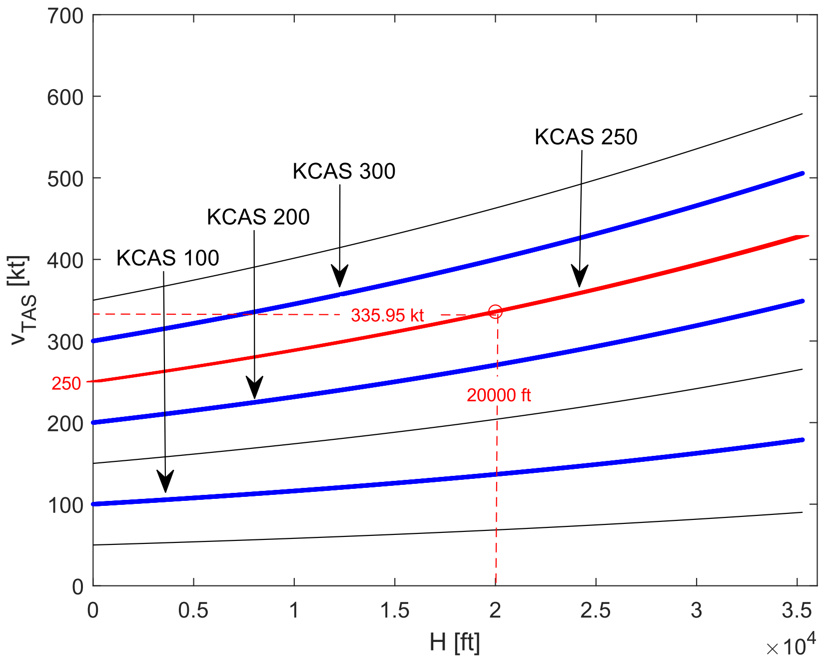

Figure 2.3 Speed conversion (KCAS to KTAS)

Relationship between geometric height h and geopotential height H:

$$h = \frac{r_{earth} \cdot H}{r_{earth} - H} \tag{2.24}$$

$$H = \frac{r_{earth} \cdot h}{r_{earth} + h} \tag{2.25}$$

r_{earth}	Earth radius	[m]

2.3 Lift Coefficients

If all geometrical parameters for the wing and the flaps are known, the lift gradients $C_{L\alpha}\ (wing)$ and $C_{L\delta}\ (flaps)$ could be calculated. The lift coefficient would be determined according to (2.26). For more detailed descriptions of some of the following contexts and geometries Chapter 7 and Chapter 12 of source (Scholz 2015) could be useful.

Lift coefficient $C_L(\alpha_w, \delta_f)$:

$$C_L(\alpha_w, \delta_f) = C_{L0} + \frac{\partial C_L}{\partial \alpha} \cdot \alpha_w + \frac{\partial C_L}{\partial \delta_F} \cdot \delta_f \tag{2.26}$$

$$C_{L,g} = C_{L0} + C_{L\alpha} \cdot \alpha_w + C_{L\delta} \cdot \delta_f \tag{2.27}$$

$C_{L,g}$	Lift coefficient, ground
$C_{L,0}$	Zero lift coefficient
$C_{L,\alpha}$	Lift coefficient gradient, wing ($\partial C_L/\partial\alpha$)
$C_{L,\delta}$	Lift coefficient gradient, flaps ($\partial C_L/\partial\beta_{\mathrm{F}}$)
α_w	Angle of attack, wing
δ_f	Flap angle

Lift curve slope (Scholz 2015**)**

$$C_{L,\alpha}(M) = \frac{2\pi A}{2 + \sqrt{A^2(1 + tan^2\,\varphi_{50} - M^2) + 4}} \tag{2.28}$$

With the aspect ratio A:

$$A = b_w^2/S_w \tag{2.29}$$

A	Aspect ratio	[-]
φ_{50}	Sweep angle [rad] (at ½)	[°], [rad]
b_w, b	Wingspan	[m]

(2.28) applies to the "clean" wing. For extended flaps, $C_{L,\alpha}$ changes as a function of the flap angle. The relationships are described in Chapter 2.7.3 (High Lift Devices) and is shown in Figure 2.4.

Converting sweep angle from $\varphi_m\ to\ \varphi_n$ at different positions:

$$tan\,\varphi_n = tan\,\varphi_m - \frac{4}{A}\left(\frac{n-m}{100} \cdot \frac{1-\lambda}{1+\lambda}\right) \tag{2.30}$$

$$tan\,\varphi_{50} = tan\,\varphi_{25} - \frac{4}{A}\left(\frac{n-m}{100} \cdot \frac{1-\lambda}{1+\lambda}\right) \tag{2.31}$$

m	Position 1 (known angle)	
n	Position 2	
φ_{25}	Sweep angle [rad] (at ¼)	[rad]
λ	Taper Ratio	[-]

In addition to the flap angle δ_f the achievable lift gains of different high lift devices differ significantly from each other. The relationship and further dependencies are described in Chapter 2.7 (High Lift Devices) and $\Delta C_{L0,flaps}$ and $\Delta C_{D0,flaps}$ are derived as a function of flap angle for single slotted fowler flaps (used for the sample aircrafts Airbus A320 & A340).

Lift coefficient $C_L(\alpha)$:

$$C_L(\alpha) = (C_{L0} + \Delta C_{L0,f}) + \frac{\partial C_L}{\partial \alpha} \cdot \alpha \tag{2.32}$$

or

$$C_L(\alpha) = (C_{L0} + \Delta C_{L0,f}) + C_{L,\alpha} \cdot \alpha \tag{2.33}$$

$$\Delta C_{L0,f} = \frac{\partial C_L}{\partial \delta_F} \cdot \delta_f \tag{2.34}$$

Lift coefficient $C_L(\alpha, M)$:

$$C_L(\alpha) = \left(C_{L0} + \Delta C_{L0,f}\right) + \alpha \cdot C_{L,\alpha}\,(M) \tag{2.35}$$

Since $v_2 \approx 1.13\ v_{s,1g}$ (see Chapter 3.2) $C_{L,2}$ can approximated with (2.36), (2.37):

$$\frac{C_{L,2}}{C_{L,max,TO}} \approx \frac{\dfrac{2W}{\rho\,S_W\,v_{2,min}^2}}{\dfrac{2W}{\rho\,S_W\,v_{s,1g}^2}} = \frac{{v_{s,1g}}^2}{\left(1.13\ v_{s,1g}\right)^2} = \frac{1}{1.13^2} \tag{2.36}$$

$$C_{L,2} \approx \frac{1}{1.13^2}\ C_{L,max,TO} \tag{2.37}$$

$C_L(\alpha, M)$	Lift coefficient as a function of AOA and Mach number	[-]
C_{L0}	Zero lift coefficient, for asymmetric airfoils typically 0.1 … 0.5	""
$C_{L,\alpha}$	Lift curve slope gradient $\partial C_L / \partial \alpha$	""
$\Delta C_{L0,f}$	Lift increment due to flaps	""
$C_{L,2}$	Lift coefficient at lift-off, also $C_{L,LOF}$	""
$C_{L,max,TO}$	Maximum (takeoff) lift coefficient in a specific flap configuration	""

W	Weight force	[N]
λ	Taper Ratio (= tip chord / root chord)	[-]
v_s	Stall Speed	[m/s], [kt]
$v_{2,min}$	Safety Speed	""
S_w	Wing surface area	[m^2]

The lift curve gradient $C_{L,\alpha}$ changes with the Mach number, the aspect ratio, the flap angle. Furthermore, it depends on the taper ratio, the aspect ratio, and the sweep angle. Figure 2.4 points out some dependencies of the lift curve gradient.

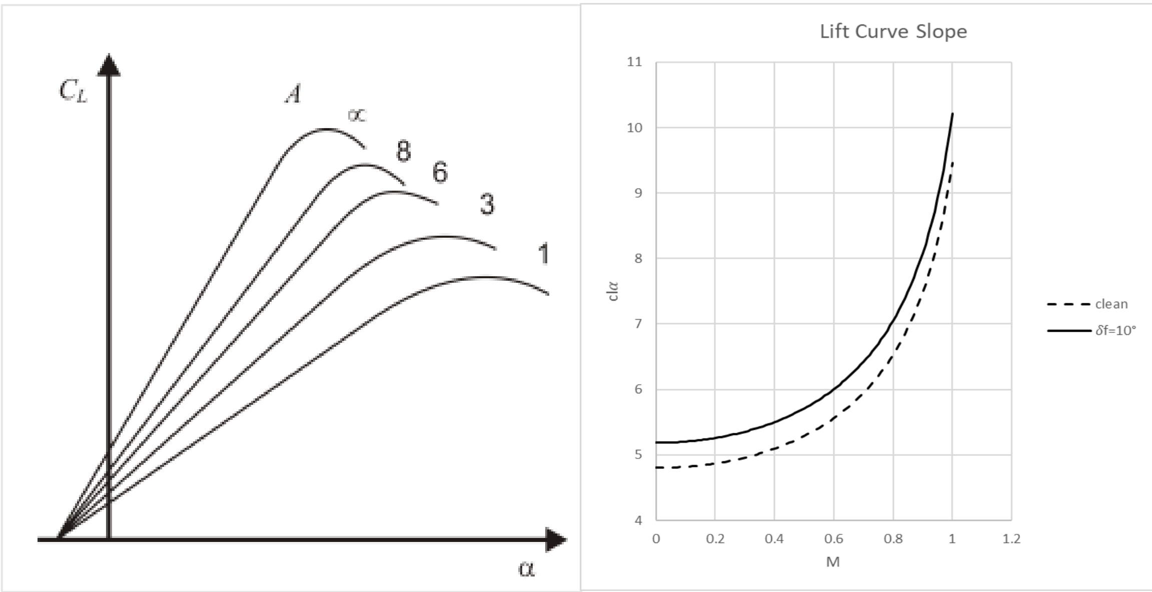

Figure 2.4 Dependencies for the lift coefficient[2]

[2] Left: (Scholz 2015), Right: generated in Excel with parameters for an Airbus A320 (Chapter 8)

2.4 Oswald Span Efficiency Factor

The e factor considers the deviation of the lift distribution over the wingspan compared to the ideal condition. An elliptical lift distribution with $e = 1$ represents the theoretical optimum (see Figure 2.5), i.e. the real Oswald span efficiency factor is smaller than 1 (typical: $0.7 <= e <= 0.85$). The Oswald span efficiency is strongly dependent on the wing geometry.

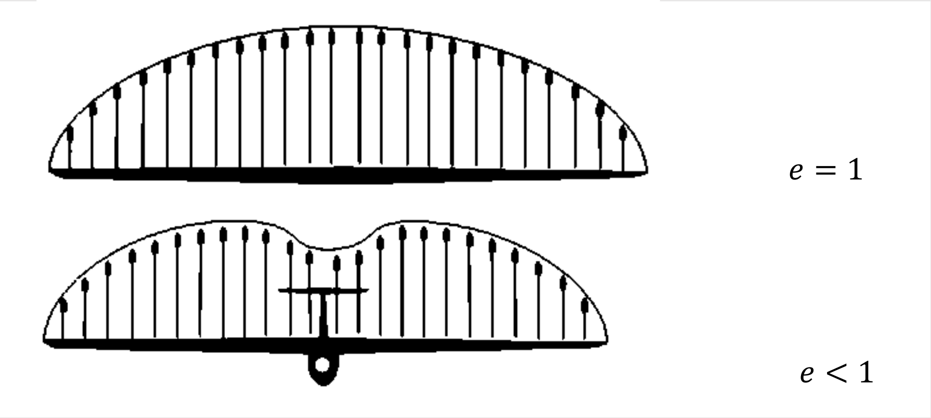

Figure 2.5 Optimal (elliptical) lift distribution (Frenslich 2022)

For the purpose of this report, Howe's approach is used, as it takes into account the most important relevant wing parameters. Howes's method is valid for subsonic flights ($M < 0.95$) with aspect ratios A > 5:

Howe (e, clean wing):

$$e = \frac{1}{(1 + 0.12\,M^6)\left(1 + \frac{0.142 + f(\lambda)\,A\,(10 \cdot t/c)^{0.33}}{cos^2(\varphi_{25})} + \frac{0.1(3\,N_e + 1)}{(4 + A)^{0.8}}\right)} \qquad (2.38)$$

$$f(\lambda) = 0.005\,[1 + 1{,}5\,(\lambda - 0.6)^2] \qquad (2.39)$$

M	Mach number
A	Aspect Ratio
t/c	Relative airfoil thickness
φ_{25}	Wing sweep
N_e	number of engines ON the wing (Airbus A320 /A340 $N_e = 0$)

For (2.39) there are no derivations from $M = 0...0.3$, therefore a value of $M = 0.3$ is used. The dependence of the Oswald factor on φ and λ is visualized with Figure 2.6.

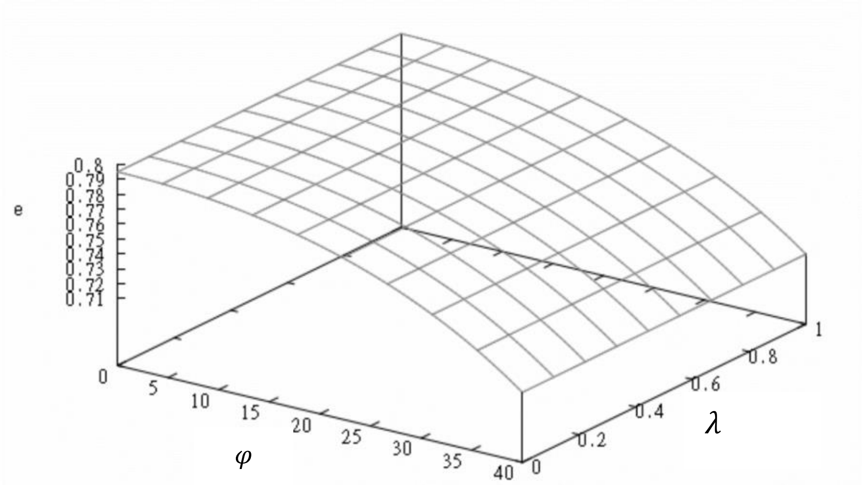

Figure 2.6 Oswald efficiency variation (Paape 2011)

For the takeoff, no speeds are reached at which compressibility effects must be taken into account. For Mach numbers above 0.3, a detailed procedure of Nita 2012 is recommended. The source (Nita 2012) provides a detailed (verified) approach for determining the Oswald Factor. Howe's method has long been recommended as part of the aircraft design lecture at HAW for estimating the Oswald factor and reaches results with deviations less than 10% according to Nita 2012. The (improved new) method from Nita 2012 has been thoroughly investigated and will be the suggested approach in the future, especially for Mach numbers at cruise speed. With respect to this report, there are only minor deviations between the calculations with Howe (A320: $e = 0.795$; A340: $e = 0.783$), therefore a simulation with adjusted values was not performed. The calculations based on Nita 2012 result in slightly smaller Oswald factors (A320: $e = 0.783$; A340-300: $e = 0.77$).

2.5 Drag Coefficients

Estimation (McCormick 79) of drag coefficient (ground) $C_{D,g}$:

$$C_{D,g} = C_{D0} + \phi \cdot \frac{C_{L,g}^2}{\pi \cdot e \cdot A} \tag{2.40}$$

Induced drag:

$$C_{D,induced} = \phi \cdot \frac{C_{L,g}^2}{\pi \cdot e \cdot A} \tag{2.41}$$

It is common to add the drag increases due to the flaps and gear on $C_{D0,clean}$.

All Engines Operative (AEO) case:

$$C_{D0} = C_{D0,clean} + \Delta C_{D0,f} + \Delta C_{D0,gear} \tag{2.42}$$

In the event of an engine failure, there is an additional drag increment $\Delta C_{D0,asym}$, which is described in sections 2.5.2 to 2.5.4.

With One Engine Inoperative (OEI) the zero lift drag coefficient becomes:

$$C_{D0} = C_{D0,clean} + \Delta C_{D0,f} + \Delta C_{D0,gear} + \Delta C_{D0,wm} + \Delta C_{D0,R} + \Delta C_{D0,sp} \tag{2.43}$$

or

$$C_{D0} = C_{D0,clean} + \Delta C_{D0,f} + \Delta C_{D0,gear} + \Delta C_{D0,asym} \tag{2.44}$$

with the summed drag coefficient increment due to the asymmetric flight conditions

$$\Delta C_{D0,asym} = \Delta C_{D0,wm} + \Delta C_{D0,R} + \Delta C_{D0,sp}\ . \tag{2.45}$$

If an aircraft operates in proximity to the ground, the vortex sheet changes. This leads to a slight increase in lift and a significant reduction in drag. The drag reduction mainly based on less vortex drag is accounted for by the factor ϕ:

$$\phi = \frac{(16\, h_w/b)^2}{1 + (16\, h_w/b)^2} \tag{2.46}$$

The "clean" zero drag coefficient is estimated according to Scholz 2017 with (2.47).

$$C_{D0,clean} = \frac{\pi\ A\ e}{4\ E_{max}^2} \tag{2.47}$$

with the maximum lift to drag ratio E_{max}:

$$E_{max} = k_E \sqrt{A/(S_{wet}/S_W)} \tag{2.48}$$

and a factor k_E

$$k_E = \frac{1}{2}\sqrt{(\pi\, e)/c_{f,eqv}} \quad . \tag{2.49}$$

$c_{f,eqv}$	Equivalent surface friction coefficient $cf, eqv = 0.003$
k_E	Factor, if unknown, statistic value => coefficient $k_E = 15.8$
$C_{D,0}$	Zero-lift drag coefficient, total
$C_{D0,\mathrm{clean}}$	Clean wing, without flap deflection $0.015 \leq C_{D,0} \leq 0.04$
$C_{D,induced}$	Induced drag
$\Delta C_{D0,f}$	Drag increment due to the flaps (for specific configuration)
$\Delta C_{D0,\mathrm{gear}}$	Drag increment due to the gear
$\Delta C_{D0,\mathrm{sp}}$	Drag increment due to the spillage effects of the failed engine
$\Delta C_{D0,\mathrm{wm}}$	Drag increment due to the windmill effect (by the engine failure)
$\Delta C_{D0,\mathrm{asym}}$	Drag increment due to the asymmetric flight conditions
$\Delta C_{D0,\mathrm{R}}$	Drag increment due to the asymmetric thrust (Compensated by the rudder)
e	Span efficiency factor, typical: $0.7 \leq e \leq 0.85$
S_{wet}	Wetted wing area [m^2]
h_w	Wing height (average), over ground [m]

2.5.1 Landing Gear Drag

The coefficient $\Delta C_{D0,gear}$ is estimated for the aircraft (Airbus A320-200 / A340-300) from statistical mean values according to Figure 2.7 corresponding to the category "Large Transports" (A340-300) and "Small / Medium Transports" (A320-200). The mean values are transferred to Excel to extract polynomial functions depending on the flap angle δ_f.

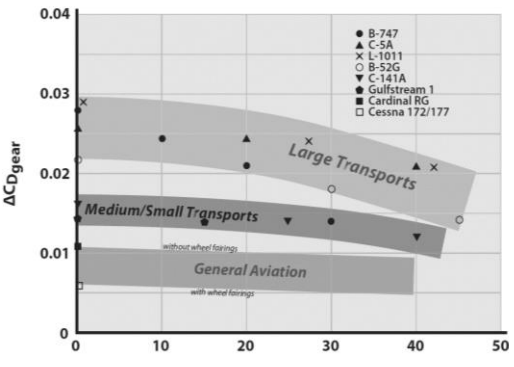

Figure 2.7 Landing gear drag coefficient (Nicolai 2010)

2.5.2 Asymmetric Drag

With OEI-conditions the drag polar must be adjusted accordingly. According to Young 2018, three main components increase the drag:

- spillage drag,
- windmilling drag and
- yaw (control) drag.

The main contribution is provided by the rudder deflection, which is necessary to compensate for the significant yaw moment created by the asymmetric thrust. (See Figure 2.8).

The asymmetric drag increases essentially with

- the distance of the engine from the center of gravity, or the line of symmetry l_E,
- the magnitude of the engine power T_0 ,
- the engine diameter (inlet) d_i

and decreases with

- the VTP lever arm l_V and
- the dynamic pressure (the velocity)

The amount of air that can pass through an engine in this condition will be substantially less than what would normally occur in a fully functioning engine at the associated flight speed, causing air to spill around the nacelle. This results in spillage drag. (Young 2018).

Additional asymmetric drag components:

- Airframe drag resulting from sideslip,
- vortex-induced drag related to the change in wing lift contribution,
- drag caused by the ailerons to compensate the asymmetric lift.

The (total) asymmetric drag is very difficult to capture. Within the scope of this thesis, the 3 essential parts "yaw-drag" and "windmill drag" and "spillage drag." are considered. Other components are neglected.

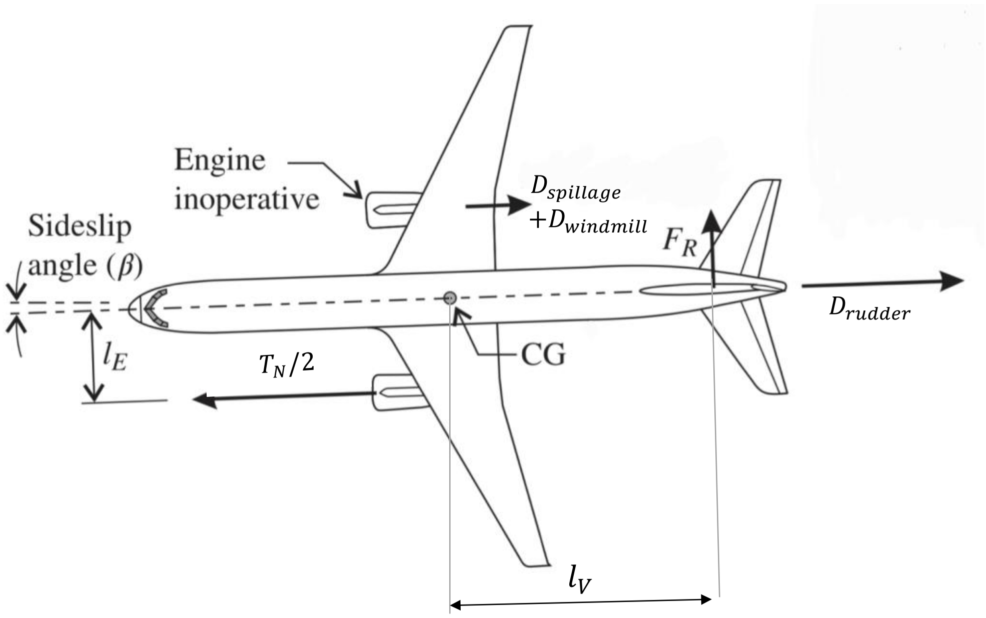

Figure 2.8 Asymmetric thrust condition (OEI), (Young 2018)

In order to estimate the corresponding drag increases, approximation methods according to (Torenbeek 1982, Appendix G-8.3) are applied. For this purpose, the geometry of the vertical stabilizer and the engines have to be determined first. Most relevant parameters could be identified regarding the 2 sample aircrafts. Other geometries, such as the rudder surface area S_r, the inner engine diameter d_i (A340) and the sweep angle of the VTP ϕ_V (A340) are derived (estimated) from the known quantities.

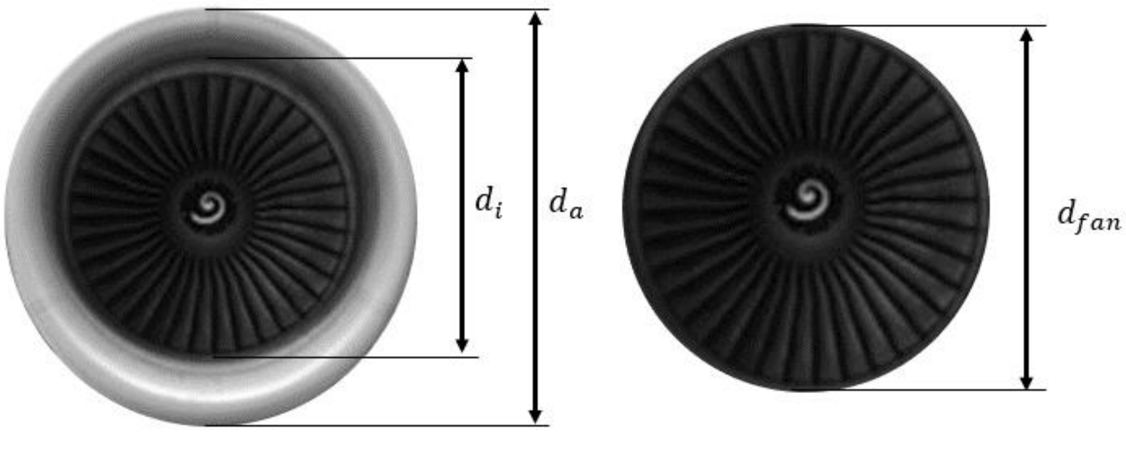

Figure 2.9 CFM56 (based on Air Team Images 2010)

The relevant engine geometry is illustrated with Figure 2.9.

For the Airbus A320, all engine parameters could be defined on the basis of available sources. For the A340, the inner diameter has to be estimated. Since the outer diameters and fan diameters have the same ratios f_d, it is assumed that this also applies (approximately) to the inner diameter because the engines are very similar.

Table 2.4 Fan parameter

	Sign	A320 [m]	A340 [m]	Ratio f_d
Outer diameter	d_a	2.30	2.43	1.057
Fan diameter	d_{fan}	1.74	1.84	1.057
Inlet diameter	d_i	1.60	?	

Thus, the inner diameter can be determined with the parameters according to Figure 2.9, with a factor from (2.50) and the values from Table 2.4.

$$d_{i,A340} = f_d \cdot d_{i,A320} = 1.69\ m \tag{2.50}$$

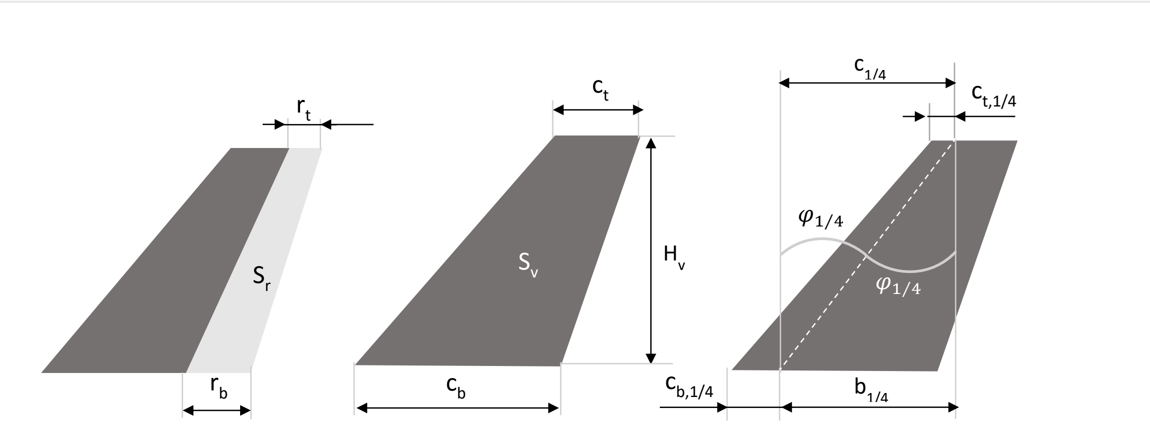

Figure 2.10 VTP parameters

For the required rudder and VTP geometry, H_v and c_b (Figure 2.10) are known. The remaining geometric parameters are derived from scaled models from Airbus 2005c & Airbus 2005d and calculated with (2.51) to (2.55) by means of trigonometry.

$$S_v = \frac{c_t + c_b}{2} \cdot H_v \tag{2.51}$$

$$S_r = \frac{r_t + r_b}{2} \cdot H_v \tag{2.52}$$

$$\varphi_{1/4} = arctan\left(\frac{c_{1/4}}{H_V}\right) \cdot \frac{180}{\pi} \tag{2.53}$$

$$c_{t,1/4} = 0.25 \cdot c_t \tag{2.54}$$

$$c_{b,1/4} = 0.25 \cdot c_b \tag{2.55}$$

Based on generalized data on plain flaps effectiveness, with (2.56) to (2.59), Torenbeek presents a method for estimating the drag increment resulting from rudder deflection required to compensate for the yaw moment in the event of an engine failure.

Drag increment due to rudder deflection (yaw moment):

$$\Delta C_{D0,R} \cdot S_W = \frac{2.3}{\pi} \sqrt{S_r \, S_v} \left(A_{V_{eff}}\right)^{-4/3} (cos\, \varphi_V)^{1/3} \cdot C_{Y_V}^2 \tag{2.56}$$

For a conventional VTP it is assumed that $A_{V_{eff}} \approx A_V$

$$C_{Y_V} = \frac{\Delta T_{OEI}}{q_V \, S_V} \cdot \frac{y_e}{l_V} \tag{2.57}$$

$$\Delta T_{OEI} = 1 \cdot \; T_0[A - K_1 v + K_2 v^2] \tag{2.58}$$

$$q_V = \frac{\rho}{2} v^2 \tag{2.59}$$

$\Delta C_{D0,R}$	$[-]$	Drag increment, rudder
S_r	$[\mathrm{m}^2]$	Rudder surface area
S_v	$[\mathrm{m}^2]$	VTP surface area (incl. rudder)
T_0	[N]	Static engine thrust, 1 engine
$A_{V_{eff}}$	$[-]$	Effective aspect ratio, VTP
φ_V	[rad]	VTP sweep angle
C_{Y_V}	$[-]$	Factor
ΔT_{OEI}	[N]	Net thrust loss (1 engine)
$\Delta C_{0,wm}$	$[-]$	Windmill drag
y_e	[m]	Lever, CG to (critical) engine position
l_V	[m]	Lever, VTP-MAC to CG
q_V	$[Pa]$	Dynamic pressure regarding the VTP

In order to demonstrate the corresponding correlations and contributions, an engine failure at 140 knots for an A320 was simulated in MATLAB. The results are visualized in Figure 2.11, Figure 2.13 for the resulting drag and Figure 2.12 for the drag coefficient increments. The "symmetrical" drag contributions are all the remaining shares that are not caused from the engine failure.

It becomes clear that the rudder portion decreases with speed, which is primarily due to the increase of the dynamic pressure, while all other portions increase. This relationship also explains the limiting speed VMCG. At low speeds, the rudder force is not sufficient to compensate for and asymmetric yaw moment. The rudder would have to deflect beyond the maximum possible / permitted deflection angle.

Figure 2.14 shows that the drag coefficient $\Delta C_{D,asym}$ increases significantly with reduced velocity. The curves approach asymptotically the y-axis. As a result, the ground roll distance would increase disproportionately at low failure speeds and the braking distance would be drastically reduced. For the study of BFL, only speed ranges that are beyond 100 knots are included. Furthermore, when calculating the stopping distance, according to the time intervals from Figure 5.9 and Table 5.8, the thrust of the remaining engine(s) is reduced to idle thrust after 1.5 seconds, after which $\Delta C_{D,asym}$ provides only an insignificant contribution to drag (see Figure 2.14) and is set to zero. If $\Delta C_{D,asym}$ were to continue to be calculated stepwise until reaching 0 knots, the values would continue to strive towards infinity even at idle thrust due to the dynamic pressure, rendering the result unusable. For the distance in the air with a failed engine, a constant velocity v_{2min} is assumed until reaching 35 ft, $\Delta C_{D,asym}$, for this reason ΔT_{OEI} , $\Delta C_{D0,wm}$ and q_V are determined based on v_{2min}. The remaining ground roll distance is also determined as part of the BFL determination at velocities well beyond 100 knots. Therefore, the procedure proposed by Torenbeek to calculate the drag increase due to asymmetric flight conditions can be applied to all distance sections. An alternative approach would be to calculate with constant average values for the asymmetric drag coefficient as proposed in (Ehrig 2012).

Indices (Figures**)**:

$asym$	Total asymmetric drag increment (coefficient)
R	Rudder
wm	Windmill
sp	Spillage
sym	Symmetric

Constant coefficients in Figure 2.12 are indicated on the Y-axis to avoid overloading the graph.

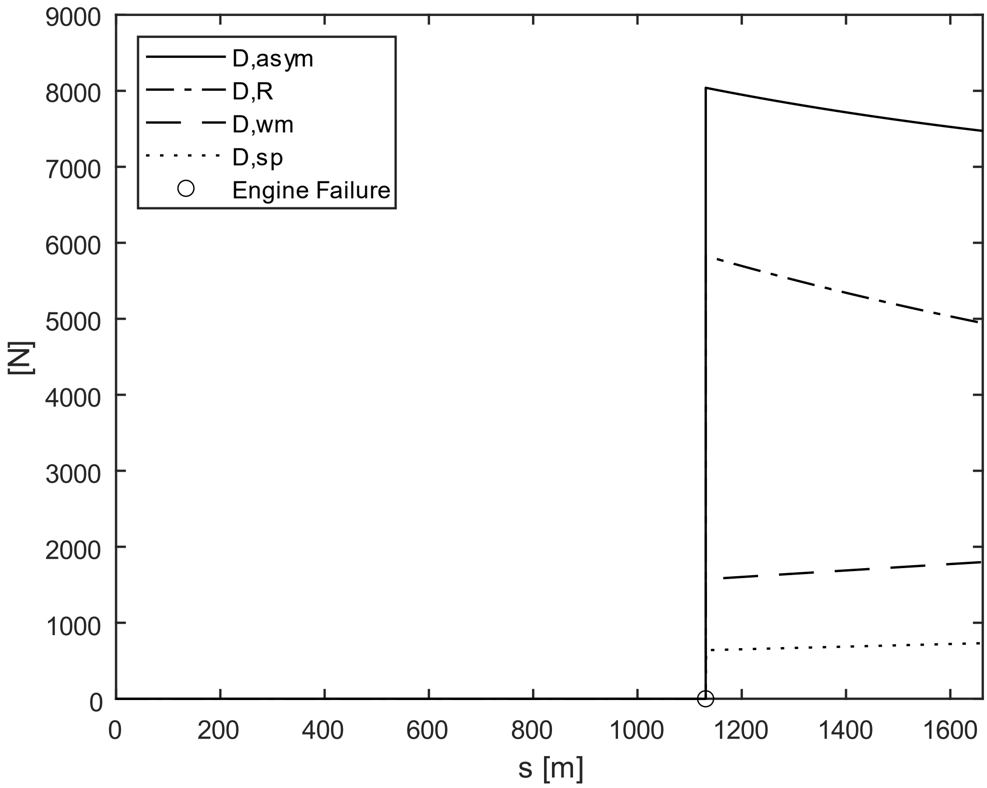

Figure 2.11 Drag breakdown (engine failure A320 with, $v_{EF} = 140\text{ knots}$)

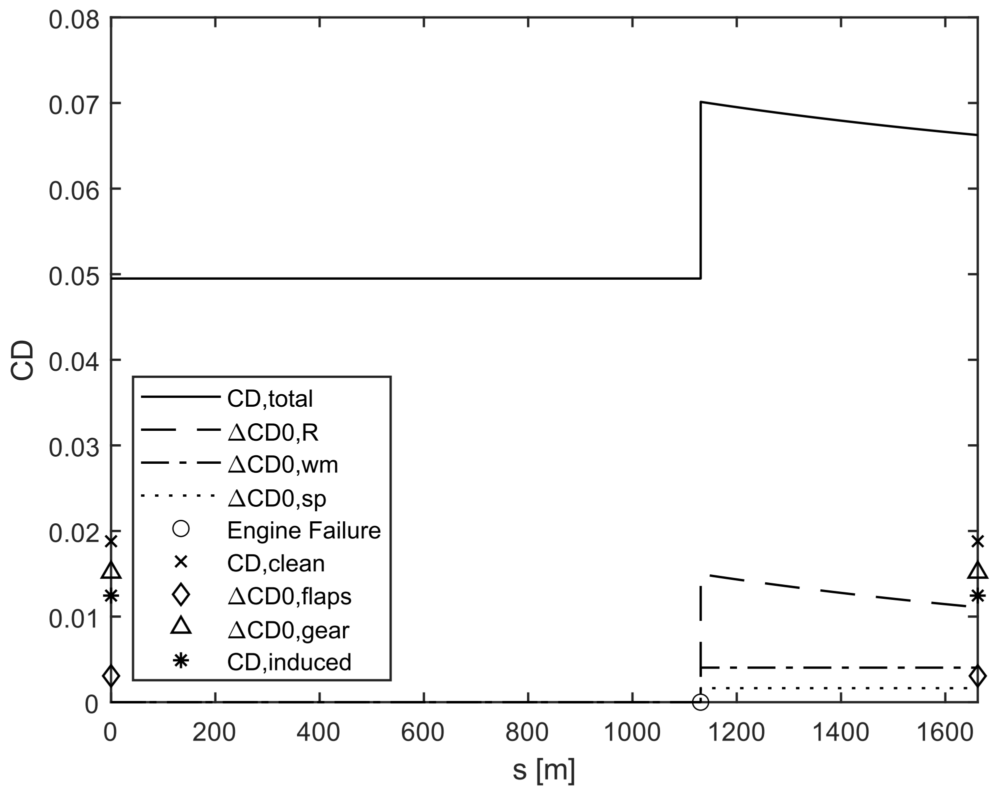

Figure 2.12 Asymmetric drag coefficient increment, A320 ($v_{EF} = 140\text{ knots}$)

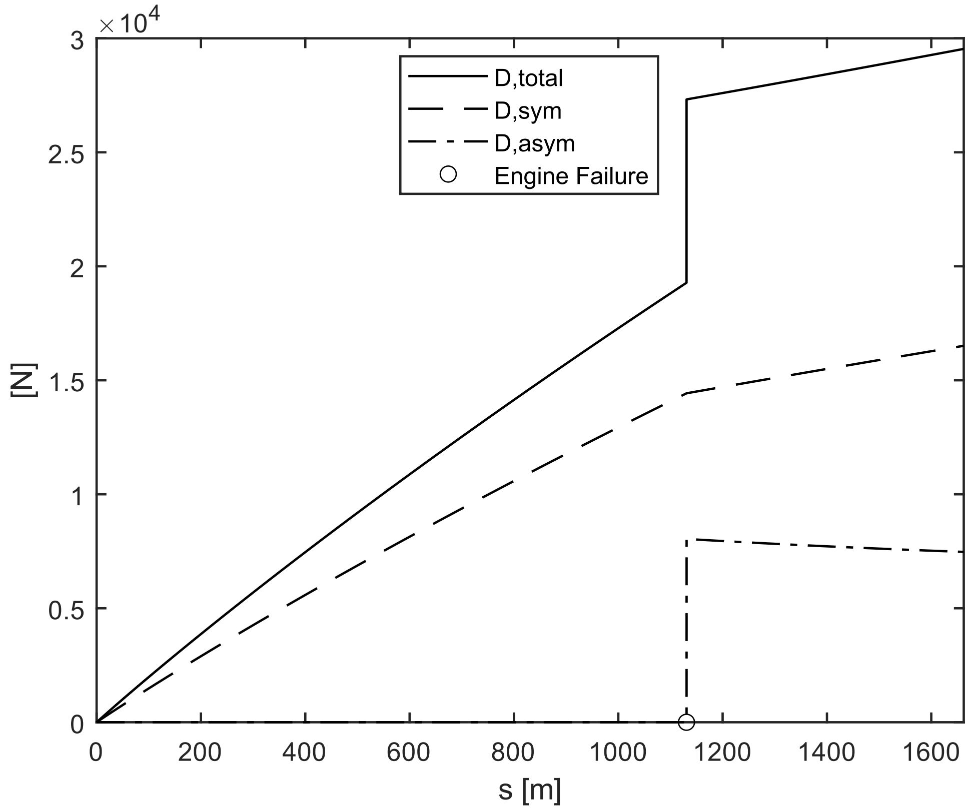

Figure 2.13 Drag coefficient breakdown (A320 with, $v_{EF} = 140$ knots)

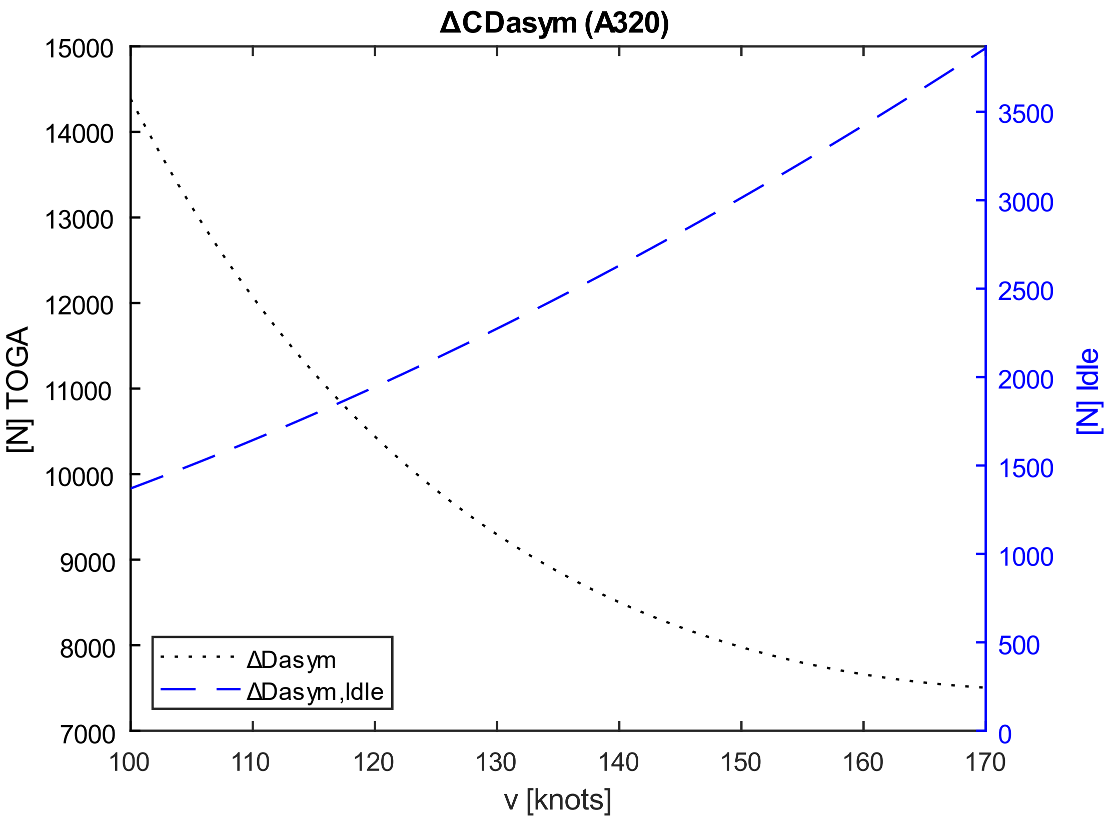

Figure 2.14 Asymmetric drag increment, A320

2.5.3 Windmill Drag

Moving air entering an inoperative engine will cause the rotating assemblies to spin. The energy needed to produce this effect, can be viewed as an effective drag force acting on the engine. This is known as windmilling drag.

Windmill drag, Jet (Torenbeek 1982, S.554):

$$\Delta C_{D0,wm} \cdot S_W = \left(d_i^2 \cdot \frac{\pi}{40} + \frac{2}{1 + 0.16 \cdot M^2} \cdot A_n \cdot \frac{v_N}{v} \cdot \left(1 - \frac{v_N}{v}\right)\right) \tag{2.60}$$

$$\Delta C_{D0,wm} = \left(0.1 + \frac{2}{1 + 0.16 \cdot M^2} \cdot \frac{v_N}{v} \cdot \left(1 - \frac{v_N}{v}\right)\right) \cdot A_n / S_W \tag{2.61}$$

$$D_{wm} = \Delta C_{D,wm} \cdot \frac{\rho}{2} \cdot v^2 \cdot S_W \tag{2.62}$$

$$A_N = d_i^2 \cdot \frac{\pi}{4} \tag{2.63}$$

$$v_{rel} = v_N / v \tag{2.64}$$

v_N/v	0.12	primary airflow of high bypass engines
	0.25	for straight turbojet & turboprop engines
	0.42	low bypass ratio engines, mixed flow
	0.92	fan airflow of high bypass engines

v_{rel}	Relative air speed
A_N	Area of a nozzle
v_N	avg velocity of engine nozzle flow
v	Flight velocity
d_i	Engine inlet diameter

The dependence on the bypass ratio is illustrated with Figure 2.15 based on the A/C parameter of Chapter 8. Although there is a dependency between the Mach number and the windmill drag coefficient, it is almost constant over the speed (see Figure 2.16)

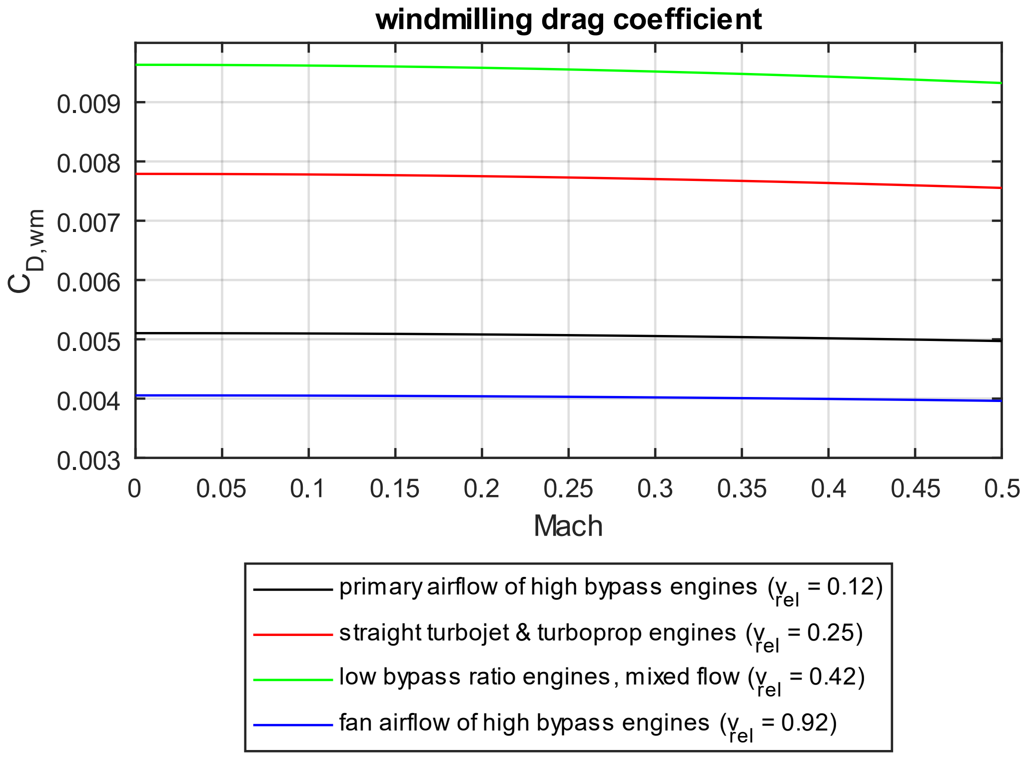

Figure 2.15 Windmill drag coefficient as a function of the relative speed

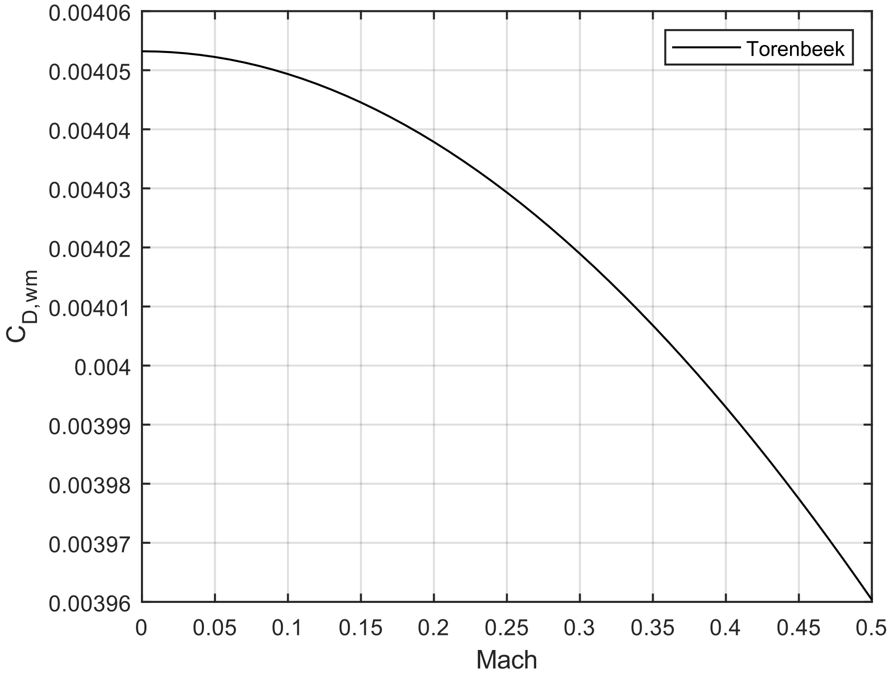

Figure 2.16 Windmill drag, A320

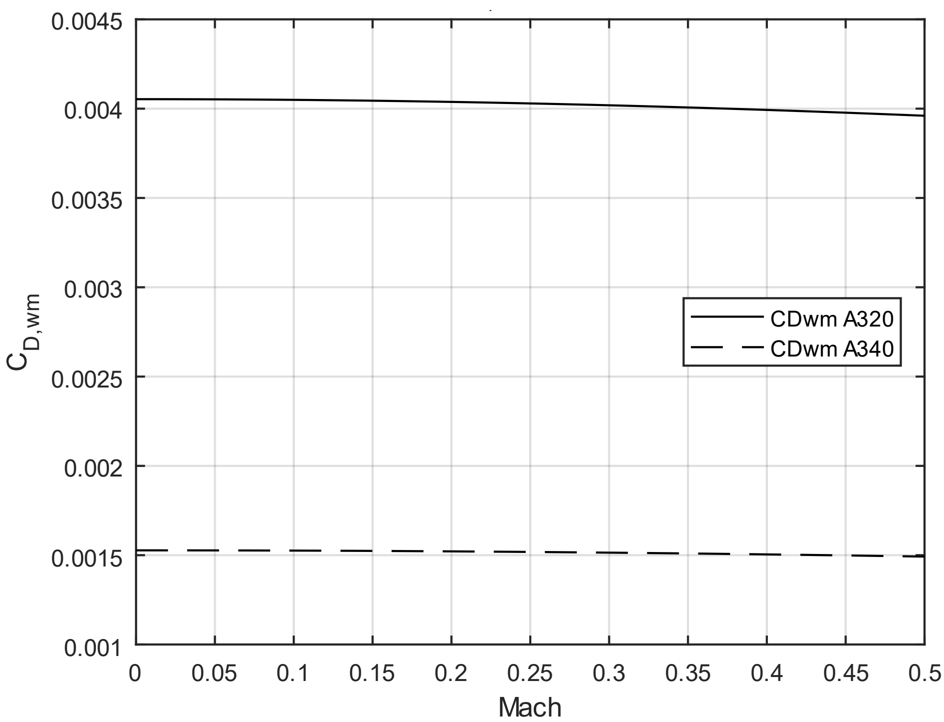

Figure 2.17 Windmill drag, comparison

For the four-engine jet, the windmill drag coefficient is significantly lower (see Figure 2.17)

An simpler approach from (Raymer 2012) gives similar results:

Jet:

$$(D/q)_{wm} = 0.3 \cdot A_N \tag{2.65}$$

$$\frac{c_{D,wm} \cdot q \cdot S_W}{q} = c_{D,wm} \cdot S_W = 0.3 \cdot A_N \tag{2.66}$$

$$\Delta C_{D0,wm} = 0.3 \cdot A_N / S_W \tag{2.67}$$

A_N engine front face surface area

2.5.4 Spillage Drag

The spillage effect can be estimated according to Torenbeek by the coefficient defined in (2.68).

$$\Delta C_{D0,sp} \cdot S_W = 0.1 \cdot \frac{\pi}{4} \cdot d_i^2 \tag{2.68}$$

2.6 Maximum Lift Coefficient at Takeoff

Definition of the lift coefficient C_L:

$$C_L = \frac{n\,W}{q\,S} \tag{2.69}$$

Dynamic pressure:

$$q = \frac{\rho}{2} v^2 \tag{2.70}$$

$$C_L = \frac{n}{v^2} \frac{2\,W}{\rho\,S} \tag{2.71}$$

with $n = 1$ and $v = v_{s1g}$ (see Figure 1.7):

$$C_{L,max} = \frac{2\,W}{S_W\,\rho\,v_{S1g}^2} \tag{2.72}$$

Conventional Stall Speed v_S:

$$v_S = 0.94\ v_{s1g} \tag{2.73}$$

With v_{s1g} from (Airbus 2005a) and (Airbus 2005b). (See Chapter 3.1)

The CLmax values, which result from the stall speeds of the FCOM according to Airbus data are summarized in Chapter 8 in Table 8.8 and Table 8.9.

m	A/C weight	[kg]
W	Weight force	[N]
$C_{L,max}$	Maximum lift coefficient (in specific flap configuration)	[-]
v_S	Stall speed	[m/s], [kt]
v_{s1g}	Stall speed at 1 g	[m/s], [kt]
n	Load factor	[-]
q	Dynamic pressure	[Pa]

The aim of the method according to (2.72) is to be able to determine C_{Lmax} as a function of the flap position and A/C weight via v_{s1g} (see Chapter 4.1).

2.7 Influence of High Lift Devices

2.7.1 Geometric Definitions

Figure 2.18 and Figure 2.19 illustrate the relevant parameters of the flap geometry.

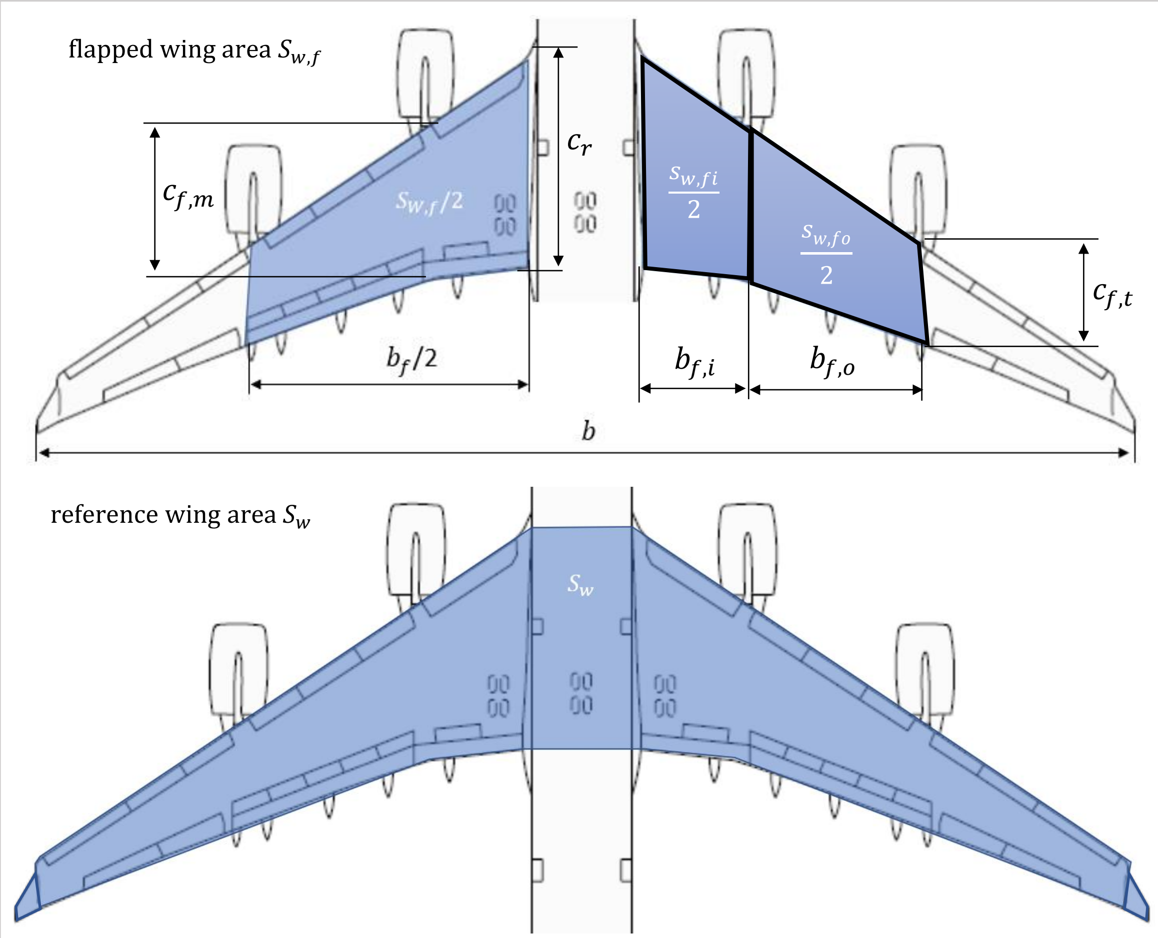

Figure 2.18 Marked (blue) reference wing areas[3]

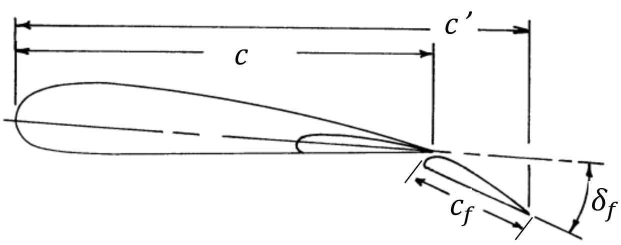

Figure 2.19 Flap parameter, (Scholz 2015)[4]

---

[3] Modified cutout, the original image is a picture of an A340 (Airbus 2005d).
[4] Edited

b_f	Flapped wingspan	[m]
$b_{f,i}$	Flapped wingspan, inside	""
$b_{f,o}$	Flapped wingspan, outside	""
c	Airfoil chord (clean, without flaps)	""
c_f	Flap chord	""
$c_{f,t}$	Wing chord at the tip of the flapped area	""
$c_{f,m}$	Wing chord at the mid of the flapped area	""
c'	Airfoil chord (extended flaps)	""
c_r	Wing root chord	""
δ_f	Flap angle	[°], [rad]
S_{wf}	Flapped wing area	[m²]
$S_{w,fi}$	Flapped wing area, inboard	""
$S_{w,fo}$	Flapped wing area, outboard	""

The flapped area is obtained by adding the two trapezoidal areas considered separately as defined in Figure 2.18.

$$S_{w,f} = S_{w,fi} + S_{w,fo} \tag{2.74}$$

$$S_{w,f}/2 = b_{f,i} \cdot \frac{c_r + c_{f,m}}{2} + b_{f,o} \cdot \frac{c_{f,m} + c_{f,t}}{2} \tag{2.75}$$

The parameters b, b_f, c_r, S_w are known from (Airbus 2005c), (Airbus 2005d), (Wikipedia 2021c) and (Wikipedia 2021d). Further parameters are derived from scaled models from the same sources, supplemented by further image sources (see Chapter 8.1).

As illustrated in Figure 2.18, by definition the flapped wing area, is not the actual flap surface area, but the wing area for the area over which the flaps span.

2.7.2 Lift Increment

In the context of this thesis, the prototype aircraft are based on the Airbus A320 - 200 and A340 - 300, both of which use "**single slotted fowler flaps**."

In this Chapter, (2.76) to (2.90), a method from (Torenbeek 1982, Appendix G) for estimating the lift increase, is presented.

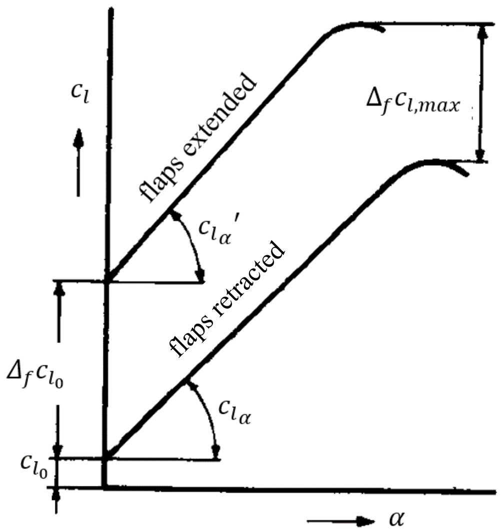

Figure 2.20 Effect of flaps on lift (Torenbeek 1982)

Figure 2.20 shows that the lift coefficient and the lift curve slope change (increase) when the flaps are extended.

$$\Delta_f C_{L_0} = \Delta_f c_{l_0} \left(\frac{C_{L_\alpha}}{c_{l_\alpha}}\right)\left[\frac{(\alpha_\delta)C_L}{(\alpha_\delta)c_l}\right] K_b \tag{2.76}$$

$$(\alpha_\delta)_{c_l} = \eta_\delta \, \alpha_\delta \tag{2.77}$$

$$\Delta_f C_{L_0} = \Delta_f c_{l_0} K_a K_b K_c \tag{2.78}$$

$$K_a = C_{L_\alpha}/c_{l_\alpha} \tag{2.79}$$

$$K_c = \frac{(\alpha_\delta)C_L}{(\alpha_\delta)c_l} \tag{2.80}$$

$\Delta_f c_{l_0}$	Lift increment 2D	
K_a	Ratio lift curve slope 3D/2D	
K_b	Flap span effectiveness factor	(Figure 2.24)
K_c	Ratio effectiveness parameter 3D/2D	(Figure 2.24)

$\Delta_f C_{L_0}$	Lift increment 3D, $\Delta_f C_{L_0} = \Delta C_{L0,flap}$	
$(\alpha\delta)C_L$	Flap effectiveness parameter 3D	
$(\alpha\delta)c_l$	Flap effectiveness parameter 2D	
$\frac{(\alpha\delta)C_L}{(\alpha\delta)c_l}$	$\frac{(\alpha\delta)C_L}{(\alpha\delta)c_l} = k_c$, ratio flap effectiveness parameter 3D / 2D	(Figure 2.24)

$$\Delta_f c_{l_0} = \Delta_f c'_{l_0}\,\frac{c'}{c} + c_{l_0}\left(\frac{c'}{c} - 1\right) \tag{2.81}$$

$$\Delta_f c'_{l_0} = 2\pi\,\eta_\delta\,\alpha'_\delta\,\delta_f \tag{2.82}$$

$$\alpha'_\delta = \frac{c_{l_\delta}}{c_{l_\alpha}} = 1 - \frac{\Theta'_f - sin\Theta'_f}{\pi} \tag{2.83}$$

$$\Theta'_f = cos^{-1}\left(2\frac{c_f}{c'} - 1\right) \tag{2.84}$$

$$c' = c + \Delta c \tag{2.85}$$

$$\Delta c = \left(\frac{\Delta c}{c_f}\right)\cdot c_f \tag{2.86}$$

c'	Increased chord due to extended (fowler) flaps
$\Delta_f c'_{l_0}$	Lift increment based on extended chord c'
η_δ	Lift effectiveness
α'_δ	Theoretical flap lift factor (based on extended chord c')
Θ'_f	Angle characterizing relative flap (based on extended chord c')
Δc	Chord increment estimation (due to extended flaps)

$0 \le \delta_f \le 5°$:

$$\Delta C/c_f = 0.0454\cdot\delta_f \tag{2.87}$$

$5 \le \delta_f \le 45°$:

$$\Delta C/c_f = 0.0053\cdot\delta_f + 0.3997 \tag{2.88}$$

$$\eta_\delta = -7.514\cdot10^{-6}\delta_f^3 + 1.731\cdot10^{-4}\delta_f^2 - 2.294\cdot10^{-3}\delta_f + 8.837\cdot10^{-1} \tag{2.89}$$

(2.87) to (2.89) are derived from Figure 2.21, respectively Figure 2.23 in Excel.

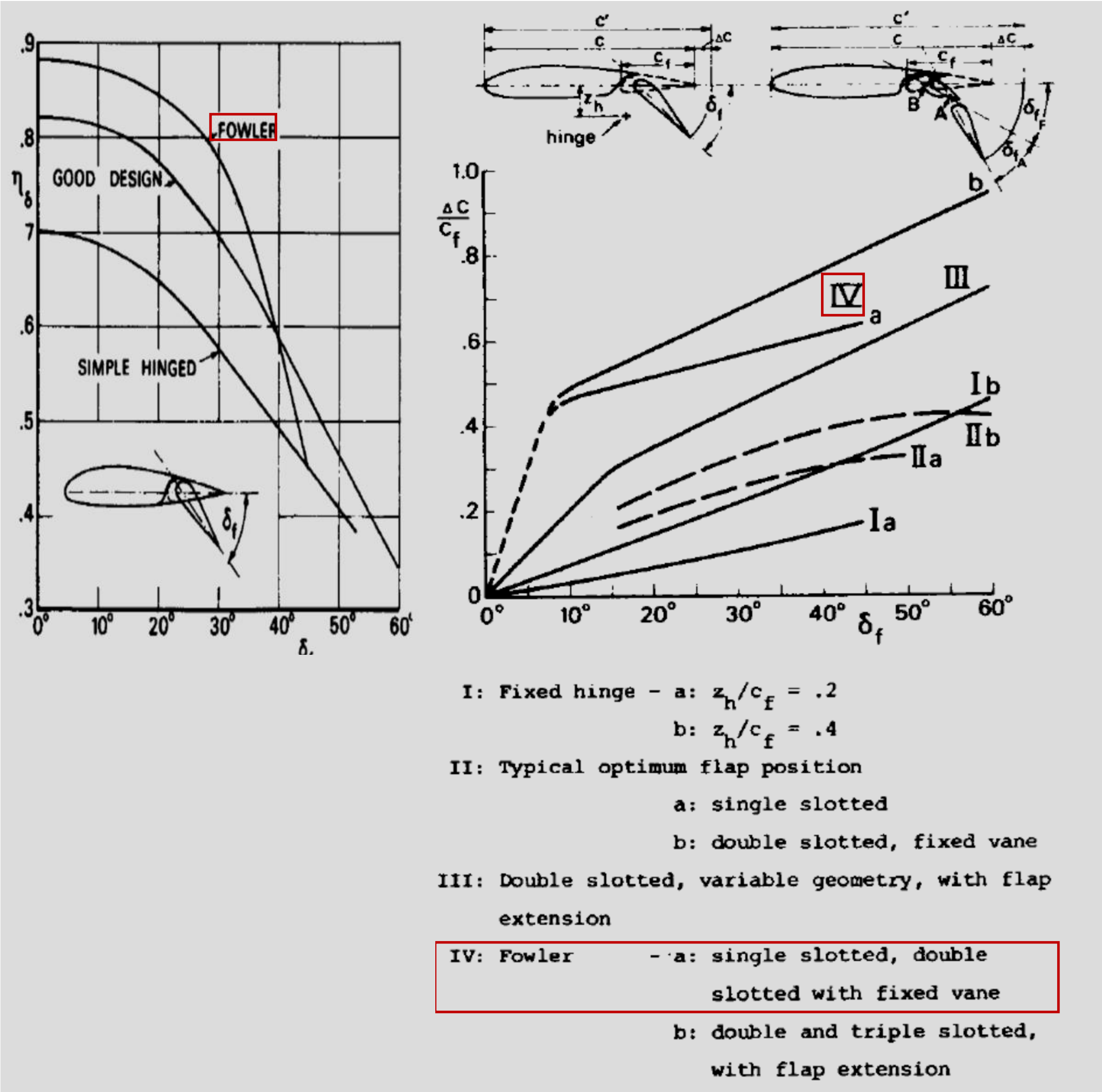

Figure 2.21 Lift effectiveness η, chord extension ratio $\Delta c/c_f$ (Torenbeek 1982)

Figure 2.22 illustrates the definition of the relative flap angle.

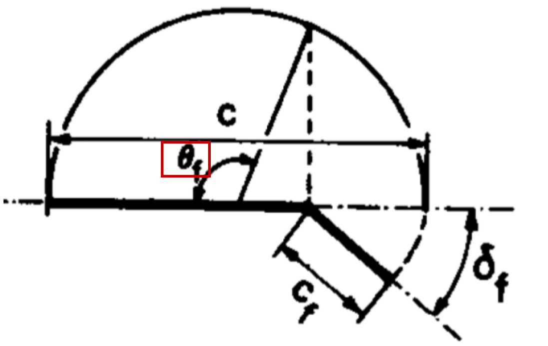

Figure 2.22 Relative flap angle Θ_f (Torenbeek 1982)

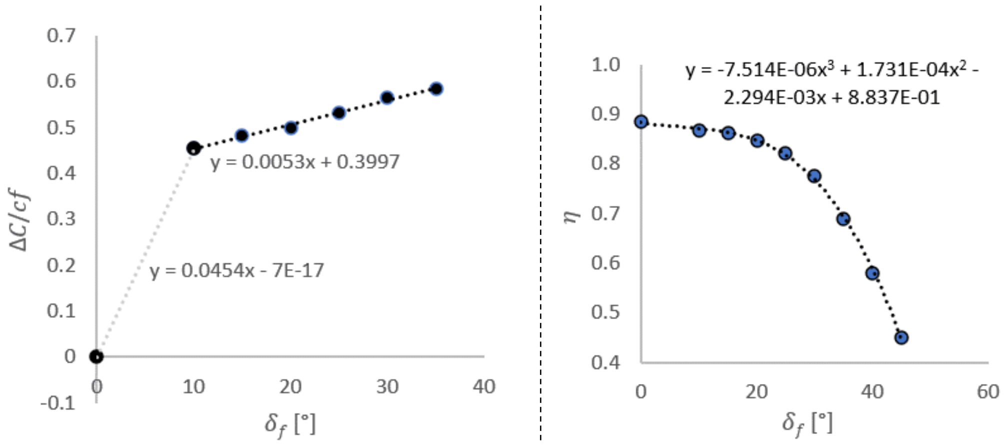

Figure 2.23 Chord extension estimate (left) / Lift effectiveness η (right)

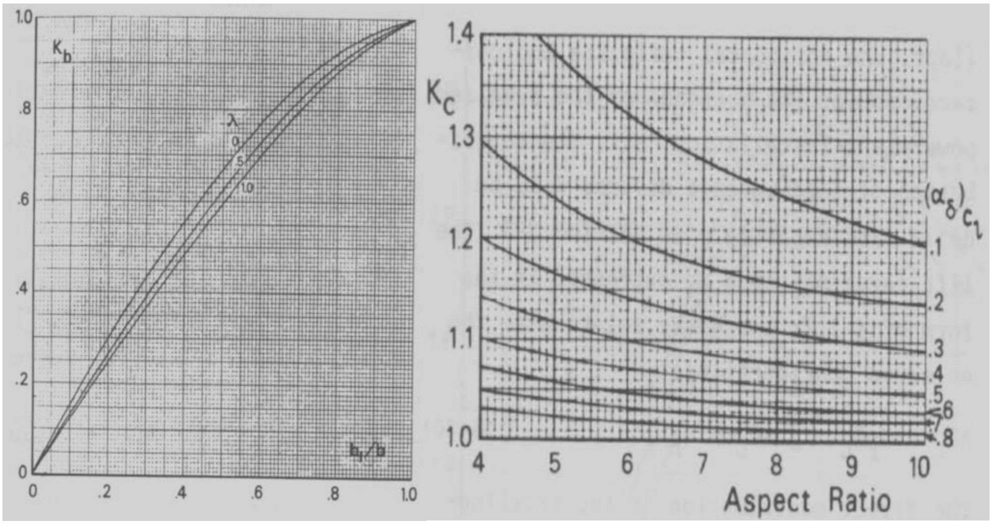

Figure 2.24 (Fowler) flap factors K_b and K_c

2.7.3 Lift Curve Slope Correction

According to (2.28), the lift curve slope coefficient (flaps retracted) is dependent on the aspect ratio and the wing sweep angle φ_{50} in addition to the Mach number. The influence of the flaps is taken into account with (2.90) from (Torenbeek 1982).

$$\frac{c'_{L\alpha}}{c_{L\alpha}} = 1 + \frac{\Delta_f C_{L_0}}{\Delta_f c_{l_0}}\left[\frac{c'}{c}\left(1 - \frac{c_f}{c'} sin^2\, \delta_f\right) - 1\right] \tag{2.90}$$

$c'_{L\alpha}$	flaps down (extended)
$c_{L\alpha}$	flaps up (retracted / clean)
$\Delta_f C_{L_0}$	three-dimensional lift increment due to flaps
$\Delta_f c_{l_0}$	two-dimensional lift increment due to flaps

Within the Mach number range of a takeoff, $C_{L,\alpha}$ can be considered approximately constant with only minor changes with a flap configuration.

2.7.4 Drag Increment

For the estimation of drag increase resulting from the extended single slotted fowler flaps, (2.91) and the factor from Figure 2.25 based on (Nicolai 2010) is applied:

$$\Delta C_{D0,f} = k_1\, k_2 \frac{S_{w,f}}{S_w} \tag{2.91}$$

$\Delta C_{D0,f}$	Zero lift drag coefficient increment due to flap extension
k_1	Factor regarding flap drag increment (Figure 2.25)
k_2	Factor regarding flap drag increment (Figure 2.25)

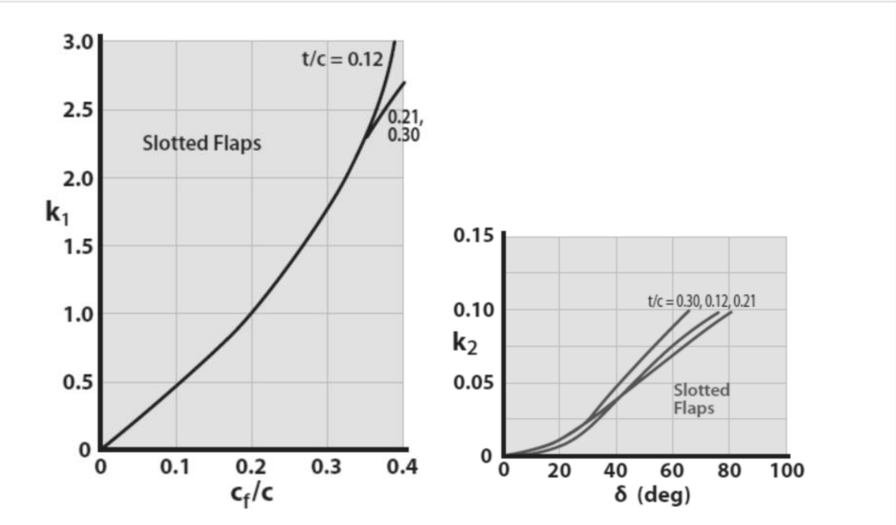

Figure 2.25 Lift increment factors for single slotted fowler flaps (Nicolai 2010)

2.7.5 Span Efficiency Factor

$$C_{D,g} = C_{D0} + \phi \cdot \frac{C_{L,g}^2}{\pi \cdot e \cdot A} \tag{2.40}$$

(2.40) is often also represented with factor k according to (2.92).

$$C_{D,g} = C_{D0} + \phi \cdot k\, C_{L,g}^2 \tag{2.92}$$

with factor k (clean):

$$k = \frac{1}{\pi \cdot e \cdot A} \tag{2.93}$$

Both the Oswald factor e and factor k vary with the flap setting. From (Sun 2020) the dependencies are estimated with (2.94) to (2.96).

For wing-mounted engines:

$$\Delta e_f = 0.0026\, \delta_f \tag{2.94}$$

(2.94) is only valid for "modern" and efficient flaps (see Figure 2.26, DC-8-63, $\Delta e / \Delta \delta_f < 0$).

The linear relationship in (2.94) was originally found by (Obert 2009, p.362-363) based on statistical data from existing aircrafts presented in Figure 2.26.

Total Oswald Factor (takeoff configuration):

$$e_{TO} = e + \Delta e_f \tag{2.95}$$

Factor k_{To} (takeoff configuration):

$$k_{TO} = \frac{1}{\frac{1}{k} + \pi\, A\, \Delta e_f} \tag{2.96}$$

k	Factor k "clean"
k_{TO}	Factor k with extended flaps (takeoff configuration)
Δe_f	Oswald Factor deviation due to flap deflection
e_{TO}	Total Oswald Factor with extended flaps (takeoff configuration)

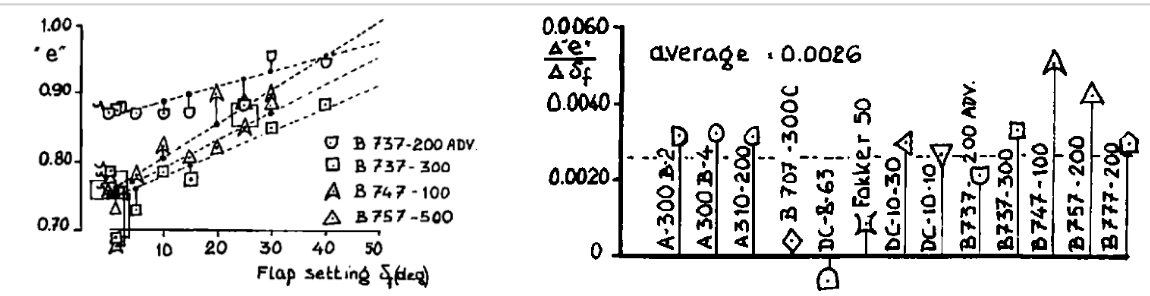

Figure 2.26 Increase in "Oswald Factor" due to flap deflection (Obert 2009)

2.8 Speed Dependent Thrust

The thrust is highly dependent on the velocity, respectively the Mach number and the bypass ratio. This dependence is taken into account in many literature sources with an equation of the form according to (2.97).

Thrust $T(v)$**:**

$$T(v) = N \cdot T_0[A - K_1 v + K_2 v^2] \tag{2.97}$$

$$A \leq 1$$

With ($\boldsymbol{A = 1}$) **coefficients** K_1 , K_2 (Scholz 1999):

$$K_1 = [2.44 \cdot 10^{-4} \cdot \lambda_{BPR} + 1.66 \cdot 10^{-3}] \frac{1}{m/s} \tag{2.98}$$

$$K_2 = [6.16 \cdot 10^{-7} \cdot \lambda_{BPR} + 4.08 \cdot 10^{-6}] \frac{1}{(m/s)^2} \tag{2.99}$$

Depending on the speed and the bypass ratio, the thrust curve is as shown in Figure 2.27.

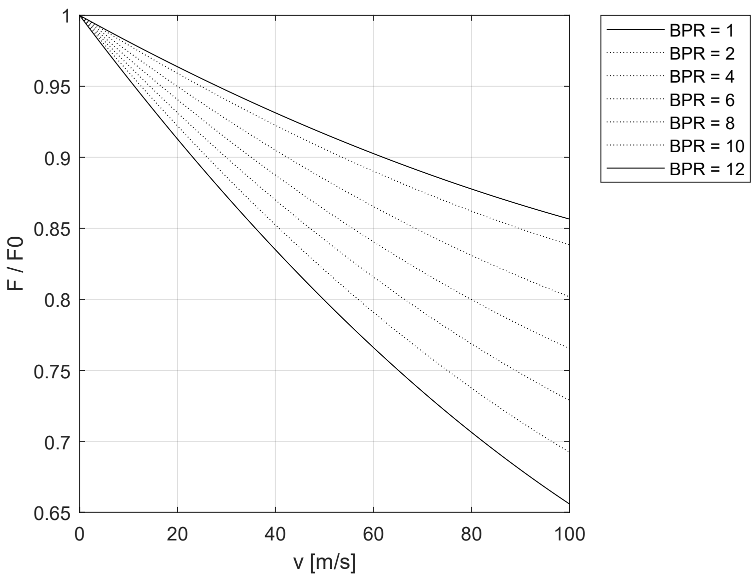

Figure 2.27 Thrust as a function of speed with varying bypass ratios (1…12)

The thrust in Figure 2.27 based on (2.97) can be used to derive thrust as a function of velocity and BPR. Furthermore, the thrust varies with the altitude. In order to be able to take into account the change in altitude with respect to the thrust in the context of parameter variation, an approach from (Bartel 2008) is employed.

Considering the height influence, (2.100) to (2.105) results:

$$T(M) = N \cdot T_0 \cdot (A - k_1 \cdot M^2 + k_2 \cdot M^2) \tag{2.100}$$

$$k_1 = \frac{0.377(1 + \lambda_{BPR})}{\sqrt{(1 + 0.82\lambda)G}} \cdot Z \cdot \frac{p}{p_0} \tag{2.101}$$

$$k_2 = \left(0.23 + 0.19\sqrt{\lambda_{BPR}}\right) \cdot X \cdot \frac{p}{p_0} \tag{2.102}$$

$$A = -0.4327\left(\frac{p}{p_0}\right)^2 + 1.3855\left(\frac{p}{p_0}\right) + 0.0472 \tag{2.103}$$

$$X = 0.1377\left(\frac{p}{p_0}\right)^2 - 0.4374 \cdot \left(\frac{p}{p_0}\right) + 1.3003 \tag{2.104}$$

$$Z = 0.9106\left(\frac{p}{p_0}\right)^2 - 1.7736 \cdot \left(\frac{p}{p_0}\right) + 1.8697 \tag{2.105}$$

$A,\ k_1\ , k_2, X$, Z	Coefficients	[-]
T_0	Static thrust (1 engine)	[N]
N	Number of engines	[-]
v	Speed	[m/s]
$T(v)$	Thrust as a function of speed	[N]
λ_{BPR}	Bypass ration (BPR)	[-]
G	Gas generator factor	[-]

The constants regarding the atmosphere are summarized in Table 2.1 and Table 2.2.

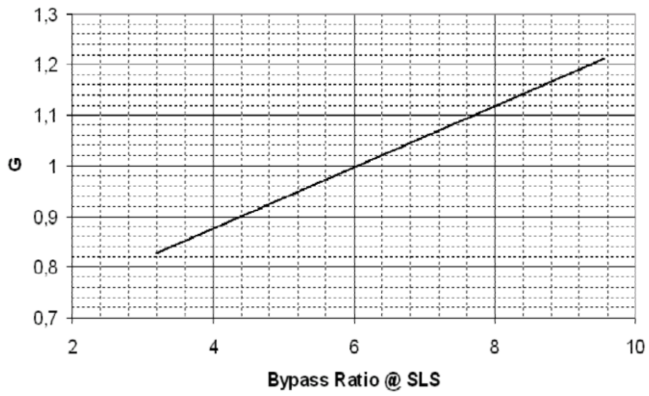

Figure 2.28 Gas generator factor (Bartel 2008)

The gas generator factor from Figure 2.28 can be mapped according to (2.106):

$$G = 0.061\,\lambda_{BPR} + 0.633 \tag{2.106}$$

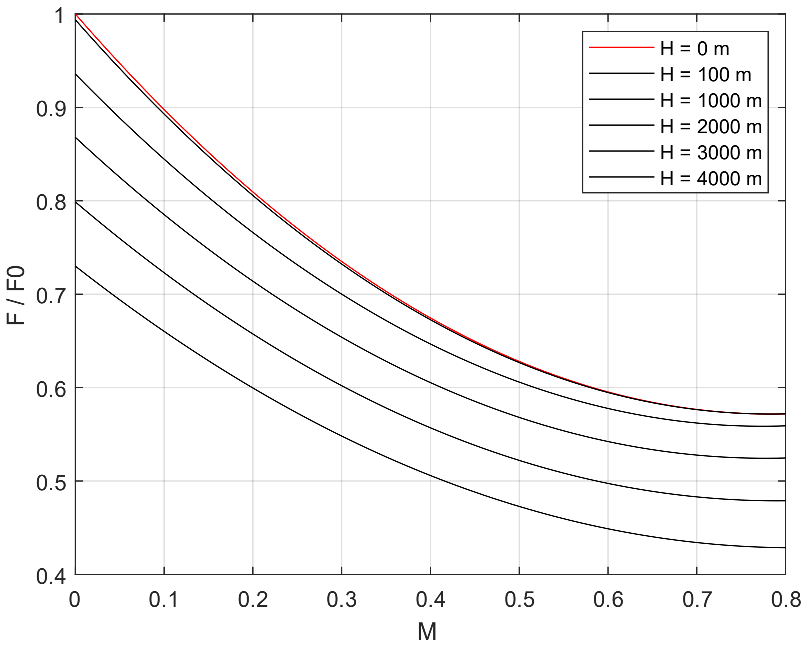

Figure 2.29 Thrust (A320) as a function of Mach number and altitude

Note: The pressure as function of altitude is determined based on (2.5) or (2.9).

The idle thrust of the A320 and A340 are not available. An Airbus A320 or A340 can start rolling with only idle thrust. Therefore, the idle thrust must provide enough thrust to overcome the friction drag. $\mu = 0.02$ at $v = 0\ kt$. Since this is only sometimes the case it needs to be less the friction the A/C has to overcome. The idle thrust is assumed to be approximately 80% of the friction (with an even runway).

$$T_{idle} \approx 0.8 \cdot \mu \cdot mg/N_e \tag{2.107}$$

3 *V*-Speed

3.1 Stall Speed

3.1.1 Airbus A320-200

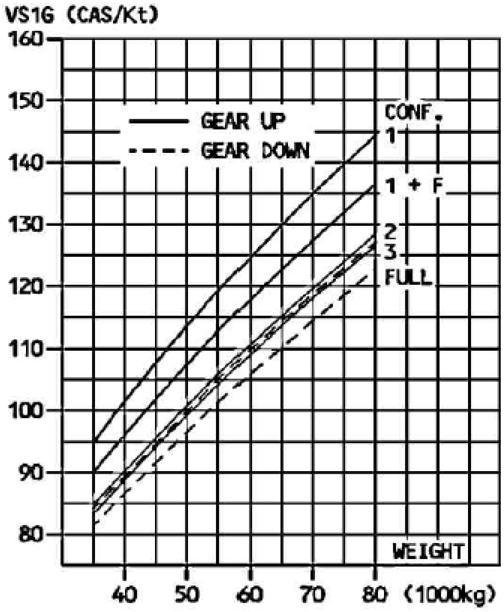

Figure 3.1 Stall speeds, vs1g, Airbus A320 (Airbus 2005a)

From Figure 3.1, values for v_{s1g} were extracted in 5000 kg interval. The results are summarized in Table 3.1:

Table 3.1 vs1g, Airbus A320

m [t]	Conf 1+F	Conf 2	Conf 3
80	137	129.5	128
75	133.75	125.5	124
70	129	121.5	119.5
65	124.5	117.5	115
60	119.5	112	110.25
55	114.5	107	105
50	109.5	102	110.25
45	103.75	97.5	95.5
40	97.5	91.5	90

In Excel, corresponding data points can be directly connected by trend lines.

From Table 3.1, the diagrams in Figure 3.2 result.

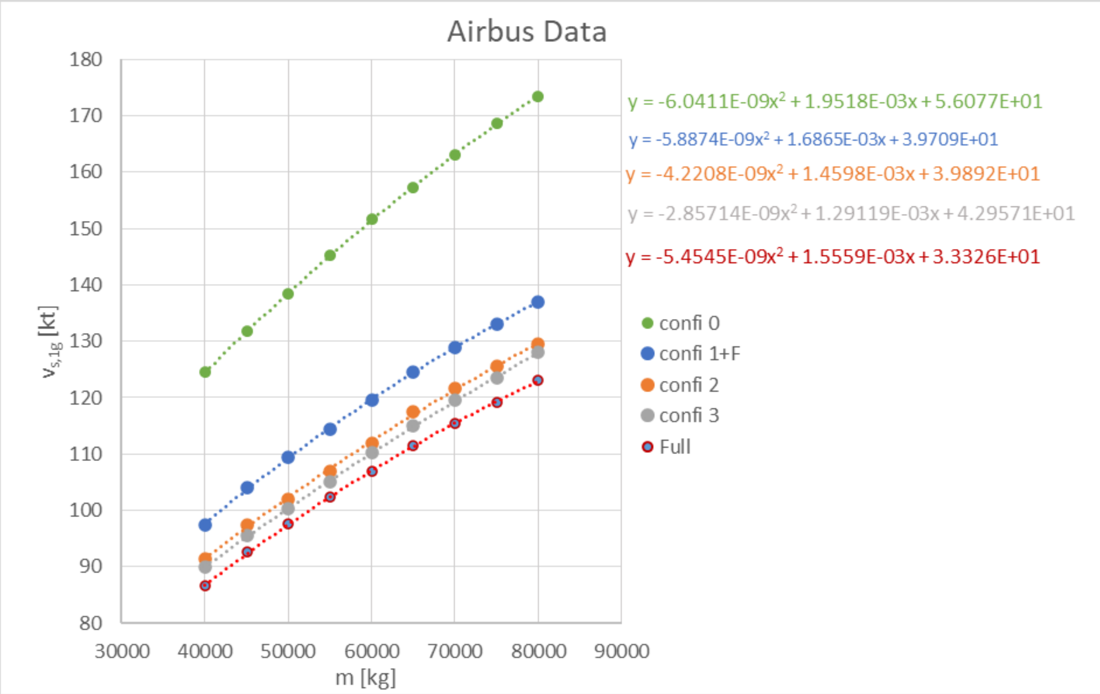

Figure 3.2 Stall speeds, vs1g, Airbus A320 (Excel)

Note: The stall speeds $vs1g$ are determined experimentally at respective aircraft mass m by stall speed maneuvers.

The corresponding 2nd degree polynomials for the potential start configurations are summarized with (3.1) to (3.3):

Confi 1+F (Takeoff):

$$v_{s,1g} = -5.8874 \cdot 10^{-9} \cdot m^2 + 1.6865 \cdot 10^{-3} \cdot m + 3.9709 \cdot 10^1 \tag{3.1}$$

Confi 2 (Takeoff):

$$v_{s,1g} = -4.2208 \cdot 10^{-9} \cdot m^2 + 1.4598 \cdot 10^{-3} \cdot m + 3.9892 \cdot 10^1 \tag{3.2}$$

Confi 3 (Takeoff / Landing):

$$v_{s,1g} = -2.85714 \cdot 10^{-9} \cdot m^2 + 1.29119 \cdot 10^{-3} \cdot m + 4.29571 \cdot 10^1 \tag{3.3}$$

Note: For an airport at sea level under ISA condition $(h = 0\text{ ft}, T = 15°\text{C})$, $v_{CAS} = v_{EAS} = v_{TAS}$. (3.1) to (3.3) apply exclusively under named conditions and only for aircrafts of the Airbus A320 family. If an airport is not located at sea level, the altitude difference (or density difference) must be taken into account and the speeds converted according to Chapter 2.1 and Chapter 2.2.

For verification, the diagrams from Figure 3.1 and Figure 3.2 were replicated using (3.1) to (3.3) (Figure 3.3):

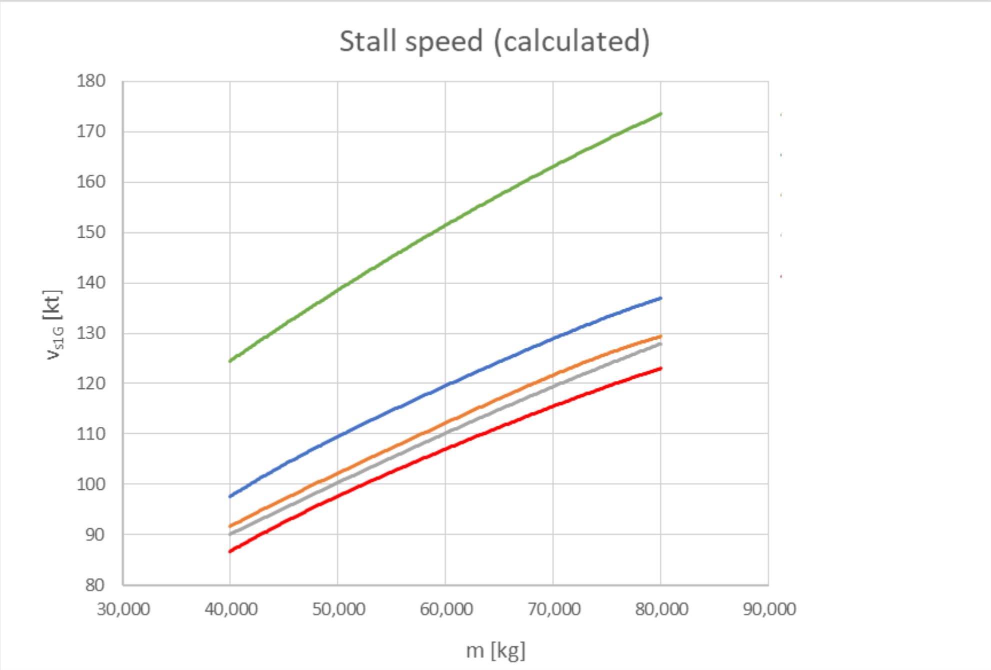

Figure 3.3 Stall speed check, vs1g, Airbus A320 (Excel)

The generic equations give the aimed result and can thus be transferred to MATLAB for the computation.

3.1.2 Airbus A340-300

The procedure for the Airbus A340-300 is analogous to that for the A320-200.

vs1g-Charts:

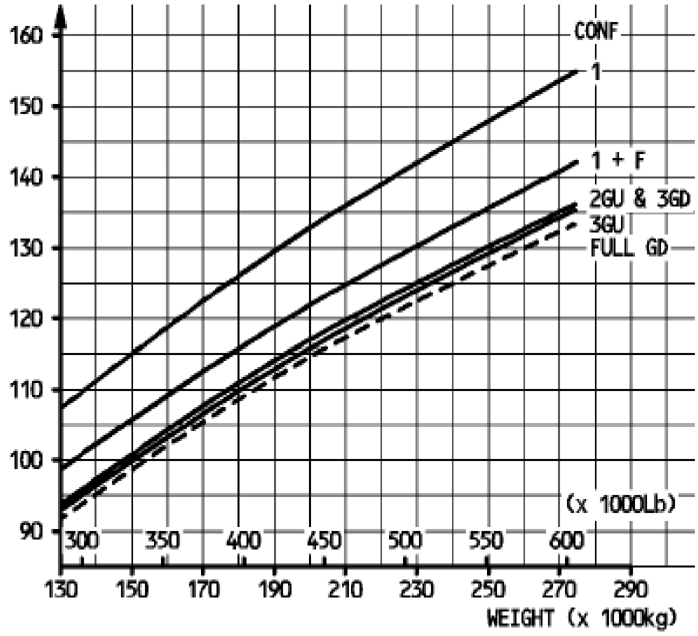

Figure 3.4 Stall speed vs1g, Airbus A340 (Airbus 2005b)

Table 3.2 vs1g, Airbus A340

m [t]	Conf 1+F	Conf 2	Conf 3
140	101.74	97.70	96.67
150	105.85	101.23	100.05
160	108.86	104.24	103.14
170	112.24	107.69	106.29
180	115.32	110.77	109.38
190	118.63	114.22	112.61
200	121.86	116.50	114.52
210	124.65	119.36	117.75
220	127.00	122.15	121.05
230	129.86	125.23	123.62
240	132.58	127.58	125.97
250	135.51	130.01	128.83
260	137.79	132.65	131.62
270	140.80	135.59	134.19

From Table 3.2, the diagrams in Figure 3.4 result Figure 3.5.

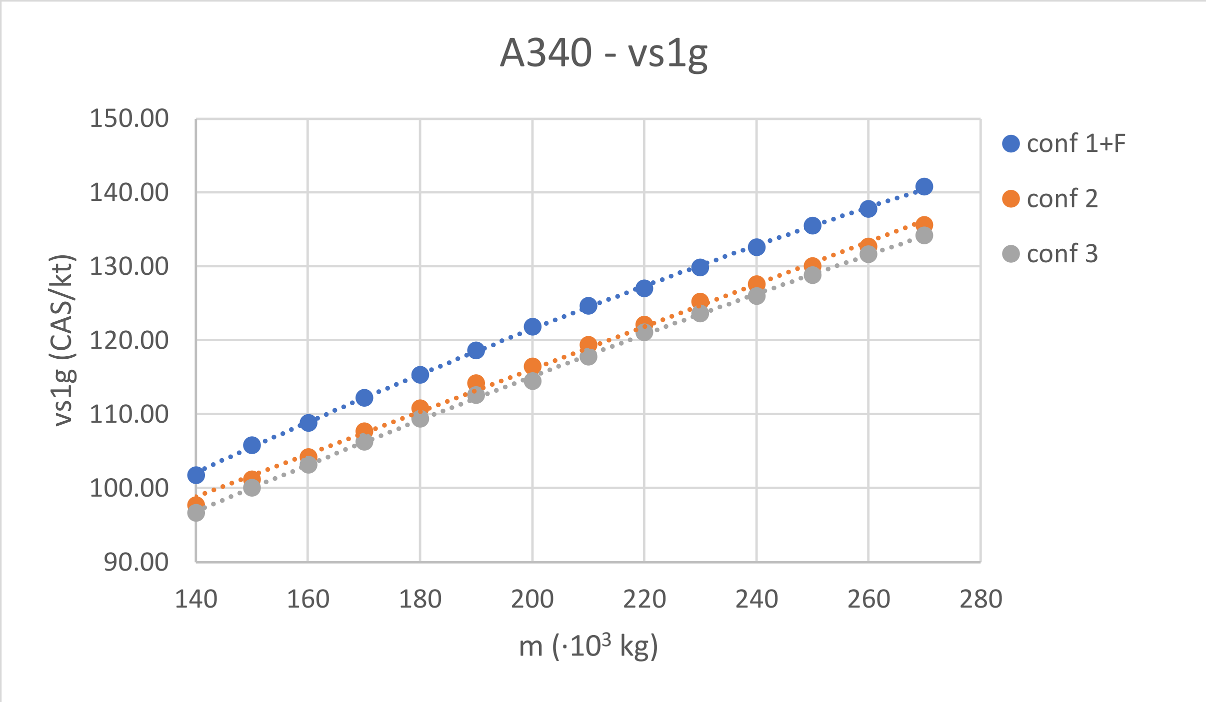

Figure 3.5 Stall speeds, vs1g-takeoff configurations, Airbus A340 (Excel)

The associated 2rd degree polynomials are summarized with (3.4) to (3.6):

Confi 1+F (Takeoff):

$$v_{s,1g} = -4.731 \cdot 10^{-10} \cdot m^2 + 4.8688 \cdot 10^{-4} \cdot m + 4.3125 \cdot 10^1 \tag{3.4}$$

Confi 2 (Takeoff):

$$v_{s,1g} = -4.3165 \cdot 10^{-10} \cdot m^2 + 4.6251 \cdot 10^{-4} \cdot m + 4.147 \cdot 10^1 \tag{3.5}$$

Confi 3 (Takeoff / Landing):

$$v_{s,1g} = -2.6552 \cdot 10^{-9} \cdot m^2 + 3.9489 \cdot 10^{-3} \cdot m + 4.6744 \cdot 10^1 \tag{3.6}$$

3.2 Safety Speed

The safety speed v_2 is derived based the requirements according to CS 25.107. It must be possible to reach v_2 at a (screen) height of 35 ft in the event of an engine failure.

=> $v_{2_{min}} \geq 1.2\ v_s$.

Assuming that $v_2 = v_{2_{min}}$, the safety speed v_2 is calculated with (3.7).

$$v_2 = 1.2\ v_s \tag{3.7}$$

where

$$v_s = 0.94 \cdot v_{s,1g} \tag{3.8}$$

and

$$v_2 = (0.94 \cdot 1.2)\ v_{s,1g} = 1.13\ v_{s,1g} \tag{3.9}$$

Without an engine failure, there is still sufficient excess thrust until 35 ft is reached and $v_{2_{min}}$ will be exceeded (see Figure 4.2). In order to distinguish v_2 (AEO) from v_2 (OEI). v_2 (AEO) is denoted by v_3.Estimate according to (Young 2018):

$$v_3 = v_{2,min} + 10\ kt \tag{3.10}$$

Approximation based on (Torenbeek 1982):

$$v_3 = 1.3\ v_{2,min} \tag{3.11}$$

For the calculations in this thesis, (3.10) is used according to (Young 2018).

3.3 Rotation Speed

Consequently, the speed at which the rotation starts (v_R) must be selected to satisfy the conditions according to (3.7) to (3.9) to achieve $v_{2,min}$ at an altitude of 35 ft. The recommendation of the Airworthiness Regulations is an average rotation rate of three degrees per second.

Rotation speed, acc. to Scholz 1999:

$$v_R \approx v_{2,min} - 3\ kt \tag{3.12}$$

3.4 Lift-Off Speed

In case of a failed engine (OEI condition), the excess thrust is significantly reduced (especially for jet with two engines, see Figure 4.2). v_2 is therefore only insignificantly greater than v_{LOF} . The conservative approach according to (3.13) therefore leads to deviations which can be neglected (Scholz 1999). Thus, $v_{2,min}$ would already be reached during lift-off and the requirement $v_{2_{min}} \geq 1.2\ v_s$ is safely satisfied.

$$v_{LOF,OEI} \approx v_{2,min} = v_2 \qquad (3.13)$$

$v_{LOF,OEI}$ lift-off speed (OEI case)

With all engines operative (AEO), there is still substantial excess thrust until lift-off, and both the lift-off speed $v_{LOF,AEO}$ and v_2 exceed $v_{2,min}$. It is assumed that approximately 50% of the discrepancy between v_3 and v_2 is achieved on the ground. In the AEO- case v_{LOF} is adjusted accordingly:

$$v_{LOF,AEO} = v_{2,min} + \left(v_3 - v_{2,min}\right) \cdot 0.5 \qquad (3.14)$$

Figure 4.2 display the effects of the engine failure on the most relevant forces and the airspeed. The significant increase in drag immediately after the failure due to the asymmetric thrust conditions can be noticed distinctly. It is also pointed out that a loss of 50% thrust $F(v)$, lead to significantly more than 50% loss of the thrust excess T_{excess}.

$v_{LOF,AEO}$ Lift-off speed, all engines operative case
$v_{LOF,OEI}$ Lift-off speed, one engine inoperative case

4 Regulations

4.1 Summary CS-25

CS 25.113 Takeoff distance and takeoff run

(a) Takeoff distance is the greater of -

(1) The horizontal distance along the takeoff path from the start of the takeoff to the point at which the aeroplane is 35 ft above the takeoff surface, determined under CS 25.111 [with a failed engine and v_2]
or

(2) 115% of the horizontal distance along the takeoff path, with all engines operating, from the start of the takeoff to the point at which the aeroplane is 35 ft above the takeoff surface, as determined by a procedure consistent with CS 25.111.

CS 25.111 Takeoff path

(a) ...

(2) The aeroplane must be accelerated on the ground to V_{EF}, at which point the critical engine must be made inoperative and remaining operative for the rest of the takeoff; and

(3) After reaching v_{EF}, the aeroplane must be accelerated to v_2.

(b) During the acceleration to speed v_2., the nose gear may be raised off the ground ... However, landing gear retraction may not be begun until the airplane is airborne.

(c) During the takeoff path determination in accordance with sub-paragraphs (a) and (b) of this paragraph -

(2) The aeroplane must reach v_2.before it is 35 ft above the takeoff surface

CS 25.109 Accelerate-Stop Distance (ASD)

(a) The accelerate-stop distance is ...

(2) The sum of the distances necessary to -

(i) Accelerate the aeroplane from a standing start to v_1 and continue the acceleration for 2.0 seconds after v_1 is reached with all engines operating; and

(ii) Come to a full stop from the point reached at the end of the acceleration period prescribed in sub-paragraph (a)(2)(i) of this paragraph, assuming that the pilot does not apply any means of retarding the aeroplane until that point is reached...

Further details concerning the ASD are described in Chapter 5.6.

The summary was edited based on (Scholz 2015)

CS 25.107 (takeoff speeds)

Requirement: $v_2 \geq 1.2\ v_s$

Changes made to the original approval requirements (Amendments) of particular relevance to this report are FAR 25 **Amendment 25-92** and **Amendment 25-42** (older version).

Amendment 25-92:
- The ASD is calculated based on the assumption that the A/C keeps a constant speed $v1$ during the 2 second delay (AFM buffer)
- Applicable to B737 - 600 /700 /800 /900, 757 - 300, 767 - 400, A321, A330 and **A340** types

Amendment 25-42:
- ASD is calculated based on the assumption that the airplane continues to accelerate
- Applicable to B777, **A320** and MD-11 according to Young 2018

4.2 Speed Limits

The takeoff speeds are defined in section CS-25.107. The essential correlations are illustrated with Figure 4.1.

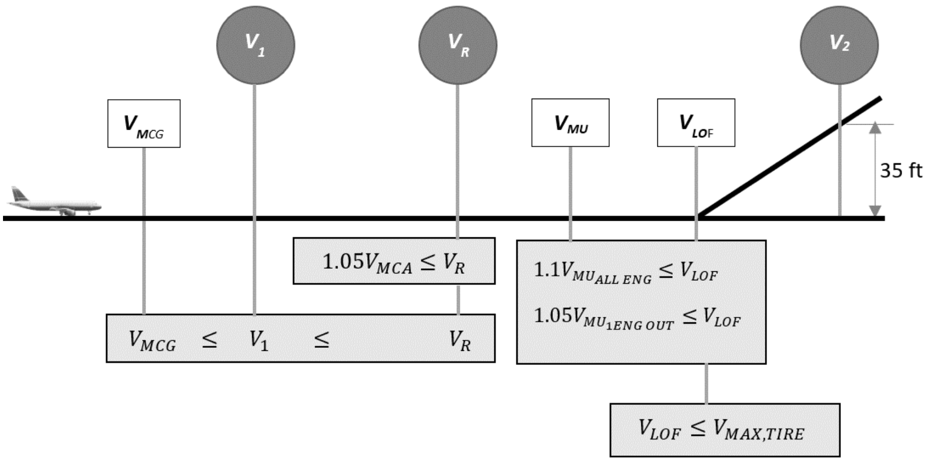

Figure 4.1 Speed Limits (based on Scholz 1998)

v_{MC}	Minimum Control Speed
v_{MCG}	Minimum Control Speed, Ground
v_{MCA}	Minimum Control Speed, Airborne
v_{MU}	Minimum Unstick Speed
v_{LOF}	Lift-off speed
v_R	Rotation speed
v_1	Decision speed
v_2	Safety speed

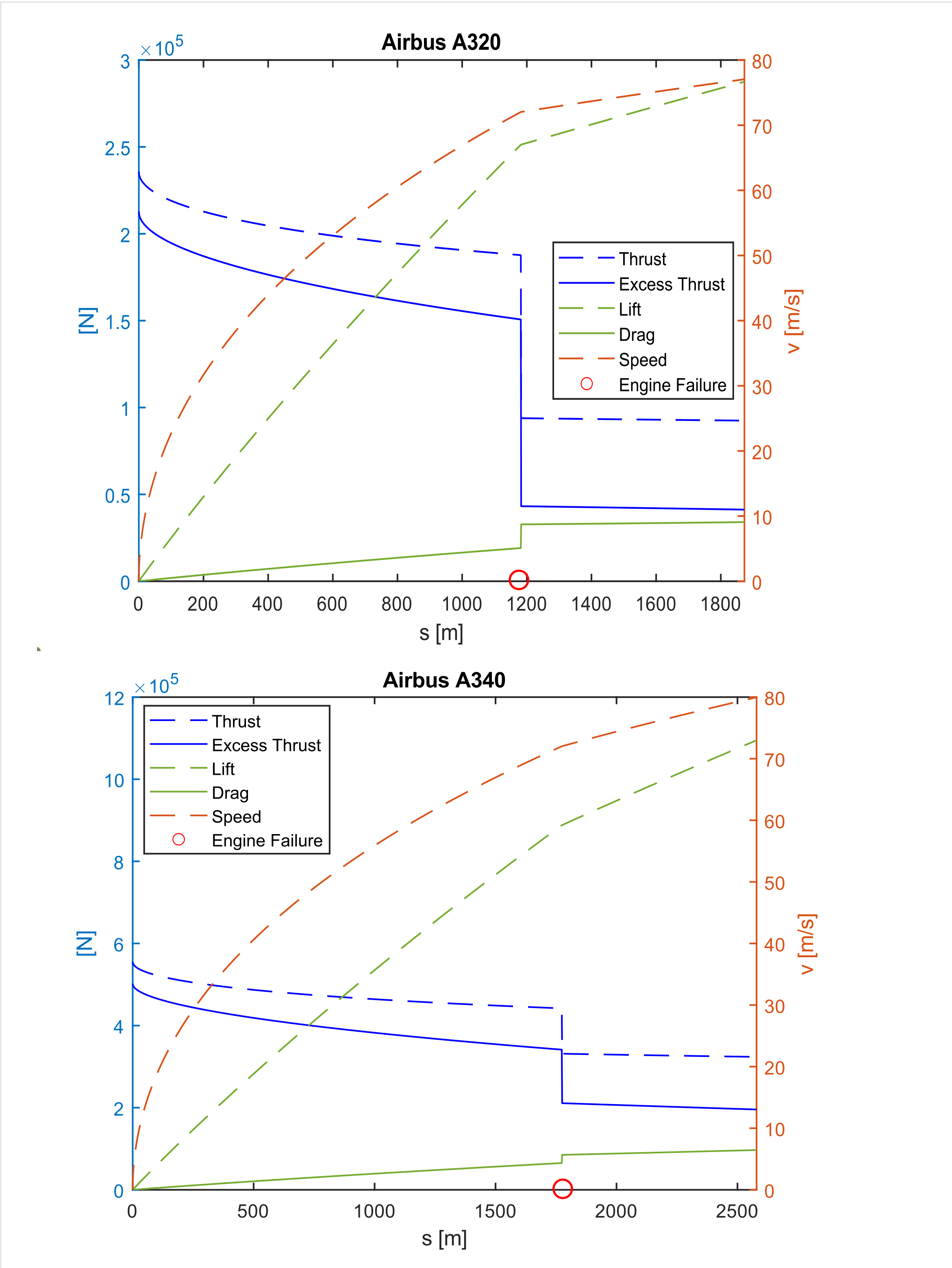

Figure 4.2 Engine Failure Effects with, $v_{EF} = 140$ knots

5 Performance

5.1 Distance Overview

This Chapter 5.1 gives an overview over the relevant distances. More detailed descriptions and derivations are provided in the following subchapters.

In all cases, a distinction is made between the All-Engines-Operative (Index: AEO) and the One-Engines-Inoperative case (Index: OEI). (5.1) to (5.7) are illustrated with Figure 1.1, Figure 1.2 and Figure 1.3.

Takeoff Distance (TOD, AEO):

$$s_{TOD,AEO} = s_{g,AEO} + s_{AIR,AEO} \tag{5.1}$$

The total ground roll distance consists of the distance $s_{g,AEO,1}$ until the rotation speed v_R is reached and the subsequent rotation distance $s_{R,AEO}$ ($= s_{g,AEO,2}$) up to the lift-off.

$$s_{g,AEO} = s_{g1,AEO} + s_{R,AEO} \tag{5.2}$$

Acceleration Go Distance (AGD**):** In the event of an engine failure, the ground roll distance is divided into 3 parts (See Table 5.1 regarding the scope):

- s_{gAEO} (ground roll with all engines operative),
- $s_{g,OEI,1}$ (ground roll with one engine inopeative) and
- $s_{R,OEI}$ (=$s_{g,OEI,2}$, rotation distance withe one engine inoperative)

The **Acceleration-Go Distance** (AGD) becomes:

$$s_{AGD} = s_{g,OEI} + s_{AIR} \tag{5.3}$$

with a total **ground roll distance**:

$$s_{g,OEI} = \left(s_{g,AEO} + s_{g1,OEI}\right) + s_{R,OEI} \tag{5.4}$$

Accelerate Stop Distance (ASD): In the Acceleration-Stop Distance, acceleration is performed to the engine failure speed v_{EF}, followed by 1 sec until recognition by the pilot. A safety margin of 2 seconds must also be considered, with either constant v_1 or acceleration with the remaining engines, depending on the aircraft type. This is being followed by deceleration to a standstill

$$s_{ASD} = s_{g,AEO} + s_{STOP} \tag{5.5}$$

Balance Field Length Condition (BFL): The balanced field length condition is described with (5.6). A detailed definition is given in Chapter 1.2. The solution algorithm is explained in Chapter 6.1.

$$s_{BFL}(v_{1,balanced}) = s_{ASD}(v_{1,balanced}) = s_{TOD}(v_{1,balanced}) \quad (5.6)$$

Factorized Takeoff Distance (TOD +15%): The factorized takeoff distance is based on the requirements. (See Chapter 4.1, CS 25.113 (a) (2))

$$s_{TOD1.15} = s_{TOD,AEO} \cdot 1.15 \quad (5.7)$$

Table 5.1 Distances, overview

	Sign	Scope
Ground Roll Distance (AEO)		
Part 1	$s_{g1,AEO}$	$0 \ldots v_R$
Rotation Distance (part 2)	$s_{R.AEO}$	$v_R \ldots v_{LOF}$
Total, AEO	$s_{g,AEO}$	$0 \ldots v_{LOF}$
Ground Roll Distance (OEI)		
Part 1 (all engines operative)	$s_{g,AEO}$	$0 \ldots v_{EF}$
Part 2 (one engine failed)	$s_{g,OEI,1}$	$v_{EF} \ldots v_R$
Rotation Distance (part 3)	$s_{R,OEI}$	$v_R \ldots v_{LOF}$
Total, OEI	$s_{g,OEI}$	$0 \ldots v_{LOF}$
Air Distance	s_{AIR}	$v_{LOF} \ldots v_2$
Takeoff Distance (AEO)	$s_{TOD,AEO}$	$0 \ldots v_3$
Takeoff Distance (OEI)	$s_{TOD,OEI}$	$0 \ldots v_2$
Factorized Takeoff Distance	$s_{TOD,1.15}$	$s_{TOD,AEO} + 15\%$
Stop Distance (numerically)	s_{STOP}	$v_{EF} \ldots 0$
Acceleration Stop Distance	s_{ASD}	$0 \ldots v_{EF} \ldots 0$
Balanced Field Length	s_{BFL}	
All Engines Operative	AEO	
One Engine Inoperative	OEI	

5.2 Ground Roll Distance

5.2.1 Derivation of the Analytical Equation

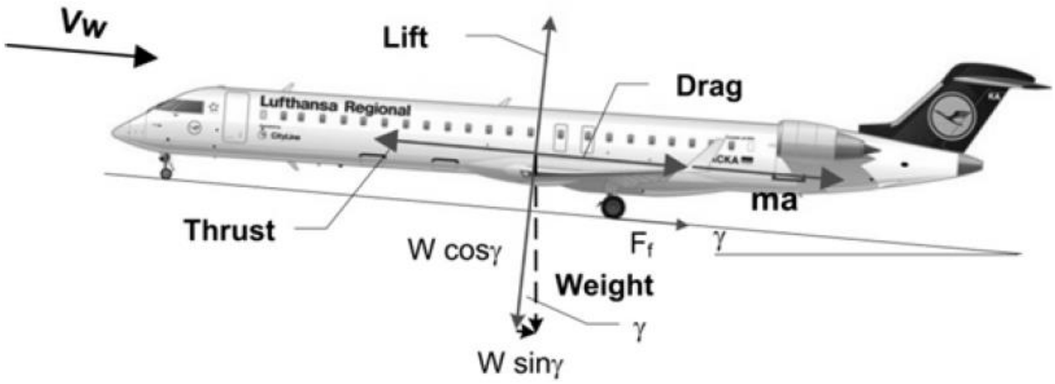

Figure 5.1 Force diagram (Scheiderer 2008)

Sum of forces in x-direction $\sum F_x$:

$$m\,a = T - D - F_f - W\,sin\,\gamma \tag{5.8}$$

Sum of forces in y-direction $\sum F_y$:

$$W\,cos\,\gamma - L - N = 0 \tag{5.9}$$

Weight force W:

$$W = mg \tag{5.10}$$

Friction force F_f:

$$F_f = \mu \cdot N = \mu \cdot (mg \cdot cos\,\gamma - L) \tag{5.11}$$

Rolling friction coefficients μ for the calculation according to (5.11), are summarized in Table 5.2. In the context of this thesis, only dry conditions are examined and a value of 0.02 is fixed for most calculations.

Table 5.2 Friction coefficients (Scholz 2015)

Surface	[KOHLMAN 92]	[TORENBEEK 1982]
Concrete or asphalt, dry or wet	0.02 bis 0.05	0.02
Solid snow	0.02	-
Ice	0.02	-
Gravel	-	0.04
Dry short grass, firm ground	0.05	0.05
Dry long grass, firm ground	0.10	0.10
Soft ground	0.10 bis 0.30	0.10 bis 0.30

Acceleration a (Separation of the variables**):**

$$a = \frac{dv}{dt} = \frac{dv}{dt} \cdot \frac{dx}{dx} = v \cdot \frac{dv}{dx} \tag{5.12}$$

From (5.8) to (5.12) results the "**basic equation**":

$$\int_{x1}^{x2} dx = \int_{v1}^{v2} \frac{m \cdot v}{T - D - F_f - W \cdot sin\,\gamma} dv \tag{5.13}$$

(5.14) gives the basic equation for the ground roll distance

$$s_g \;= \int_{v_A}^{v_B} \frac{m \cdot v}{T - D - \mu \cdot (mg - L) - mg \cdot sin\,\gamma}\, dv \tag{5.14}$$

γ	Slope, flight path angle	[%], [°]
L	Lift	[N]
D	Drag	""
N	Normal force	""

The integration limits are differentiated based on the case (AEO or OEI).

With all engines operative **AEO:**
- $v_A = 0$
- $v_B = v_{\mathrm{R}}$

If an engine has failed, the ground roll distance is further divided into a distance up to the engine failure and the remaining distance up to the initiation of rotation. The rotation distance s_R (see Chapter 5.3) is considered separately. However, by definition, the rotation distance belongs to the ground roll distance.

Integration limits part 1 (AEO):
- $v_A = 0$
- $v_B = v_{\mathrm{E}}$

Integration limits part 2 (OEI):
- $v_A = v_{\mathrm{E}}$
- $v_B = v_{\mathrm{R}}$

With the **excess thrust** T_{excess}

$$T_{excess} = T - D - F_f - mg \cdot sin\,\gamma \;\;, \tag{5.15}$$

the **lift L**

$$L = L(v) = \frac{\rho}{2} v^2 \, C_{L,g} \, S_W \,, \tag{5.16}$$

as well as the **drag D**

$$D = D(v) = \frac{\rho}{2} \, v^2 \, C_{D,G} \, S_W \,. \tag{5.17}$$

In the following Subchapters 5.2.2 to 5.2.4, three different solution approaches for the integration of the basic equation are presented:

1. integration of the basic equation by means of an average thrust:$T = T(v_{av}) = const.$,
2. integration of the basic equation by means of an speed dependent thrust: $T = T(v)$ and
3. Numerical integration considering a speed dependent thrust $T = T(v) \neq const.$.

The most common method is to calculate an average speed based on the mean dynamic pressure, since L, D and T are a function of the dynamic pressure q.

Mean dynamic pressure q_{av} considering the wind speed

$$q_{av} = \frac{\rho}{2} v_{av}^2 = \frac{1}{2}\left(q + q_{v_w}\right) \tag{5.18}$$

$$\frac{\rho}{2} v_{av}^2 = \frac{1}{2}\left(\frac{1}{2} \, \rho \, v_w^2 + \frac{1}{2} \rho \, v^2 \right) \tag{5.19}$$

$$v_{av}^2 = \frac{1}{2}\left(\, v_w^2 + \, v^2 \, \right) \tag{5.20}$$

$$q_{av} = \frac{1}{2} \cdot \frac{\rho}{2} v^2 \left(1 + \left(\frac{v_W}{v}\right)^2\right) \tag{5.21}$$

The approach $q_{av} = (\rho/2) \, v_{av}^2$ gives the average inflow velocity v_{av}:

$$\frac{v_{av}}{v} = \sqrt{\frac{1}{2}\left(1 + \left(\frac{v_W}{v}\right)^2\right)} \tag{5.22}$$

Without wind, the outcome would be (5.23):

$$\bar{v} = 0.707 \cdot v_{LOF} \tag{5.23}$$

AEO-Case (0 ... v_R):

$$\frac{v_{av}}{v_R} = \sqrt{\frac{1}{2}\left(1 + \left(\frac{v_W}{v_R}\right)^2\right)} \tag{5.24}$$

Average thrust (constant) T_{av}:

$$T_{av} = T_0[A - K_1 M_{av} + K_2\, M_{av}^2] \tag{5.25}$$

Thrust factors k_1, k_2, A based on Chapter 2.8.

$$T_{excess} = T_{av} - D(v) - F_f(v) - mg\ sin\gamma \tag{5.26}$$

$$mg = L = \frac{1}{2} \cdot C_{L,max,To} \cdot \rho \cdot S_w \cdot v_{s1g}^2 \tag{5.27}$$

With an appropriate average thrust, (5.14) can hence forth be solved analytically using an integral table.

5.2.2 Analytical with Average Thrust and variable Drag and Lift

Assumptions:

- $T_{excess} \neq constant$
  - $D = D(v)$
  - $L = L(v)$
- $T = T_{av} = const.$

The drag D and the lift L according to (5.16) and (5.17) are proportional to v^2 with regard the basic equation from (5.14). With an average thrust according to (5.25) an the given assumptions, (5.28) is obtained:

$$s_g = m \int_{v_A}^{v_B} \frac{v}{T_{av} - \frac{\rho}{2} v^2 \, C_{D,g} \, S_w - \mu \cdot mg - \mu \frac{\rho}{2} \, v^2 \, C_{L,g} \, S_w - mg \, sin\gamma} dv \tag{5.28}$$

By bracketing out and reshaping, the **wing loading** m/S_w and **thrust to weight ratio** $T \,/\, (mg)$ can be used in (5.29):

$$s_g = \frac{1}{g} \int_{v_A}^{v_B} \frac{v}{\frac{T_{av}}{mg} - \frac{\rho}{2g} v^2 \, C_{D,g} \frac{S_w}{m} - \mu - \mu \frac{\rho}{2g} v^2 \, C_{L,g} \frac{S_w}{m} - \sin\gamma} dv \tag{5.29}$$

To obtain an integral form that can be solved with common integral tables, variable v is separated accordingly.

$$s_g = \frac{1}{g} \int_{v_A}^{v_B} \frac{v}{\frac{T_{av}}{mg} - \mu - \sin\gamma - \frac{\rho}{2g} \frac{S_w}{m} \, v^2 \left(C_{D,G} - \mu C_{L,g}\right) v^2} dv \tag{5.30}$$

$$s_g = \frac{1}{\frac{\rho}{2} \frac{S}{m} \left(C_{D,G} - \mu \, C_L\right)} \int_{v_A}^{v_B} \frac{v}{\frac{\frac{T_{av}}{mg} - \mu - \sin\gamma}{\frac{\rho}{2g} \cdot \frac{S_w}{m} \left(C_{D,G} - \mu \, C_{L,G}\right)} - v^2} dv \tag{5.31}$$

$$s_g = \frac{2(m/S_w)}{\rho\left(C_{D,G} - \mu \, C_{L,G}\right)} \cdot \int_{v_A}^{v_B} \frac{v}{\frac{2g(m/S_w)\left(\frac{T_{av}}{mg} - \mu - \sin\gamma\right)}{\frac{\rho}{2}\left(C_{D,G} - \mu \, C_{L,G}\right)} - v^2} dv \tag{5.32}$$

The result is an integral of the form:

$$F(v) = 2b \int \frac{v}{a^2 - v^2} dv \tag{5.33}$$

An integral of the form according to (5.33) can be solved with an integral table. According to (Merziger 2010):

$$\int \frac{x}{a^2 - x^2} dx = -\frac{1}{2} \cdot ln(a^2 - x^2) \tag{5.34}$$

Transferred to (5.33) follows:

$$2b \int \frac{v}{a^2 - v^2} dv = -b \; ln \; (a^2 - v^2) \tag{5.35}$$

To eliminate the negative sign:

$$2b \int_0^v \left(\frac{v}{a^2 - v^2}\right) dv = b \cdot ln \left(\frac{1}{1 - \frac{v^2}{a^2}} \right) \tag{5.36}$$

If the terms substituted with a and b according to (5.37) as well as (5.38) are inserted into (5.36), the searched ground roll distance s_g follows with (5.39).

$$b = \frac{(m/S)}{\rho\left(C_D - \mu \, C_{L,G}\right)} \tag{5.37}$$

$$a^2 = \frac{2g(m/S)\left(\frac{T_{av}}{mg} - \mu - sin \, \gamma\right)}{\frac{\rho}{2}\left(C_{D,G} - \mu \, C_{L,G}\right)} \tag{5.38}$$

Ground roll distance $\boldsymbol{s_g}$ with the integration limits $\boldsymbol{v_A}$ & $\boldsymbol{v_B}$

$$s_g = \frac{2(m/S_W)}{\rho(C_{D,g} - \mu C_{L,g}} \; ln \left. \left(\frac{1}{1 - \frac{\frac{\rho}{2}\left(C_{D,g} - \mu \, C_{L,g}\right) v^2}{g\left(\frac{m}{S_W}\right)\left(\frac{T_{av}}{mg} - \mu - sin \, \gamma\right)}} \right) \right|_{v_A}^{v_B} \tag{5.39}$$

Chapter 5.2.2 is the result of (Scholz 1998).

5.2.3 Analytical with Depending Forces

In order to optimize the accuracy of the calculation the thrust is now to be included in (5.50) as a function of the speed as well.

$$s_g = \int_{v_A}^{v_B} \frac{m \cdot v}{T(v) - D(v) - \mu \cdot [mg - L(v)] - mg \cdot sin\,\gamma}\, dv \tag{5.40}$$

With respect to the thrust model from (2.97):

$$\int_{v_A}^{v_B} \frac{v\, dv}{N \cdot T_0[A - K_1 v + K_2 v^2] - \frac{\rho}{2}\, C_{D,g}\, S_w\, v^2 - mg\,(\mu + sin\,\gamma) + \mu \frac{\rho}{2}\, C_{L,g}\, S_w\, v^2} \tag{5.41}$$

Transformation results in:

$$\int_{v_A}^{v_B} \frac{v\, dv}{\left[N\, T_0\, K_2 - \frac{\rho}{2} C_{D,g}\, S_w + \mu \frac{\rho}{2}\, C_{L,g}\, S_w\right]\, v^2 - [\,N\, T_0\, K_1]v + [\,N\, T_0\, A - mg\,(\mu + sin\,\gamma)]} \tag{5.42}$$

With k_1, k_2 form (2.101) and (2.102) and speed of sound c_{sd}:

$$\int_{v_A}^{v_B} \frac{v\, dv}{\left[N\, T_0 \frac{k_2}{c_{sd}^2} - \frac{\rho}{2} C_{D,g}\, S_w + \mu \frac{\rho}{2}\, C_{L,g}\, S_w\right]\, v^2 - \left[N\, T_0\, \frac{k_1}{c_{sd}}\right] v + [\,N\, T_0\, A - mg\,(\mu + sin\,\gamma)]} \tag{5.43}$$

This gives an integral of the form:

$$\int \frac{x\, dx}{a\, x^2 + b\, x + c}. \tag{5.44}$$

With:

$x = v$

$a\, x^2 = [N\, T_0\, K_2 - (\rho/2)\, C_{D,g}\, S_w + \mu\, (\rho/2)\; C_{L,g}\, S_w\,]\; v^2$

$b\, x = -[\,N \cdot\, T_0\, K_1]\, v,$

$c = [\,N \cdot\, T_0\, A - \mu \cdot mg\,(\mu + \sin\gamma)].$

Integral limits:

$v_B = \mathrm{v_R},$

$v_A = 0.$

If the rotation distance isn't solved separately.

Integral is be solved analytical by Papula 2015 complemented by Goudreault 2013:

$$\Delta = 4\,ac - b^2 \tag{5.45}$$

$\Delta > 0$:

$$\int \frac{x\,dx}{a\,x^2 + b\,x + c} = \frac{1}{2a} ln\,\left|ax^2 + bx + c\right| - \frac{b}{2a} \cdot \frac{2}{\sqrt{\Delta}} \cdot atan\left(\frac{2ax + b}{\sqrt{\Delta}}\right) \tag{5.46}$$

$\Delta < 0$:

$$\int \frac{x\,dx}{a\,x^2 + b\,x + c} = \frac{1}{2a} ln\,\left|ax^2 + bx + c\right| - \frac{b}{2a} \cdot \frac{1}{\sqrt{|\Delta|}} ln \left|\frac{2ax + b - \sqrt{|\Delta|}}{2ax + b + \sqrt{|\Delta|}}\right| \tag{5.47}$$

$\Delta = 0$:

$$\int \frac{x\,dx}{a\,x^2 + b\,x + c} = \frac{1}{2a} ln\left|ax^2 + bx + c\right| - \frac{b}{2a} \cdot \frac{2}{2ax + b} \tag{5.48}$$

This offers a method to analytically solve the ground roll distance with drag, lift AND thrust as a function of velocity. By applying Young's thrust model, the height difference could also be taken into account in addition to the piston slope.

While in Chapter 5.2.2 the ground roll distance was still reduced (simplified) to an integral of the form $x/(ax^2 + c)$, in Chapter 5.2.3 an (integral of the type $x/(ax^2 + bx + c)$ is solved and thus has generally more valid character

The concept and the proposed solution with the help of the thrust model was found at the end of the thesis, when all numerical solutions had already been completed. The same approach can also be applied to the stop distance. With this approach, there is now a method to completely eliminate the need for numerical solution methods without sacrificing accuracy. The found approach will be part of a new project or thesis at the HAW Hamburg under the supervision of Professor Scholz.

The numerical results from Chapter 9 can be understood as an analytical result, where the ground roll distance and stop distance were calculated using the method derived in this chapter. The results are identical.

5.2.4 Numerical Integration

The next accuracy level for the solution of an ordinary DGL of 1st order is achieved with the simple Euler method, a one-step numerical integration method. A more accurate solution (when using the same step size) is provided by the Runge-Kutta method (4th order). Both methods were compared in the context of ground roll distance. It was found that the same accuracy can be achieved with the Euler method, provided that the time interval is reduced. From a time interval of $\Delta t = 0.1$, the deviations are less than 0.1%. Therefore, the one-step Euler method was used to verify the numerical results from MATLAB. Moreover, most of the plots were created based on the Euler method.

As a measure for the "correct" results, the outputs from MATLAB via "ode45 function" a solver for solving ordinary differential equations with automatic step size adjustment are used. A redundant numerical analysis of the ground and stop distances is intended to secure the results against each other, since otherwise errors can easily occur unnoticed in complex loops.

Remark: The accuracy of the integration procedures can be controlled (optimized) by the adjustment (reduction) of the step size. To approach the accuracy of the Runge-Kutta method with the Euler method, a smaller step size would have to be selected. Smaller step sizes require more computing time. Regarding the task of this thesis, the computing time is not a relevant factor. With a laptop of medium computing power, computation times of a maximum of 10 seconds are generated within the scope of the task.

Assumptions:
$T_{excess} \neq constant$
$T = T(v)$, respectively. $T = T(M)$
$D = D(v)$
$L = L(v)$

An initial value problem has to be solved:

$$a_n(v) = \frac{dv_g}{dt} = \frac{d^2 s_g}{dt^2} = \frac{1}{m}\left[T(v) - D(v) - F_f(v)\right] - g \cdot sin\,\gamma \tag{5.49}$$

Thereby the differential equation has the form:

$$\frac{d^2 s}{dt^2} = \frac{dv_g}{dt} = f(t, v_g) \tag{5.50}$$

Numerical Integration with MATLAB

MATLAB offers several functions based on the Runge-Kutta method. Corresponding functions all start with "ode" as an acronym for ordinary differential equation. The differential equation to be solved can be solved with the solver **ode23** or **ode45.** Solutions are calculated step by step, using the solution of the previous point for the solution of each point. The step size of the single steps takes a prominent role for the accuracy of the result. With the solver ode23 a 2nd and 3rd order method is used for each point, while with ode45 4th and 5th order methods are applied. If the results differ too far from each other, this would be an indication that the step size became too large. If this is the case, MATLAB will automatically adjust the step size in the next step.

Ode45 solves 1st order DGL. The basic equation, i.e., the acceleration a corresponds to the 2nd time derivative of the distance s. With reference to the distance, this results in a 2nd order DGL. For the solution, the DGL is transformed into a system of 1st order ODE functions.

General form of the ode function in MATLAB:

$$\dot{x} = f(t, x) \tag{5.51}$$

In the context of the task, live scripts are used in MATLAB for the main program, via which the parameters are defined by means of input fields and can be modified if necessary. First, an equation is defined in an m-file, which can be accessed in the main program (*mlx-file). Thereby the function in the m-file has the following structure according to (5.51): transferred.

function $\dot{x} = Functionname(t, x)$

With: t => Independent variable,
x => Dependent variable.

The function name can be chosen arbitrarily if the characters are chosen according to the rules. In MATLAB, there is no superscript in the code. In the original, x˙ would be substituted by, for example, "xdot":

function $xdot = Funktionsname(t, x)$

A first order DGL with x as the dependent variable and t as the independent variable must be passed. The acceleration $\ddot{s}$ with reference to the distance s is a 2nd order DGL with the speed $\dot{s}$. In order to use the ode function according to the problem definition, a two-column matrix S is passed instead of a single variable s:

$$S(1,1) = s_1 \tag{5.52}$$

$$S(1,2) = s_2 \tag{5.53}$$

This yields in:

$$\text{function } \dot{S} = Functionname(t,X)$$

respectively:

$$\text{function } Sdot = Functionname(t,X)$$

with:

- $\dot{S}(1,1) = v$
- $\dot{S}(1,2) = a$

If corresponding correlations are transferred to MATLAB, the following exemplary extract from the m-file for the calculation of the takeoff distance results:

```
function Sdot=Functionname(t,S)

s=S(1);
v=S(2);

vG = v + vW;
L   = rho/2*(v)^2*CLg*Sw;
D   = rho/2*(v)^2*CDg*Sw;
Ff  = mu*(m*g*cos(gammaRad)-L);

Sdot(1,1)=vG;
Sdot(2,1)=1/m*(T-D-Ff)-g*sin(gammaRad);
```

Note: The original code is considerably more extensive. This is a (short) extract.

Table 5.3 Parameter - MATLAB (m-file, ground roll distance)

Sign	**Definition**	**Unit**
Sdot	Result - Matrix $Sdot(n,m)$	
L	Lift	[N]
D	Drag	[N]
Ff	Friction force	[N]
rho	Density ρ	$[kg/m^3]$
CL	Lift coefficient, ground $C_{L,g}$	$[-]$
CD	Drag coefficient, ground $C_{D,G}$	$[-]$
Sw	Wind surface area S_w	$[-]$
T	Thrust	[N]
mu	Friction coefficient μ	$[-]$
m	A/C Weight	[kg]
g	Earth acceleration	$[m/s^2]$
gammaRad	Flight path angle γ_{rad}	[rad]

Table 5.3 gives an overview over the matrices and variable uses in MATLAB-Code

$C_{L,G}$, $C_{D,G}$, γ_{rad} are calculated by the m-file. The input parameters ρ, S_W, μ, m, g, γ are entered via live script. The output matrix Sdot is an n x 2 - matix (two-column matrix). The number of rows n depends on the size of the interval and the chosen (time) step size Δt.

The ode function "ode45" is used. The following excerpt from the MATLAB script shows the main function for solving the DGL:

```
options = odeset('NonNegative',1,"MaxStep",0.1);
[t,Sdot]=ode45(@Functionname,[tmin:dt:tmax],[s0,v0],options);
```

Parameter are defined in Table 5.4.

Table 5.4 Parameter-descriptions (MATLAB-script, ground roll distance)

Variable	Definition	Unit
t	Time-Vector (n rows)	[s]
tmin	Lower limit for time t	[s]
dt	Time interval	[s]
tmax	Upper limit for time t	[s]
s0	Initial value, distance at t_{min}	[m]
v0	Initial value, speed at t_{min}	[m/s]
options	Additional restrictions (ode-options)	
Sdot	Output-Matrix $Sdot(n, m)$	[m], [m/s]
Sdot(n,1)	Distance s	[m]
Sdot(n,2)	Speed v	[m/s]

In the context of this thesis, SI metric units will be used throughout. For alternative unit systems, the defined universal constants would have to be adapted in the MATLAB script and the input parameters would then have to be specified in accordance with the units.

Figure 5.2 and Figure 5.3 show a typical curve for the ground roll distance as a function of time and speed (for an Airbus A320, based on parameters in Chapter 8, with $H = 0$, confi $1 + F$, $slope = 0$). The rotation speed v_R is marked accordingly.

Note: The rotation distance is part of the ground distance. The rotation distance s_R is calculated according to (5.54). In the case of the Airbus A320 described above, $s_R = 298.32$ m and $s_{g,total} = 1612.61$ m.

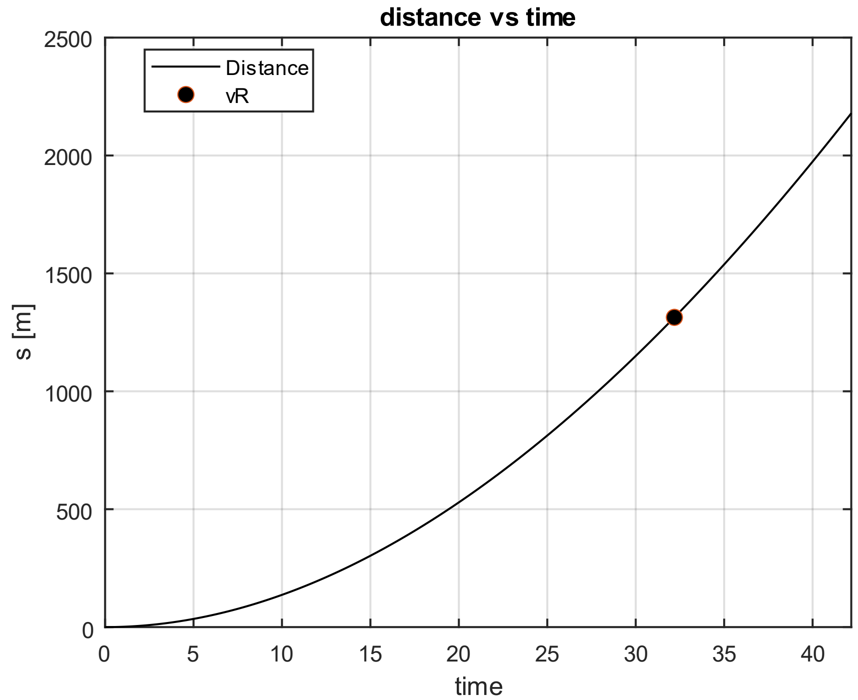

Figure 5.2 Ground roll distance (A320): MATLAB diagram (distance vs. time)

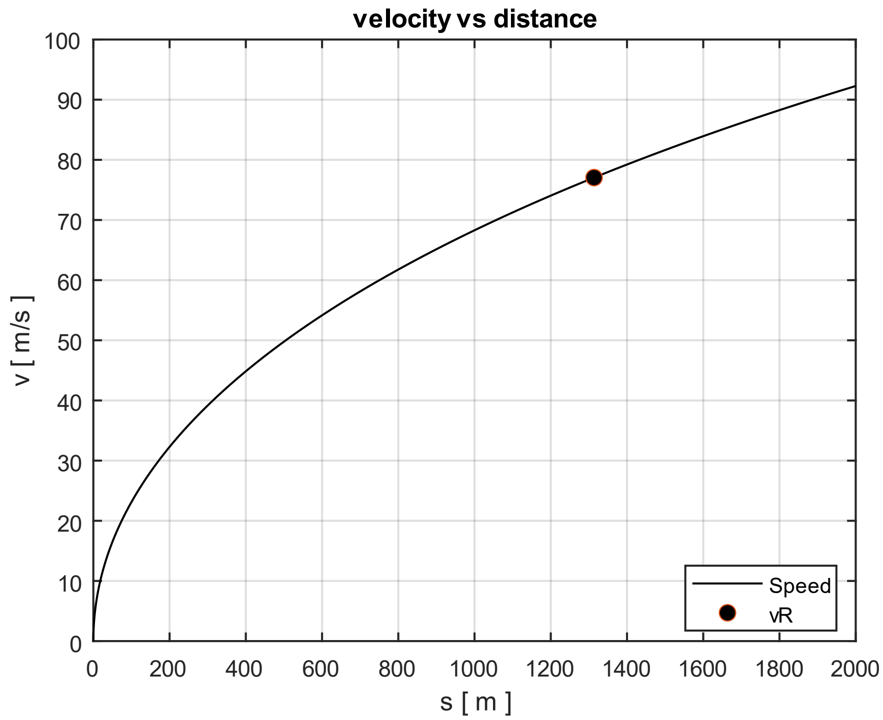

Figure 5.3 Ground roll distance (A320, 78 t, 117.9 kN)

The ode45 function from MATLAB gives a ground roll distance 1314.29 m ($v_0 \ldots v_R$). A numerical solution in Excel based on the Euler method according to Figure 5.4 achieves the result 1313.86 m with $\Delta t = 0.01$ (a discrepancy of 0.03%).

		t_n [s]	$v_{G,n}$ [m/s]	T_n [N]	D_n [N]	Ln [N]	$F_{f,n}$ [N]	a_n [m/s²]	s_n [m]
Equation		(3.25)	(3.26)	(2.3)	(2.26)	(2.25)	(2.18)	(3.23)	(3.28)
Initial-Condition		0	0	235,800	0	0	0	2.827	**0**
Initial-Condition	Δt	0.01	0	235,779	0	0	15,298	2.827	0.00
1	Δt	0.02	0.06	235,757	0.01	0.16	15,298	2.826	0.00
2	Δt	0.03	0.08	235,736	0.03	0.36	15,298	2.826	0.00
3	Δt	0.04	0.11	235,714	0.05	0.63	15,298	2.826	0.00
4	Δt	0.05	0.14	235,693	0.07	0.99	15,298	2.826	0.00
5	Δt	0.06	0.17	235,672	0.11	1.43	15,298	2.825	0.01
6	Δt	...	...	...	...	...	...	...	...
...	Δt	32.18	77.04	*185,891*	*22,232*	*294,836*	*9,402*	*1.978*	**1313.53**
3219	Δt	*32.19*	*77.06*	*185,880*	*22,243*	*294,988*	*9,399*	*1.977*	***1314.30***
		t_R 32.18	v_R 77.0499						s_R **1313.86**

Figure 5.4 Ground roll distance (A320): Euler method (Excel), $\Delta t = 0.01$

		t_n [s]	$v_{G,n}$ [m/s]	T_n [N]	D_n [N]	Ln [N]	$F_{f,n}$ [N]	a_n [m/s²]	s_n [m]
Equation		(3.25)	(3.26)	(2.3)	(2.26)	(2.25)	(2.18)	(3.23)	(3.28)
Initial-Condition		0	0	235,800	0	0	0	2.827	**0**
Initial-Condition	Δt	0.1	0	235,586	0	4	15,298	2.824	0.03
1	Δt	0.2	0.57	235,373	1.20	15.86	15,298	2.821	0.08
2	Δt	0.3	0.85	235,160	2.69	35.66	15,298	2.819	0.17
3	Δt	0.4	1.13	234,947	4.78	63.33	15,297	2.816	0.28
4	Δt	0.5	1.41	234,735	7.45	98.86	15,296	2.813	0.42
5	Δt	0.6	1.69	234,523	10.72	142.22	15,296	2.810	0.59
6	Δt	...	...	...	...	...	...	...	...
...	Δt	32.10	76.91	*185,959*	*22,159*	*293,869*	*9,421*	*1.979*	**1311.39**
322	Δt	*32.2*	*77.11*	*185,853*	*22,273*	*295,383*	*9,391*	*1.977*	***1319.10***
		t_R 32.17	v_R 77.0499						s_R **1316.65**

Figure 5.5 Ground roll distance (A320): Euler method (Excel), $\Delta t = 0.1$

By increasing Δt *to* 0.1 (Figure 5.5) the Euler method generates a ground roll distance of 1316.65 m (a discrepancy of 0.18%). With $\Delta t = 1$ the deviation would rise to 2.29% (1344.45 m).

5.3 Rotation Distance

According to Nicolai 2010 or Young 2018, (5.54) achieves sufficient accuracy for the rotational distance:

$$s_R \approx t_R \cdot \frac{v_R + v_{LOF}}{2} \tag{5.54}$$

The time for the rotation t_R, i.e., from the first actuation of the stick until it is lifted off, results from 2 parts:

1.) Time until constant rotation speed is reached $0 \geq t \geq t_1$
2.) Time with constant rotation speed until lift-off $t_1 > t \geq t_R$

The rotation time t_R is highly dependent on the pilot's skills. There are recommendations from Airbus for the Standard Operation Procedures (SOP) as to which (constant) rotation speed ω should be aimed for. A rotation speed of 3 °/s is recommended. For the Airbus 340, studies showed that the average rotation time is considerably longer (see Balzer 2021), which has a significant impact on performance. A reduction of 1 °/s results in an increase of the takeoff distance of up to 300 m for an Airbus A340-300. The rotation speed is adjusted to 2.5 °/s (A340) with respect to the performance calculations. This shall ensure that the speed when reaching the target angle is sufficient to be able to take off. Otherwise (if the rotation is too fast), the pilot might continue to rotate and exceed the maximum allowable pitch attitude (until the tail strikes the ground). In the OEI case, it is (generally) recommended that the rotation speed be reduced another 0.5 °/s to ensure that v_{2min} can be achieved in 35 ft, since only very little excess thrust remains after takeoff in the OEI case (see Figure 4.2). On short runways, however, a too slow rotation speed would additionally be problematic, since the pilot would run the risk of missing the end of the runway

It usually takes about one second for the pilot to reach the corresponding (constant) angular speed with careful (gentle) acceleration after pulling the stick. To estimate a plausible value for the total time for rotation according to the recommendations of Airbus, a constant angular acceleration is assumed until ω_1 is reached. Furthermore, it is assumed that the pilot reaches constant angular speed after one second. The (Airbus) pilot usually rotates to a target pitch attitude between 12.5° and 15° (in the air), whereby the target pitch attitude does not correspond to the lift-off angle α_{LOF}. For the Airbus A320 (or Airbus A340), the lift-off angle α_{LOF}, i.e., the angle at which the aircraft takes off, is typically 10° (Balzer 2021). To estimate t_R, α_{LOF} =10° is applied. The described relationships are visualized with Figure 5.6.

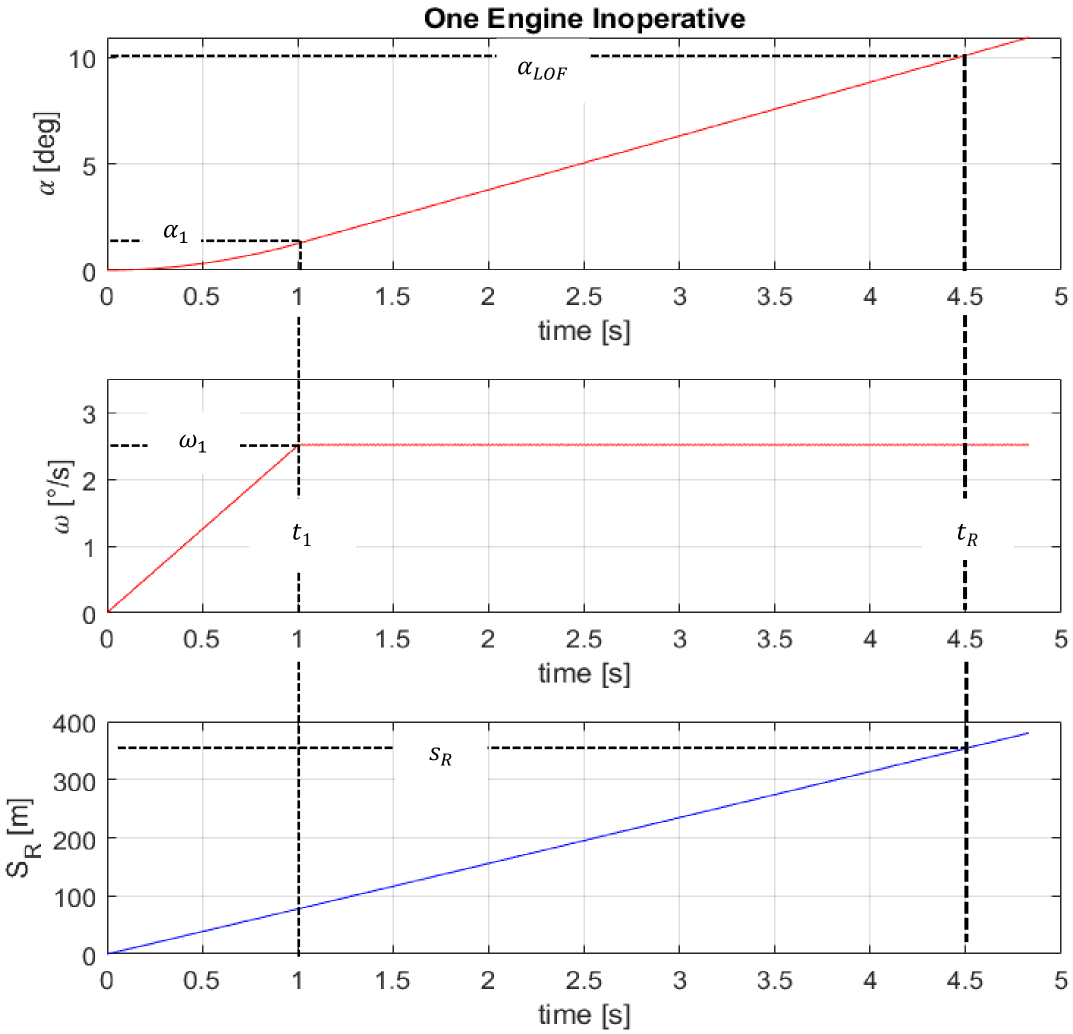

Figure 5.6 Rotation-Plots, A320 (OEI)

(5.55) to (5.68) describe the general relationships of angular acceleration $\dot{\omega}$, angular velocity ω, Angle of Attack α and time t:

$$\omega = \dot{\alpha} = \frac{d\alpha}{dt} \tag{5.55}$$

$$\dot{\omega} = \ddot{\alpha} = \frac{d\omega}{dt} \tag{5.56}$$

$$\dot{\omega}(t) = \dot{\omega} = const \tag{5.57}$$

$$\omega(t) = \dot{\omega}\int_{t_0}^{t} dt = \omega_0 + \dot{\omega}\cdot(t - t_0) \tag{5.58}$$

$$\alpha(t) = \int_{t_0}^{t} \omega(t)\,dt = \omega_0\,(t - t_0) + \dot{\omega} \cdot \frac{(t^2 - t_0^2)}{2} + \alpha_0 \tag{5.59}$$

$0 \geq t \geq 1$:

Table 5.5 Initial conditions, rotation, interval 1

$\dot{\omega}_0$	$[°/s^2]$	Angular Acceleration at $t = t_0$	(5.61)
ω_0	$[°/s]$	Angular Speed at $t = t_0$	0
α_0	$[°]$	Angle of Attack at $t = t_0$	0
t_0	$[s]$	Time when the rotation starts	0

From the initial conditions of Table 5.5, the initial values for the 2nd time interval are first determined for the time interval $\mathbf{0 \geq t \geq 1}$**:**

$$\omega(1) = \omega_1 = \dot{\omega}_0 \cdot t_1 \tag{5.60}$$

$$\rightarrow\ \dot{\omega}_0 = \omega_1 / t_1 \tag{5.61}$$

$$\alpha(1) = \alpha_1 = \dot{\omega}_0 \cdot \frac{t_1^2}{2} \tag{5.62}$$

followed by the interval $\boldsymbol{t_1 > t \geq t_{LOF}}$ based on the initial values of Table 5.6:

Table 5.6 Initial conditions, rotation, Interval 2

$\dot{\omega}_1$	$[°/s^2]$	Angular Acceleration at $t = t_1$	0
ω_1	$[°/s]$	Angular Speed at $t = t_1$	2.5 / 3
α_1	$[°]$	Angle of Attack at $t = t_0$	(5.62)
t_1	$[s]$	Time when the rotation starts	1

For the 2nd time interval, the time variable t is substituted corresponding to (5.64).

$$\tau = t - t_1 \tag{5.63}$$

$$t = \tau + t_1 \tag{5.64}$$

With τ and the initial values from Table 5.6, the time domain $t_1 > t \geq t_{LOF}$ results in:

$$\alpha(\tau) = \alpha_1 + \omega_1 \cdot \tau \tag{5.65}$$

With the known (assumed) lift-off angle α_{LOF} and the corresponding time τ_{LOF}:

$$\alpha(\tau_{LOF}) = \alpha_{LOF} = \alpha_1 + \omega_1 \cdot \tau_{LOF} \tag{5.66}$$

by re-substitution with

$$t_{LOF} = \tau_{LOF} + t_1 \tag{5.67}$$

results in the required rotation time t_R

$$t_R = \frac{\alpha_{LOF} - \alpha_1}{\omega_1} + t_1 \tag{5.68}$$

$\dot{\omega}, \ddot{\alpha}$	Angular Acceleration	$[°/s^2]$
$\dot{\omega}_0$	Angular Acceleration at $t = 0\ s$	""
$\dot{\omega}_1$	Angular Acceleration at $t = 1\ s$	""
$\omega, \dot{\alpha}$	Angular Speed	""
ω_0	Angular Speed at $t = t_0$	""
ω_1	Angular Speed at $t = 1\ s$	""
α	Angle of Attack	[°]
α_0	Angle of Attack at $t = t_0$	""
α_1	Angle of Attack at $t = 1\ s$	""
α_{LOF}	Angle of Attack at when the A/C becomes airborne (lift off)	""
t	Time variable	$[s]$
t_0	Initial value, interval $0 \geq t \geq 1$, $t_0 = 0$	""
t_1	End of time interval 1, $t_1 = 1$ s	""

From the assumptions described at the beginning and the preceding equations, the results are obtained according to Table 5.7.

Table 5.7 Rotation times t_R

		A320		A340	
		AEO	OEI	AEO	OEI
$\dot{\omega}_1$	[°/s²]	3	2.5	2.5	2
t_1	[s]	1	1	1	1
α_1	[°]	1.5	1.25	1.25	1
ω_1	[°/s]	3	2.5	2.5	2
t_R	[s]	3.83	4.50	4.50	5.50

5.4 Air Distance

The Air distance (the distance from lift-off until 35 ft is achieved at v_2) is estimated based on a common method provided in Raymer 1989, Scholz 1999, Nicolai 2010 or Gudmundsson 2014. This approach divides the aircraft trajectory (after the A/C becomes airborne) into 2 separate trajectories, the bow-shaped trajectory (rotation phase in the air) and the linear trajectory (climb phase) at a constant climb angle (see Figure 5.7).

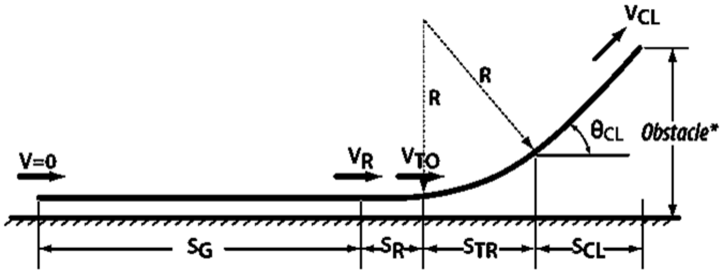

Figure 5.7 Schematic visualization of the takeoff phase. (Nicolai 2010)

Obstacle Height (Screen Height)

- Commercial = 35 ft
- Military = 50 ft

Transition Distance

During the transition section, the aircraft flies with a constant velocity an arc of radius R. Inspired by (Ehrig 2012) the load factor n of the aircraft becomes:

$$n = \frac{L}{W} = \frac{{}^{1}\!/_{2} \cdot C_{L,LOF} \cdot \rho \cdot S \cdot v_{LOF}^2}{{}^{1}\!/_{2} \cdot C_{L,max,TO} \cdot \rho \cdot S \cdot v_s^2} = \frac{v_{LOF}^2}{v_s^2} \cdot \frac{C_{L,LOF}}{C_{L,max,TO}} \tag{5.69}$$

It can be assumed that (based on Scholz 1999 and Nicolai 2010):

$$\frac{C_{L,LOF}}{C_{L,max,TO}} \approx 0.8 \tag{5.70}$$

This results in a load factor:

$$n = \frac{\mathrm{v}_{\mathrm{LOF}}^2}{\mathrm{v}_{\mathrm{s}}^2} \cdot \frac{C_{L,\mathrm{LOF}}}{C_{L,\mathrm{max}}} \approx \left(\frac{1.2 \cdot v_s}{v_s}\right)^2 \cdot 0.8 = 1.152 \tag{5.71}$$

and a Radius R:

$$R = \frac{v_{LOF}^2}{g(n-1)} = \frac{v_{LOF}^2}{0.15\, g} \tag{5.72}$$

Transition Distance s_{TR}:

$$s_{TR} = R\, sin\Theta_{CL} \tag{5.73}$$

Climb Distance s_{CL}:

$$s_{CL} = \frac{h_{obst} - h_{TR}}{tan\,\Theta_{CL}} \tag{5.74}$$

$$h_{TR} = R - R\,cos\,\Theta_{CL} = R(1 - cos\,\Theta_{CL}) \tag{5.75}$$

$$\Theta_{CL} = arcsin\left(\frac{T - D}{W}\right) \tag{5.76}$$

Since the climb angle Θ_{CL} remains constant after reaching the height h_{TR}, the speed dependent thrust $F(v)$ and drag $D(v)$ may be calculated with $v = v_{LOF}$. The resulting angle is valid up to the obstacle height h_{SC}. Thus, the part of the takeoff distance in the air can be solved time-independently, in pure geometrical terms.

The total flight distance results from the sum of the transition distance and climb phase (see Figure 5.8, left):

Total Air Distance s_{air}:

$$s_{AIR} = s_{TR} + s_{CL} \tag{5.77}$$

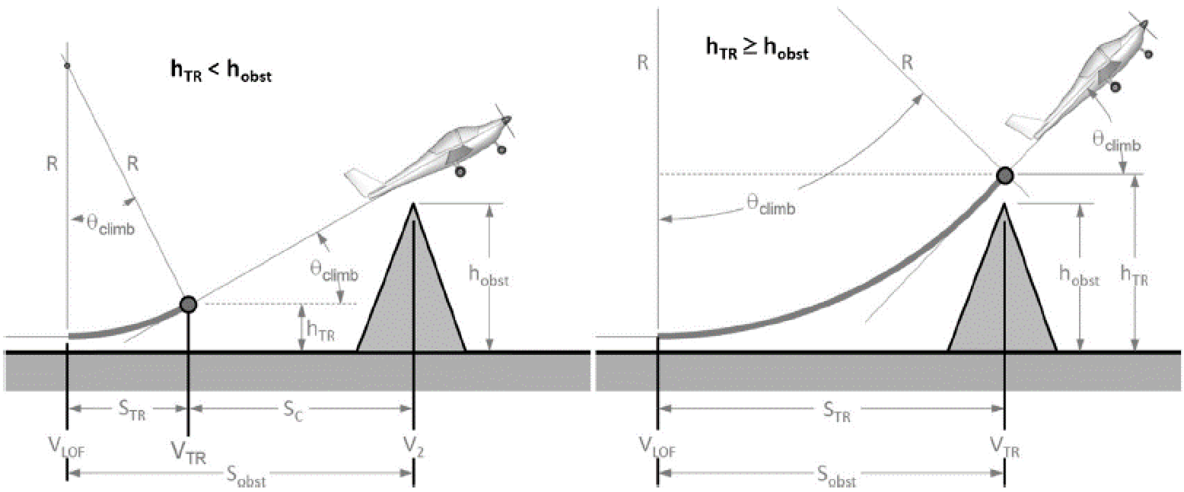

Figure 5.8 Transition & rotation phase (Gudmundsson 2014)

If $h_{TR} \geq h_{SC}$:

$$R^2 = s_{obst}^2 + (R - h_{obst})^2 \tag{5.78}$$

$$s_{AIR} = s_{obst} = \sqrt{R^2 - (R - h_{obst})^2} \tag{5.79}$$

$$s_{CL} = 0 \tag{5.80}$$

h_{obst}	Screen height (obstacle* in **Figure 5.7**)	[m], [ft]
h_{TR}	Height at transition from rotation to climb phase	“”
Θ_{CL}	Climb angle	[rad]
R	Bow radius	[m]
$C_{L,\mathrm{LOF}}$	Lift coefficient at lift-off	[-}
$C_{L,max,TO}$	Maximum lift coefficient in a specific flap configuration	"
n	Load factor	"
s_{CL}	Climb Distance	[m]
s_{TR}	Transition Distance	""

5.5 Stop Distance

5.5.1 Time intervals

For the calculation for the BFL on dry runaways no reverse thrust is considered. In Scheiderer 2012 the AFM transition time is explained as illustrated in Figure 5.9. When an engine failure occurs, one second must be assumed at v_{EF} until the pilot notices the failure. Two extra seconds (AFM buffer) are added to account for potential human individual error. Then, in order, the brake is applied, the thrust is set to idle, and the speed brakes are actuated. The time for active operation is determined in flight tests from at least six such start aborts, according to Scheiderer 2012 and average values are formed as the result. In total, for the safety margin, the brakes, the thrust reduction, and the speed brakes, this results in about 3 seconds. The individual time intervals are summarized in Table 5.8.

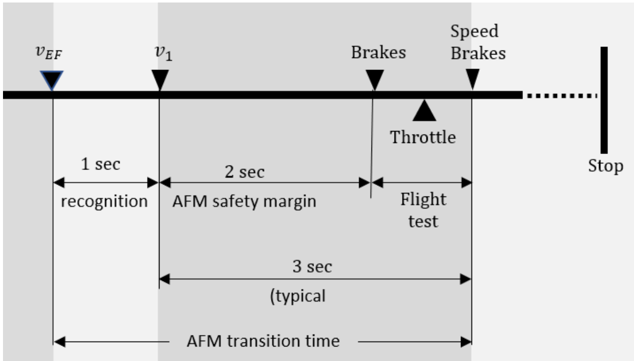

Figure 5.9 AFM transition time

Table 5.8 AFM Transition time

			Time		**Speed**	**Acceleration**	
		Action	Σ [s]	Σ [s]	[m/s]	AM 25.42 (A320)	AM 25.92 (A340)
AFM Transition Time		Engine failure	0		v_{EF}	$a > 0$	$a > 0$
		Recognition time	1	1	v_1	$a > 0$	$a > 0$
		AFM buffer	2	3		$a > 0$	$a = 0$
		Reaction					
	1st	Brake actuation	0.5	3.5			
	2nd	Thrust lever (idle thrust)	0.5	4.0		$a < 0$	$a < 0$
	3rd	Spoiler	…	…		$a < 0$	$a < 0$
				t_{stop}	0	0	0

Besides, it is assumed that the braking force develops linearly within two seconds. The distinction regarding the acceleration according to Amendment 25.92 and Amendment 25.42 shall be clarified with Figure 5.10 and Figure 5.11. In each case, an engine failure at 140 knots is simulated.

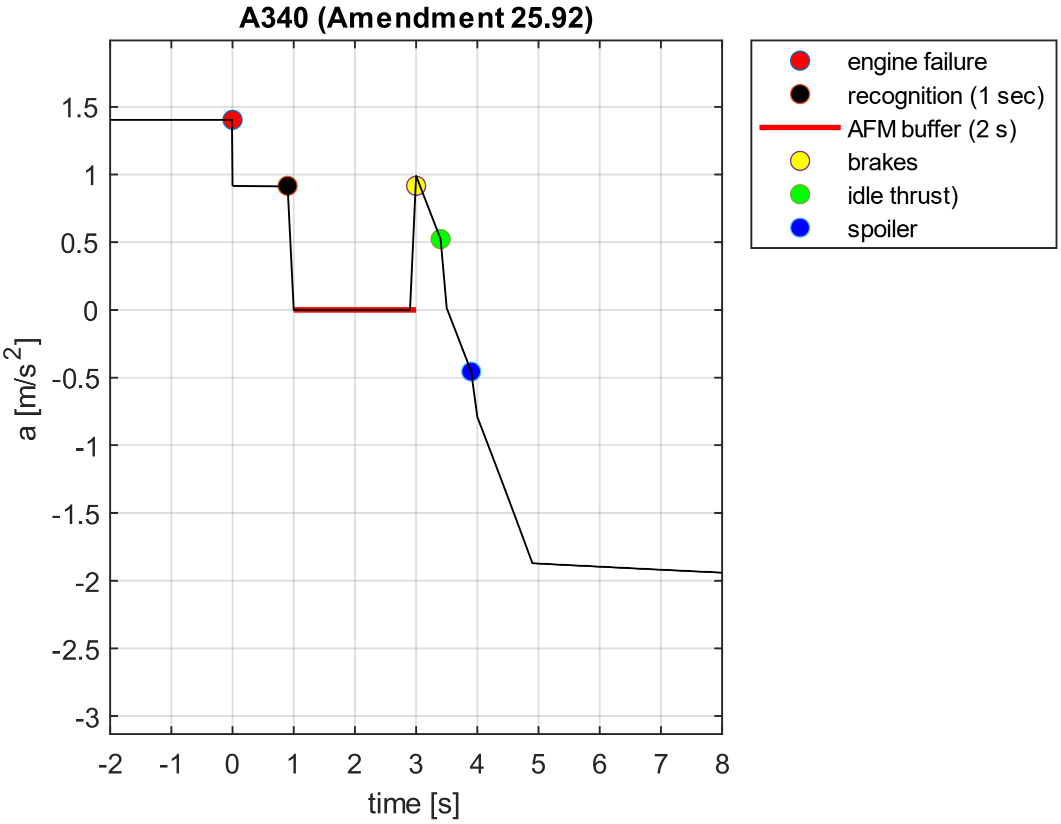

Figure 5.10 Deceleration: A340; $v_{EF} = 140\ kt$

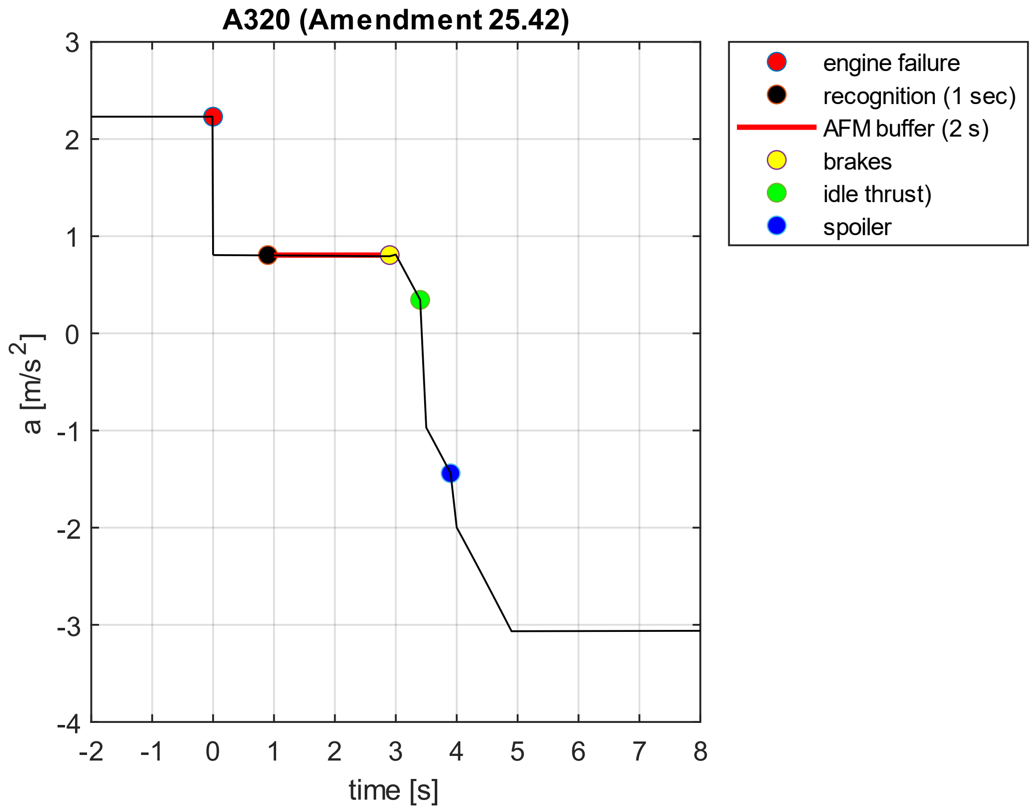

Figure 5.11 Deceleration: A320; $v_{EF} = 140\ kt$

5.5.2 Numerical Solution

The Stop distance is solved numerically, similar to the ground roll distance.

Analogous to (5.8):

$$a = \frac{1}{m}[T - D - F_B - mg\,sin\,\gamma] \tag{5.81}$$

Reverse Thrust, dry => not to be considered

Braking force:

$$F_B(v) = \mu_B(f_L \cdot W \cdot cos\,\gamma - L(v)) \tag{5.82}$$

Only part of the weight rests on the main landing gear. This is considered via the load factor f_L. According to Scholz 1999, values between 0.8 and 0.95 are suitable for jets. For Jets with nose wheel brakes the value becomes 1. f_L depends on the C.G. position and varies with the weight distribution (fuel, passengers, cargo, etc.). In the context of the thesis, a value of 0.91 is used (most forward position).

The braking coefficient depends on the runway condition. For dry asphalt or concrete a value between 0.3 and 0.6 is characteristic (see Table 5.10)

Table 5.9 Brake coefficient (Scheiderer 2018)

Code	Bremswirkung	Bremskoeffizient ICAO	Bremskoeffizient CIS[12]
9	Unreliable	9 - unreliable	9 - unreliable
5	Good	> 0,40	> 0,50
4	Medium-good	0,39 – 0,36	
3	Medium	0,35 – 0,30	0,50 – 0,30
2	Medium-poor	0,29 – 0,26	
1	Poor	< 0,25	< 0,30[13]

Table 5.10 Brake coefficients

	Gudmundsson 2014	Nicolai 2010
μ_B dry asphalt or concrete	0.3-0.5	0.3-0.6

CIS: Commonwealth of Independent States

Regarding the simulation the upper "Medium" of Table 5.9 value $\mu_B = 0.35$ is set.

By changing the sign, since the acceleration is less than 0:

$$a = \frac{1}{m}[F_B(v) + D(v) + W \cdot sin\gamma - T(v)] \tag{5.83}$$

$$a = \frac{g}{m\,g}\left[\mu_B\left(f_L \cdot W\,cos\,\gamma - L(v)\right) + C_{D,g}\ \frac{\rho}{2}\ v^2\ S_w + W\,sin\,\gamma - T(v)\right] \tag{5.84}$$

with thrust from (2.97):

$$T(v) = T_0[A - K_1 v + K_2 v^2] \tag{2.97}$$

Transformation:

$$a = \frac{g}{W}\left[\mu_B\left(f_L\ W\,cos\,\gamma - C_{L,g}\frac{\rho}{2}\ v^2\ S_w\right) + C_{D,g}\ \frac{\rho}{2} v^2\ S_w + W\,sin\,\gamma - T(v)\right] \tag{5.85}$$

$$a = g \cdot \mu_B\left[f_L\ cos\,\gamma - C_{L,g}\ \frac{\rho}{2}\frac{S_w}{W}\ v^2 + \frac{C_{D,g}}{\mu_B}\ \frac{\rho}{2}\cdot\frac{S_w}{W}\cdot v^2 + \frac{sin\,\gamma}{\mu_B} - \frac{T(v)}{W\ \mu_B}\right] \tag{5.86}$$

$$a = \frac{dv}{dt} = \frac{d^2s}{dt^2} = g\ \mu_B\left[\left(f_L\ cos\,\gamma + \frac{sin\,\gamma}{\mu_B} - \frac{T(v)}{W\ \mu_B}\right) + \frac{\rho}{2}\ \frac{S_W}{W}\left(\frac{C_{D,g}}{\mu_B} - C_{L,g}\right)v^2\right] \tag{5.87}$$

Spoiler:

If the spoiler geometry is known, a procedure by Scholz 1997 is recommended to account for the deceleration of the extended spoiler:

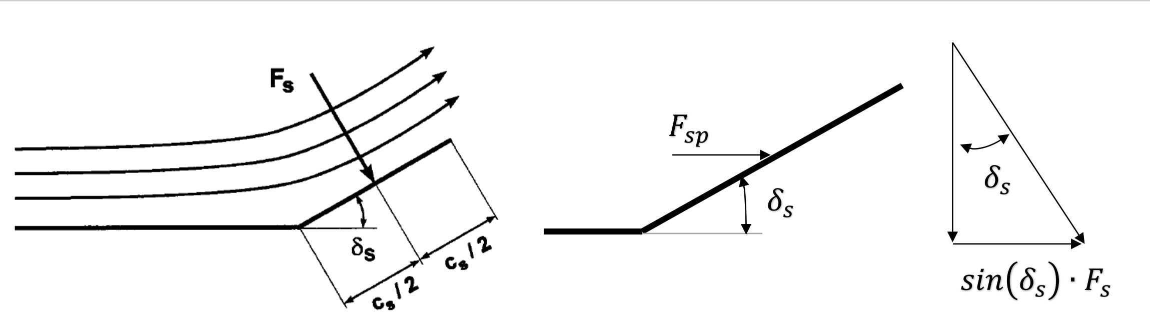

Figure 5.12 Deceleration due to spoiler (Scholz 1997)

$$\boldsymbol{F_{sp}} = C_{D,sp} \cdot \rho/2 \cdot v^2 \cdot S_{sp} \cdot \sin(\delta_s) \tag{5.88}$$

Calculations for spoilers of A310, A320, A340 resulted in spoiler coefficients:

- $C_{D,sp} \leq 2$ (Infinitely large spoilers $C_{D,sp} = 2$)
- $\boldsymbol{C_{D,sp} \approx 1.8}$ (Multiple spoilers extended)
- $C_{D,sp} \approx 1.5$ (Spoiler with rather square shape)

According to Scholz 2015, a maximum spoiler deflection of $\boldsymbol{\delta_s = 50°}$ can be assumed. The spoiler data for the sample aircraft are provided by (Niederkleine 1999)

Stop Distance (numerical solution):

With thrust $T = T(v)$ the DGL regarding the stop distance is solved numerically. Corresponding to the ground roll distance with (5.50):

$$\frac{d^2 s}{dt^2} = \frac{dv_g}{dt} = f(t, v_g) \tag{5.50}$$

Deceleration incl. Spoiler:

$$a = g\mu_B \left[\left(\frac{F_{SP}}{W\mu_B} + f_L \cos\gamma + \frac{\sin\gamma}{\mu_B} - \frac{T(v)}{W\mu_B} \right) + \frac{\rho}{2} \frac{S}{W} \left(\frac{C_{D,g}}{\mu_B} - C_{L,g} \right) v^2 \right] \tag{5.89}$$

(5.50) must be solved numerically based on the deceleration according to (5.89) with time intervals on the basis of Table 5.8 . Before the brakes are applied $\mu = 0.02$. With brake actuation $\mu = \mu_B = 0.35$ based on Table 5.9 and Table 5.10 .

5.6 Accelerate Stop Distance

Total distance at aborted takeoff s_{ASD}:

$$s_{ASD} = s_{g,AEO} + s_{Stop} \tag{5.90}$$

Stop Distance s_{Stop}:

$$s_{Stop} = s_{g,v1} + s_{g,AFM} + s_B \tag{5.91}$$

$s_{\mathrm{g,AEO}}$	Ground roll distance from v_0 to v_{EF} with AEO	[m], [ft]
$s_{g,v1}$	Transition distance, 1 second recognition (v_{EF} ... v_1).	""
s_{gAFM}	AFM safety margin, 2 seconds	""
s_B	Braking distance, brake actuation until $v = 0$	""
s_{Stop}	Total stop distance	""

Figure 5.13 and Figure 5.14 show the ASD simulation with MATLAB for an A320 / A340 in the event of a simulated engine failure at 140 knots (parameters according to Chapter 8, with $H = 0$, $slope = 0\%$, confi 1+F, $v_W = 0$). Figure 5.14 corresponds to the curve according to Figure 5.15 from (Young 2018) based on amendment 25.92, in which the individual intervals are described. Figure 5.13 differs qualitatively only in the 2 seconds of the AFM buffer.

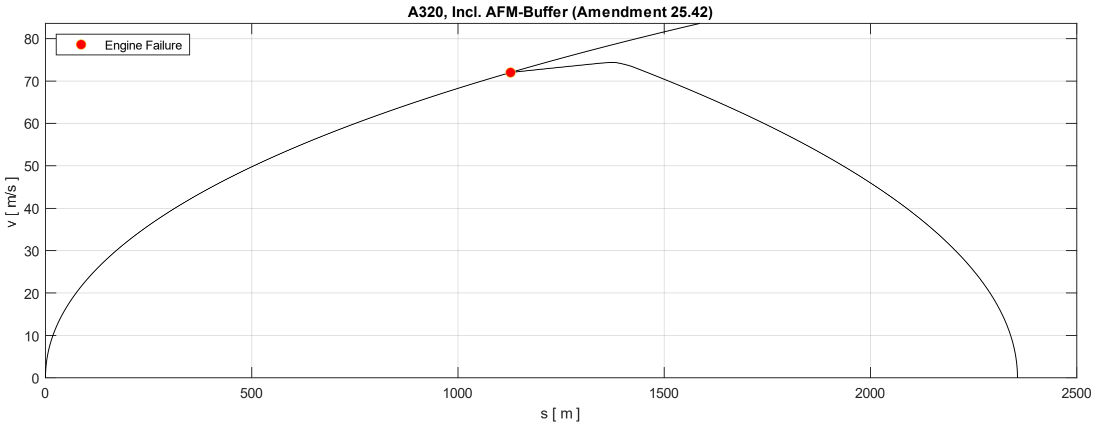

Figure 5.13 ASD (2356 m), A320 with $v_1 = 140\ \mathrm{kt}\ (72.02\ \mathrm{m/s})$

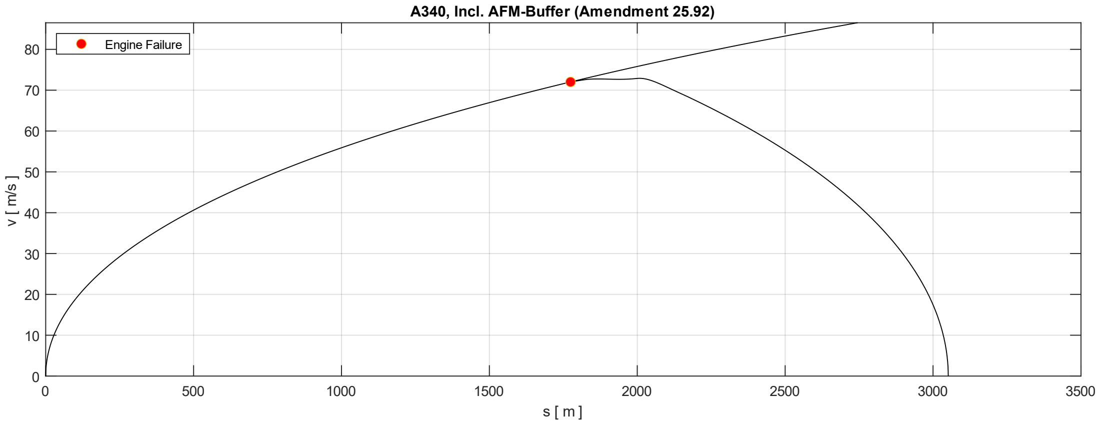

Figure 5.14 ASD (3051 m), A340 with $v_1 = 140\ \mathrm{kt}\ (72.02\ \mathrm{m/s})$

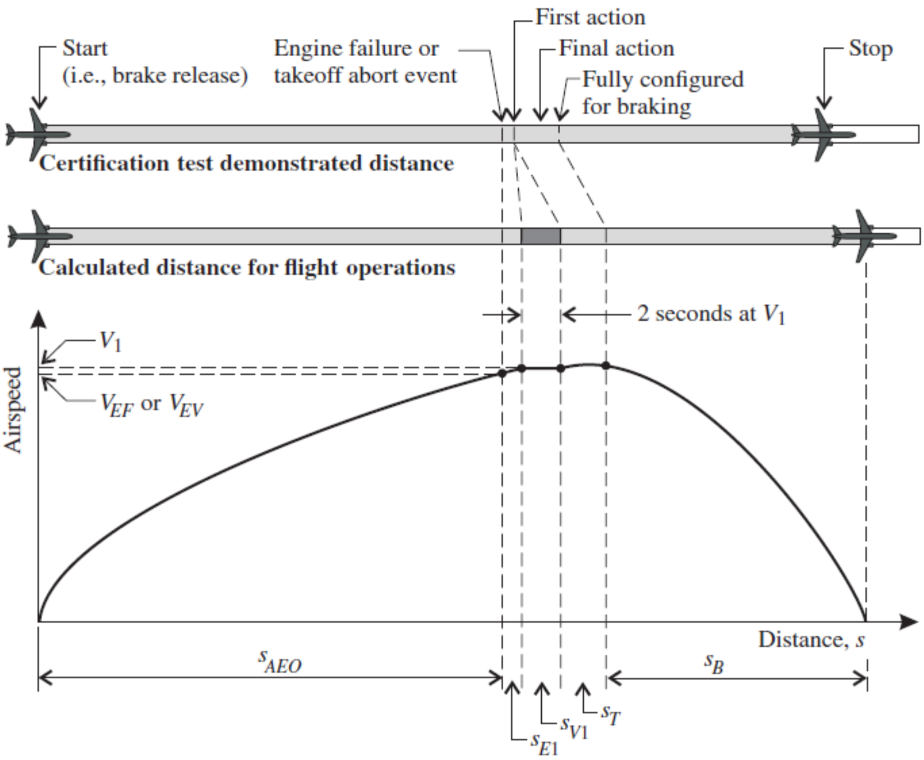

Figure 5.15 Rejected takeoff, accelerate–stop distance, AM 25.92 (Young 2018)

6 Balanced Field Length

6.1 Numerical Solution

The condition for the Balance Field Length with a balanced decision speed $v_{1,balanced}$ is:

$$s_{BFL} = s_{ASD}(v_1) = s_{AGD}(v_1) \tag{6.1}$$

The **One Engine Inoperative Takeoff Distance** $s_{AGD}(v_1)$ is determined from (5.3) and the **Acceleration Stop Distance** $s_{ASD}(v_1)$ based on (5.90).

A detailed definition for the Balanced Field Length is provided in Chapter 1.2.

A loop is programmed in MATLAB with an interval for engine failure speeds from v_{MCG} to v_R based on the requirement that $v_{MCG} \leq v_1 \leq v_R$ (see Figure 4.1), with minimum control speeds from Table 6.1.

Table 6.1 Minimum Control Speeds

		Confi 1+F	Confi 2	Confi 3
v_{MCG} (A320)	[kt]	125	125	125.5
v_{MCG} (A340)	[kt]	109.5	107.5	107

The **deviations Δs** of the distances $s_{TOD}(v_1)$ and $s_{ASD}(v_1)$ are calculated in each loop:

$$\Delta s = \left| s_{AGD}(v_1) - s_{ASD}(v_1) \right| \tag{6.2}$$

All result is stored in a **matrix Z** of the form:

$$Z = \begin{bmatrix} s_{AGD}(v_{1,i=1}) & s_{ASD}(v_{1,i=1}) & v_{1,i=1} & \Delta s_{i=1} \\ \dots & \dots & \dots & \dots \\ s_{AGD}(v_{1,i=n}) & s_{ASD}(v_{1,i=n}) & v_{1,i=n} & \Delta s_{i=n} \end{bmatrix} \tag{6.3}$$

i Loop count variable
n End of the loop (= rows of the matrix)

The distances $s_{TOD}(v_{1,i})$ and $s_{ASD}(v_{1,i})$ correspond to the searched balanced field length at the position $\Delta s_i = 0$. The associated "balanced" decision speed $v_{1,\mathrm{bal}}$ and the BFL are determined by interpolation based on $\Delta s_i = 0$.

6.2 Analytical Solution from Torenbeek

(6.4) presents an analytic method of calculating the BFL widely used in literature works of aircraft design as for example in (Raymer 2012). The method is based on Egbert Torenbeek

$$BFL = \frac{0.863}{1+2.3G}\left(\frac{W/S}{\rho\ g\ C_{L,2}} + h_{sc}\right)\left(\frac{1}{T_{av}/W - u} + 2.7\right) + \left(\frac{655}{\sqrt{\rho/\rho_{SL}}}\right) \tag{6.4}$$

With flaps in takeoff position parameter u becomes:

$$u = 0.01\ C_{Lmax,TO} + \mu \tag{6.5}$$

in most literatures (for example Raymer 2012) with $\mu = 0.02$ (concrete):

$$u = 0.01\ C_{Lmax,TO} + 0.02 \tag{6.6}$$

Average Thrust for Jets:

$$T_{av} = 0.75\ T_0 \left[\frac{5+\lambda_{BPR}}{4+\lambda_{BPR}}\right] \tag{6.7}$$

Factor G:

$$G = \gamma_2 - \gamma_{min} \tag{6.8}$$

Climb angle γ_2:

$$\gamma_2 = arcsine\left[\frac{T_{av}}{W} + \frac{C_{D,2}}{C_{L,2}}\right] \tag{6.9}$$

γ_2	1-engine-out, climb speed, also called: γ_{climb}
γ_{min}	Minimum climb gradient allowed by the airworthiness regulations two-engines: 0.024 3-engines: 0.027 four-engines: 0.030
$C_{L,2}$	C_L at climb speed ($v_2 = 1.2\ v_{stall}$), also called $C_{L,climb}$
$C_{D,2}$	C_D at climb speed v_2
h_{SC}	Screen height: 35 ft commercial, 50 ft military
λ_{BPR}	Bypass ratio
G	Difference: $\gamma_{climb} - \gamma_{min}$, often also called: $\Delta\gamma_2$
ρ	Density at height H
ρ_{SL}	Density at sea level (H=0)
$C_{Lmax,TO}$	Maximum C_L in a specific (takeoff) flap position
T_{av}	Average thrust

6.2.1 Derivation of the Decision Speed

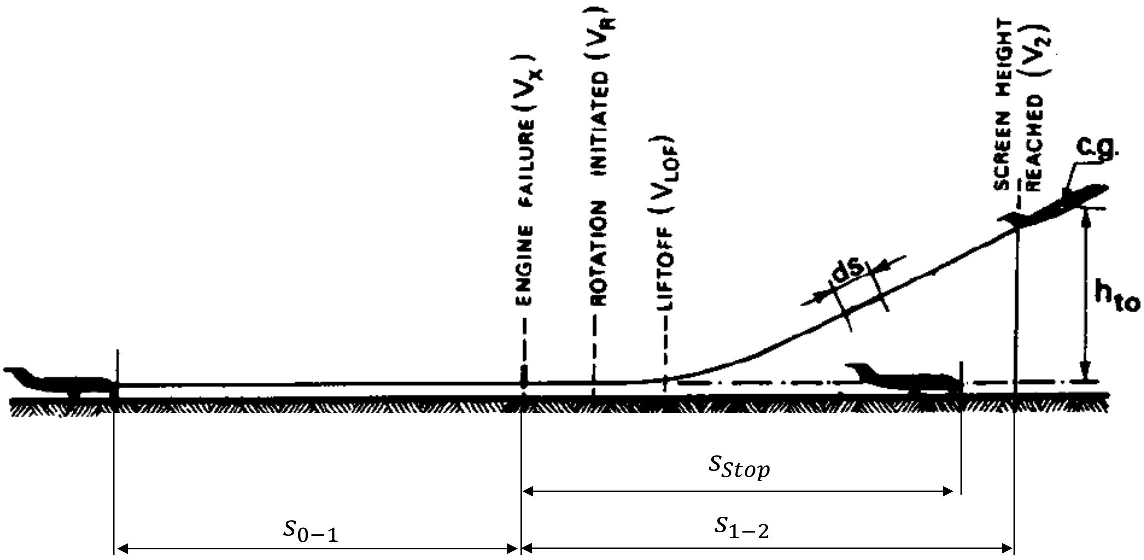

Figure 6.1 Takeoff phases (Torenbeek 1982)

Torenbeek divided the takeoff is into 2 phases (as illustrated in Figure 6.1):
Phase 1: Acceleration from standstill to engine failure at v_E,resp. v_1
Phase 2: Motion after engine failure up to an altitude of 10.7 m (35 ft) with safety speed v_2

Note: Torenbeek operates with the approximation $v_{EF} \approx v_1$.

Distance Phase 1 ($\boldsymbol{v = v_0 \dots v_1}$)

$$s_{0-1} = \frac{v_1^2}{2\,\bar{a}_{0-1}} \tag{6.10}$$

with a mean acceleration $\bar{a}_{0-1}$:

$$\left({}^{\bar{a}_{0-1}}/_{g}\right) = \frac{1}{mg} \cdot \left(T_{av} - D_{av} - F_f\right) \tag{6.11}$$

$$\left(\frac{\bar{a}_{0-1}}{g}\right) = \frac{T_{av}}{W_{TO}} - \mu - (C_D - \mu C_L)\,\frac{\rho}{2}\frac{v_1^2\,S_w}{W_{TO}} \tag{6.12}$$

Distance phase 2 ($\boldsymbol{v = v_1 \dots v_2}$)

$$s_{1-2} = \frac{1}{\bar{\gamma}} \cdot \left(\frac{v_2^2 - v_1^2}{2\,g} + h_{TO}\right) \tag{6.13}$$

Torenbeek defines the equivalent climb gradient $\bar{\gamma}$ regarding the distance s_{1-2} as followed:

$$\bar{\gamma} = 0.06 + \Delta\gamma_2 \tag{6.14}$$

(6.14) is approximated based on empiric data.

The distance needed to complete the standstill:

$$s_{stop} = \frac{v_1^2}{2\,\bar{a}_{stop}} + v_1 \Delta t \tag{6.15}$$

The inertia time Δt is basically influenced by the thrust-weight ratio at v_1.

Resulting from the condition for a balanced Takeoff Field Length $s_{ASD}(v_1) = S_{TOD}(v_1)$:

$$s_{0-1} + s_{STOP} = s_{0-1} + s_{1-2} \tag{6.16}$$

Respectively:

$$s_{STOP} = s_{1-2} \tag{6.17}$$

If (6.13) and (6.15) are inserted, it is obtained that:

$$\frac{v_x^2}{2\,\bar{a}_{stop}} + v_x \cdot \Delta t = \left(\frac{v_2^2}{2\,\bar{\gamma}\,g} + \frac{h_{to}}{\bar{\gamma}}\right) - \frac{v_x^2}{2\,\bar{\gamma}\,g} \tag{6.18}$$

Further transformation gives:

$$\frac{v_x^2}{2\,\bar{a}_{stop}} + \frac{v_x^2}{2\,\bar{\gamma}\,g} + v_x \cdot \Delta t = \left(\frac{v_2^2}{2\,\bar{\gamma}\,g} + \frac{h_{to}}{\bar{\gamma}}\right) \tag{6.19}$$

and

$$v_x^2 + \frac{2\,\bar{\gamma}\,g \cdot \bar{a}_{stop}\,\Delta t}{\left(\bar{a}_{stop} + \bar{\gamma}\,g\right)}\; v_x - \frac{2\,\bar{\gamma}\,g \cdot \bar{a}_{stop}}{\bar{a}_{stop} + \bar{\gamma}\,g}\left(\frac{v_2^2}{2\,\bar{\gamma}\,g} + \frac{h_{to}}{\bar{\gamma}}\right) = 0 \tag{6.20}$$

v_x Engine Failure Speed

By zero-point calculation:

$$v_x = -\frac{2\,\bar{\gamma}\,g \cdot \bar{a}_{stop}\,\Delta t}{2\left(\bar{a}_{stop} + \bar{\gamma}\,g\right)} \pm \sqrt{\left(\frac{2\,\bar{\gamma}\,g \cdot \bar{a}_{stop}\,\Delta t}{2\left(\bar{a}_{stop} + \bar{\gamma}\,g\right)}\right)^2 + \left(\frac{2\,\bar{\gamma}\,g \cdot \bar{a}_{stop}}{\bar{a}_{stop} + \bar{\gamma}\,g}\left(\frac{v_2^2}{2\,\bar{\gamma}\,g} + \frac{h_{to}}{\bar{\gamma}}\right)\right)} \tag{6.21}$$

Only the positive result is relevant and yields finally:

$$\frac{v_x}{v_2} = \frac{1}{v_2^2} \sqrt{\left(\bar{a}_{stop}\, \bar{\gamma}\, g \right)^2 \Delta t^2 + \frac{\left(\bar{a}_{stop} + \bar{\gamma}\, g\right)}{\bar{a}_{stop}} \left(1 + \frac{2\, h_{to}\, g}{v_2^2}\right)} - \frac{\bar{\gamma}\;\, g\, \Delta t}{v_2} \tag{6.22}$$

Approximation $v_1\,/v_2$ from Torenbeek 1972:

$$\frac{v_1}{v_2} = \left\{ \frac{1 + 2g\, h_{TO}/v_2^2}{1 + {\bar{\gamma}}\big/{(\bar{a}/g)_{stop}}} \right\}^{1/2} - \frac{\bar{\gamma}\, g(\Delta t - 1)}{v_2} \tag{6.23}$$

The simulation indicated that the results are consistently too low (for the two-engine jet). To optimize the output over as wide a range of parameters as possible, the BFL is corrected correspondingly according to (6.24).

Corrected BFL (two-engine jet):

$$BFL \;\; = 1.05 \left[\frac{0.863}{1 + 2.3G} \left(\frac{W/S}{\rho\, g\, C_{L,2}} + h_{sc} \right) \left(\frac{1}{T_{av}/W - u} + 2.7 \right) + \left(\frac{655}{\sqrt{\rho/\rho_{SL}}} \right) \right] \tag{6.24}$$

6.2.2 Derivation of the Balanced Field Length

Derived from the condition: $v_1 < v_R$ and $s_{1-2} = s_{stop}$:

$$BFL = \frac{v_2^2}{2g\left\{1+\frac{\bar{\gamma}}{(\bar{a}/g)_{stop}}\right\}}\left[\frac{1}{(\bar{a}/g)_{0-1}}+\frac{1}{(\bar{a}/g)_{stop}}\right]\left(1+\frac{2g\,h_{TO}}{v_2^2}\right)+\left(\frac{\Delta s_{TO}}{\sqrt{\sigma}}\right) \tag{6.25}$$

The inertial distance of 200 m (655 ft) with $\Delta t = 4.5$ s result according to Torenbeek from "typical" values from combinations for the wing and thrust loads. The values apply to propellers as well as jet engines.

$\Delta\gamma_2$ is the difference between the lift gradients for the 2nd segment and the minimum lift gradients, limited by the "airworthiness regulations."

The safety speed v_2^2 is derived based on the corresponding coefficient c_{L_2}:

$$v_2^2 = \frac{2\,W}{\rho\,S_W\,c_{L_2}} \tag{6.26}$$

For the average acceleration $\overline{a}_{stop}$, a statistical value of $\overline{a}_{stop} = 0.37g$ was determined based on 15 different (transport) jet. For optimal braking with lift dampers and nosewheel braking, (negative) accelerations, or braking effects, of $\bar{a}_{stop} = 0.45\,g$ to $\bar{a}_{stop} = 0.55\,g$ are possible on dry surfaces.

If all correlations and equations are taken into account, the following is obtained:

$$\begin{aligned} BFL = {} & \frac{\frac{2\,W}{\rho\cdot S_W\cdot c_{L_2}}}{2g\left\{1+\frac{0.06+\Delta\gamma_2}{0.37}\right\}} \\ & \cdot\left[\frac{1}{\frac{T}{W_{TO}}-\mu-(C_D-\mu C_L)\cdot\frac{\rho}{2}\cdot\frac{S_W\cdot C_{L2}}{W}\cdot\frac{2\,W}{\rho\cdot S_W\cdot c_{L_2}}}+\frac{1}{0.37}\right] \\ & \cdot\left(1+\frac{2g\cdot h_{TO}}{\frac{2\,W}{\rho\cdot S_W\cdot c_{L_2}}}\right)+\left(\frac{\Delta s_{TO}}{\sqrt{\sigma}}\right) \end{aligned} \tag{6.27}$$

With

$$\mu' = \mu - (C_D - \mu C_L) \tag{6.28}$$

results:

$$\begin{aligned} BFL &= \frac{1}{\left\{\frac{0.43}{0.37} + \frac{\Delta\gamma_2}{0.37}\right\}} \left[\frac{1}{\frac{T}{W_{TO}} - \mu'} + 2.7\right] \frac{W/S_W}{\rho \cdot S_W \cdot c_{L_2}} \\ &\cdot \left(1 + \frac{2g \cdot h_{TO}}{\frac{2\,W}{\rho \cdot S_W \cdot c_{L_2}}}\right) + \left(\frac{\Delta s_{TO}}{\sqrt{\sigma}}\right) \end{aligned} \tag{6.29}$$

By further transformation finally (6.4) evolves:

$$BFL = \frac{0.863}{1 + 2.3 \cdot \Delta\gamma_2} \cdot \left(\frac{W_{TO}/S}{\rho\ g\ C_{L2}} + h_{TO}\right)\left(\frac{1}{T_{av}/W_{TO} - u'} + 2.7\right) + \left(\frac{\Delta s_{TO}}{\sqrt{\sigma}}\right) \tag{6.4}$$

Often (as in Raymer 2012) the equation is given with statistical mean values for Δs_{TO}

With: $\Delta s_{TO} = 200$ m (655 ft)
$h_{TO} = 10.7$ m (35 ft)

This yields in:

$$BFL = \frac{0.863}{1 + 2.3 \cdot \Delta\gamma_2} \cdot \left(\frac{W_{TO}/S}{\rho\ g\ C_{L2}} + 10.7\right)\left(\frac{1}{T_{av}/W_{TO} - u'} + 2.7\right) + \left(\frac{200}{\sqrt{\sigma}}\right) \tag{6.30}$$

6.3 Analytical Solution from Kundu

Kundu assumes an average acceleration $\bar{a}$ until reaching the obstacle height of 35 ft and a corresponding speed v_2, thus summarizing the sections on the ground and in the air:

$$s_{TOFL} = \int_0^{v_2} \frac{v}{\bar{a}} dv = \frac{1}{\bar{a}} \int_0^{v_2} \frac{v}{\bar{a}}\, dv = \frac{v_2^2}{2\bar{a}} \tag{6.31}$$

$$\bar{a} = [(T - D) - \mu(W - L)] \cdot \frac{g}{W} = g\left(\frac{T}{W}\right)\left[1 - \frac{D}{T} - \frac{\mu W}{T} + \frac{\mu L}{T}\right] \tag{6.32}$$

$$v_2^2 = \frac{2 \cdot 1.2^2\, W/S}{\rho\, C_{Lmax,TO}} \tag{6.33}$$

As well as Loftin by omitting the term " $-\frac{D}{T} - \frac{\mu W}{T} + \frac{\mu L}{T}$ " due to the small(er) contribution:

$$s_{TOFL} = \frac{1}{[g(T/W)]} \frac{1.44\, W/S}{\rho\, C_{Lmax,TO}} \tag{6.34}$$

$$s_{TOFL} = \frac{1.44/\rho_0}{g\, \rho/(\rho_0)\;\, C_{Lmax,TO}} \frac{(W/S)}{(T/W)} \tag{6.35}$$

$$s_{TOFL} = \frac{(1.44\,)\,/\rho_0}{g\, \sigma\, C_{Lmax,TO}} \frac{(W/S)}{(T/W)} \tag{6.36}$$

For two-engine Jet Kundu recommends a factor of 0.5 due to the failed engine applied on the static net thrust ():

$$s_{TOFL} = \frac{1.44}{0.5\, g\, \rho_0} \cdot \frac{1}{\sigma\, C_{Lmax,TO}} \frac{(W/S)}{(\,T/W)} \tag{6.37}$$

For four-engine Jet Kundu suggests a factor of 0.75 (loss of thrust by a fourth) regarding the net static thrust due to the failed engine ($T_{OEI} \approx 0.75\, T_{TO}$):

$$s_{TOFL} = \frac{1.44}{0.75\, g\, \rho_0} \cdot \frac{1}{\sigma\, C_{Lmax,TO}} \frac{(W/S)}{(\,T/W)} \tag{6.38}$$

For four-engine Jet Kundu (corrected)

$$s_{TOFL} = \frac{1.44}{0.57\, g\, \rho_0} \cdot \frac{1}{\sigma\, C_{Lmax,TO}} \frac{(W/S)}{(\,T/W)} \tag{6.39}$$

Based on the findings (Chapter 9), the factor 0.75 (four engines) according to (6.38) does not lead to satisfactory results. The factor was adjusted in accordance with (6.39)

7 Takeoff Field Length

The Takeoff Field Length is the longest of the following three distances:

1. Accelerate Stop Distance with an engine failure 1 second before the decision speed v_1 (without reverse thrust in case of a dry runway),
2. Takeoff Distance (s_{AGD}) until the screen height (35 ft) is reached with an engine failure one second before the decision speed v_1,
3. (Factored) Takeoff Distance ($s_{TOD1.15}$) with all engines operative (AEO) until the screen height (35 ft) is reached plus an additional 15% safety margin

7.1 Numerical

For the (partial) numerical calculation of the TOFL, the BFL is calculated according to Chapter 6.1. In addition, the ground roll distance, the rotation distance, as well as the air distance in the AEO case are determined, whereby the sum results in the TOD s_{TOD}. The TOD incl. 15% markup then yields the factorized TOD $s_{TOD1.15}$. The greater distance of $s_{TOD1.15}$ and s_{BFL} consequently gives the TOFL s_{TOFL}. The correlations are summarized in table Table 7.1.

Table 7.1 Numerical Takeoff Field Length Calculation

Sign	Condition	Chapter
$\mathrm{TOD}_{1.15}$	= 1.15·[Ground Roll Distance (AEO)	Chapter 5.2.4 (numerical)
	+ Rotation Distance (AEO)	Chapter 5.3 (analytical)
	+ Air Distance (AEO)]	Chapter 5.4 (analytical)
BFL	Condition: ASD (v1) = TOD (v1)	Chapter 6.1
TOFL	= max ($\mathrm{TOD}_{1.15}$, BFL)	

7.2 Analytical from Loftin

Ground Roll Distance S_{TOG} based on Chapter 5.2.1:

$$S_{TOG} = \frac{1}{2} \cdot \frac{m_{TO} \cdot (v_{LOF} - v_W)^2}{T_{TO} - D_{TO} - \mu(mg - L_{TO}) - m_{TO}\, g \sin\gamma} \tag{5.14}$$

With a **lift coefficient ratio**:

$$\frac{C_{L,LOF}}{C_{L,max,TO}} = \frac{\frac{2\,w}{v_{LOF}^2\, S_W\, \rho}}{\frac{2\,w}{v_s^2\, S_W\, \rho}} \tag{7.1}$$

$$\frac{C_{L,LOF}}{C_{L,max,TO}} = \frac{v_s^2}{v_{LOF}^2} = \frac{v_s^2}{(1.2 \cdot v_s)^2} \tag{7.2}$$

$$C_{L,LOF} \approx \frac{1}{1.2^2}\, C_{L,max,TO} \tag{7.3}$$

Lift-off speed:

$$v_{LOF} = \sqrt{\frac{2g}{\rho} \cdot \frac{m_{TO}}{S_w} \cdot \frac{1}{C_{L,LOF}}} \tag{7.4}$$

Assumptions:

- $v_w = 0$
- $\gamma = 0$
- $\mathrm{v_s} = 1.2 \cdot \mathrm{v_2} \approx 1.2 \cdot \mathrm{v_{LOF}}$
- $T \gg D \,\&\, F_f$

By neglecting the term " $- D_{TO} - \mu(mg - L_{TO}) - m_{TO}\, g\, sin\gamma$ " and the above assumptions:

$$s_{TOG} = \frac{1}{\rho \cdot C_{L,LOF}} \cdot \frac{m_{MTO}/S_W}{T_{TO}/(m_{MTO} \cdot g)} \tag{7.5}$$

Note: Due to the simplifications, the ground roll distance given by (7.5) is too short and only serves as a basis for further calculations to determine the TOFL.

k_x is a factor introduced by Loftin which is used as a markup on the ground roll distance to derive the TOFL from it.

$$S_{TOFL} = s_{TOG}\, k_x \tag{7.6}$$

$$S_{TOFL} = k_x \frac{1}{\rho \cdot C_{L,LOF}} \cdot \frac{m_{MTO}/S_W}{T_{TO}/(m_{MTO} \cdot g)} \tag{7.7}$$

Further transformation gives:

$$S_{TOFL} = k_x \frac{1.2^2\ \rho_0}{\rho_0} \cdot \frac{1}{\rho \cdot\ C_{L,max,TO}} \cdot \frac{m_{MTO}/S_W}{T_{TO}/(m_{MTO} \cdot g)} \tag{7.8}$$

Constant values are combined to a factor k_{TO}:

$$k_{TO} = k_x \frac{1.2^2}{\rho_0} \tag{7.9}$$

This leads to the final equation:

$$S_{TOFL} = k_{TO} \cdot \frac{1}{\sigma \cdot C_{LmaxTO}} \cdot \frac{m_{MTO}/S_W}{T_{TO}/(m_{MTO} \cdot g)} \tag{7.10}$$

A statistical evaluation of Loftin in a variety of jet aircraft resulted in an average of $k_{TO} = 2.34$.

7.3 Analytical from Kroo

Kroo adopted a similar procedure but did not apply a linear approach and made a distinction according to the number of engines. A statistical evaluation yielded:

Two engines:

$$S_{TOFL,2eng} = 857.4 + 28.43\,x + 0.0185\,x^2 \tag{7.11}$$

Four engines:

$$S_{TOFL,4eng} = 486.7 + 26.20\,x + 0.0093\,x^2 \tag{7.12}$$

with **Thrust $\boldsymbol{T(v)}$ at $\boldsymbol{v = 0.7 \cdot v_{LOF}}$** (based on Chapter 2.8):

$$T_{.7\,v_{LO}} = N\,[1 - K_1\,(0.7\,v_{LOF}) + K_2\,(0.7\,v_{LOF})^2] \tag{7.13}$$

K_1, K_2 from (2.98) and (2.99).

Index variable x

$$x = \frac{W^2}{\sigma\,CL_{max,TO}\,S_W\,T_{.7\,VLO}} \tag{7.14}$$

Weight (imperial)	W	[lbs]
Thrust at 0.7 v_{LOF} (imperial)	$T_{.7\,VLO}$	[lbf]
index variable	x	[lbs/ft^2]

The curves for the TOFL depending on the index (from (7.14)) according to (7.11) and (7.12) are visualized with Figure 7.1.

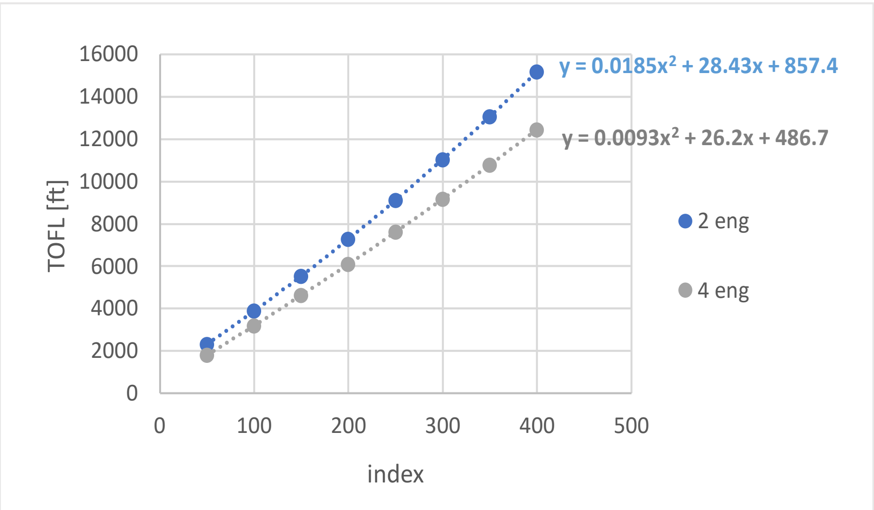

Figure 7.1 TOFL curves (Kroo)

7.4 Modified Analytical Solution from Loftin

Following the analytical method of Loftin, the index x from (7.15) is used to statistically evaluate the TOFL using the main aircraft parameters m_{MTO}/S_W, $T_{TO}/(m_{MTO} \cdot g)$ and C_{LmaxTO}. The values for the parameters and TOFL are taken from the source Jenkinson 2001.

Index variable x:

$$x = \frac{1}{\sigma \cdot C_{LmaxTO}} \cdot \frac{m_{MTO}/S_W}{T_{TO}/(m_{MTO} \cdot g)} \tag{7.15}$$

For the (linear) trend line, unlike Loftin, no intersection point was forced at the origin. This results in a classical linear equation:

$$S_{TOFL} = m \cdot x + b \tag{7.16}$$

$$S_{TOFL} = m \cdot \frac{1}{\sigma \cdot C_{LmaxTO}} \cdot \frac{m_{MTO}/S_W}{T_{TO}/(m_{MTO} \cdot g)} + b \tag{7.17}$$

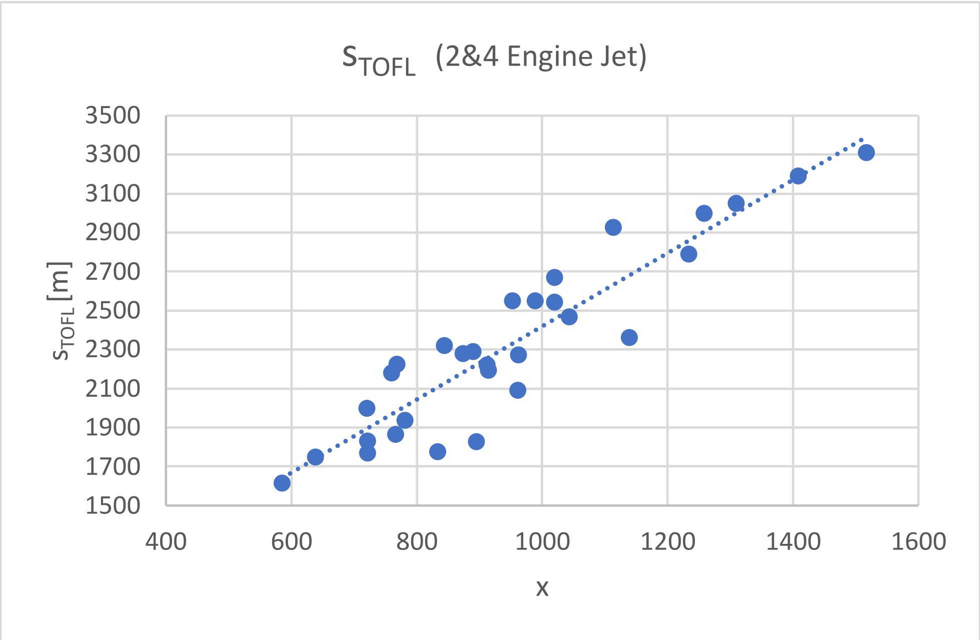

Figure 7.2 Statistical TOFL evaluation

An evaluation results in (7.18) according to Figure 7.2.

$$s_{TOFL} = 1.876\,x + 543.28 \tag{7.18}$$

This leads to a coefficient of determination (R^2) of 0.8553 with maximal deviation from -293 m to + 393 m (see Figure 7.3).

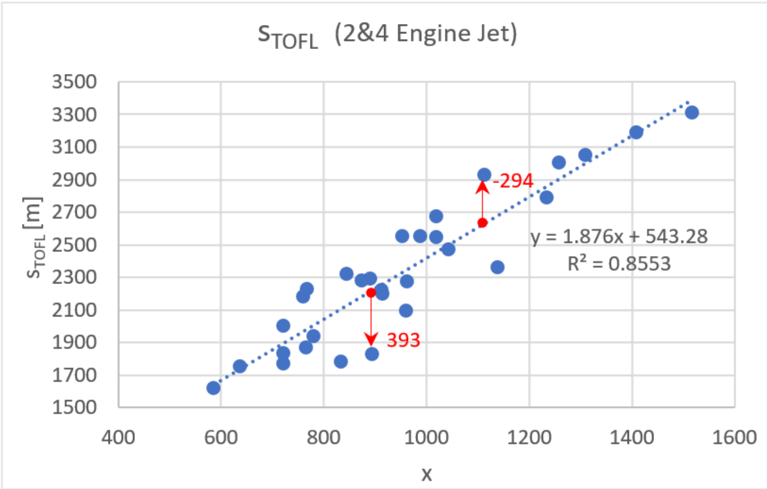

Figure 7.3 Residuals (statistical TOFL evaluation)

If a height difference is also to be considered, the start thrust must be adjusted (reduced). For this purpose, the thrust equation from Chapter 2.8 was evaluated according to Bartel 2008 as shown in Figure 2.29. The mean value for the thrust decrease per meter height difference was determined with (7.19). A scale of values was evaluated for velocities in the takeoff-relevant range between 0 ma and 0.3 ma as well as from 0 m to 3000 m

$$T/T_0 = 1 - 5.2224 \cdot 10^{-5} \cdot H \tag{7.19}$$

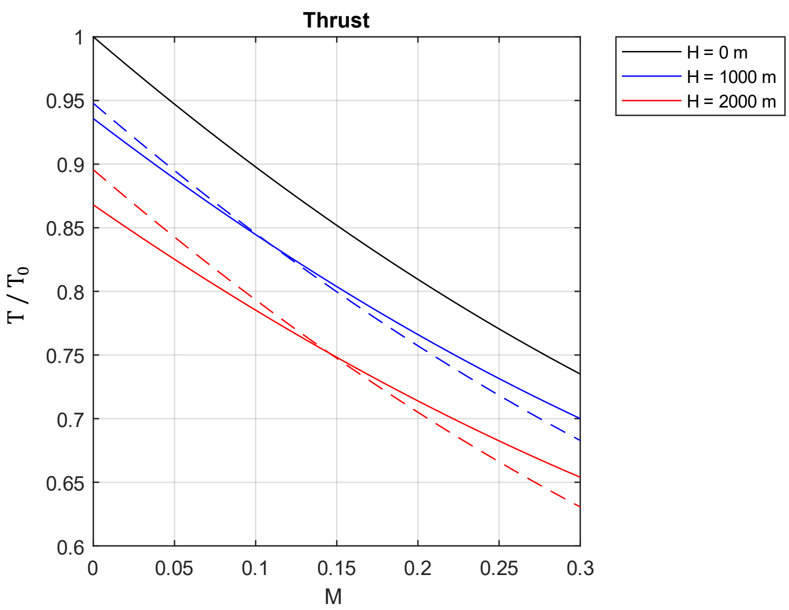

Figure 7.4 Average height dependent thrust reduction

Figure 7.4 shows the curves that result at an altitude of 0 m, 1000 m and 2000 m by using (2.100) from Bartel 2008. The dashed lines result in each case from a thrust ratio that was calculated using (7.19). (7.19) is used as follows for the evaluation of all analytical procedures where the maximum net thrust is used to adjust the thrust according to an altitude variation.

8 Sample Aircraft Parameters

In order to compare the analytical (simplified) equations with the results from the numerical solution methods, an aircraft type must be selected for which the results are compared using the computational algorithms presented. The input values, i.e., all geometries and coefficients, must be used consistently in all equations in order to make the results comparable. The aim is not to exactly reproduce the performance of specific aircraft models. For this, all geometries, polars, coefficients, ...etc. would have to be known in detail. Rather, 2 models should be used, which provide realistic parameters and thus offer feasible results for the performance. In the context of this Thesis 2 model airplanes are analyzed with respect to the takeoff performance. Although not all parameters are publicly available from the aircraft manufacturers, they can often be estimated with good approximation. In some places, statistical values are applied. The two sample aircrafts will basically be based on two Airbus models:

1.) Airbus A320-200
2.) Airbus A340-300

Two models were chosen for which a sufficient number of parameters are accessible in order to make the analysis as real as possible. An aircraft with 2 engines and another with four engines are to be considered, since the limiting takeoff distance differ from one another. For jet with four engines, the factorized takeoff distance (TOD + 15%) is usually the limiting element, while for jet aircraft with two engines, the BFL is the limiting factor. This relationship is confirmed with the results from Chapter 9. All equations are tested for both aircraft types.

8.1 Geometry of the Flaps

Both Airbus models are equipped with single-slotted Fowler flaps. The flap geometry was not available for the sample models. Therefore, the flap geometry had to be estimated from different image sources. Known parameters (b_f, b, c_r, S_w) from (Airbus 2005c) (Airbus 2005d), (Wikipedia 2021c) and (Wikipedia 2021d) were taken as a basic measure to estimate the relations from the sources according to Table 8.1, Table 8.2 and scaled models in (Airbus 2021c) as well as in (Airbus 2021d). The results are presented in Table 8.3.

Table 8.1 Source, flap geometry (A320)

A320 Sources	
Archived	Bitly-Link
https://perma.cc/F4ZN-9FQG	https://bit.ly/3HWcNhg
https://perma.cc/GY88-ZBXG	https://bit.ly/3l3V0Lf

Table 8.2 Source, flap geometry (A340)

A340 Sources	
Archived	Bitly-Link
https://perma.cc/7E4G-JZ62	https://shutr.bz/3nKugBi
https://perma.cc/2ATJ-8X7Q	https://shutr.bz/3nHoZKs
https://perma.cc/N8KS-JP8K	https://bit.ly/3nHVvfs
https://perma.cc/F5H2-JBKD	https://bit.ly/30Yj7Uy

Table 8.3 Flap parameter results

	Unit	A320 Value	A340 Value
c	[m]	3.73	7.44
c_f	[m]	0.89	1.6
b_f	[m]	24.54	32.90
$S_{w,f}$	[m2]	80.92	244.74
c_f / c	[-]	23.87%	21.51%
$S_{w,f}/S_w$	[-]	70.14%	67.40%
b_f / b	[-]	67.18%	56.72%

Note: All specified chords are mean chords (MAC).

8.2 Geometry of the Vertical Tailplane

The parameters necessary for the performance calculation are collected in Table 8.4.

Table 8.4 VTP / rudder parameter

		A320		A340	
Sign	**Unit**	**Value**	**Source**	**Value**	**Source**
h_V	[m]	5.87	[Airbus 2005c]	8.3	[Airbus 2005d]
l_V	[m]	12.53	[Jenkinson 2001]	27.5	[Jenkinson 2001]
l_E	[m]	5.75	[Airbus 2005c]	19.22	[Airbus 2005d]
S_V	[m2]	21.5	[Wikipdia 2021c]	45.3	(2.51)
S_r	[m2]	7.19	(2.52)	14.15	(2.52)
Φ_V	[-]	1.6	(2.29)	1.52	(2.29)
$\varphi_{V\,25}$	[°]	34.95	(2.53)	40.96	(2.53)

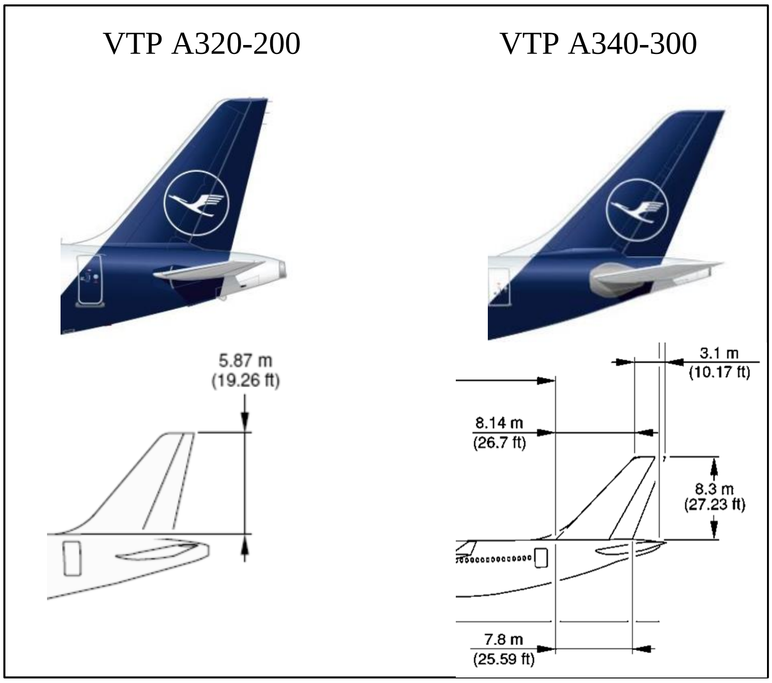

Figure 8.1 VTP images (Lufthansa 2021a & 2021b, Airbus 2005c, & 2005d)

The VTP parameters are scaled according to given dimensions (H_V, c_b), based on Figure 2.10 and Figure 8.1.

8.3 General Aircraft Parameter

The main parameters are summarized in Table 8.5.

Table 8.5 Main aircraft parameter

		A320		A340	
Sign	**Unit**	**Value**	**Source**	**Value**	**Source**
General Aircraft Parameter					
m	[t]	78	[Wikipedia 2021c]	271	[Wikipedia 2021d]
W	[kN]	765	(5.10)	2,658	(5.10)
Wing					
h_w	[m]	3.31	[Airbus 2005c]	4.73	[Airbus 2005d]
b_w	[m]	34.1	[Wikipedia 2021c]	58	[Jenkinson 2001]
S_w	[m²]	122.6	[Wikipedia 2021c]	363.1	[Jenkinson 2001]
A	[-]	9.5	(2.29)	9.26	(2.29)
λ	[-]	0.24	[Jenkinson 2001]	0.251	[Jenkinson 2001]
φ_{w25}	[°]	25	[Jenkinson 2001]	29.7	[Jenkinson 2001]
Coefficients					
μ	[-]	0.02	[Table 5.2]	0.02	[Table 5.2]
e (clean)	[-]	0.795	(2.38)	0.783	(2.38)
$C_{D,0,clean}$	[-]	0.0194	(2.47)	0.0193	(2.47)
$C_{L,0,clean}$	[-]	0.2	Estimated (typical value)	0.2	Estimated (typical value)
$C_{L,alpha}$	[-]	4.83	(2.28)	4.66	(2.28)
$C'_{L,alpha}$	[-]	5.21	(2.90)	4.80	(2.90)
Breaking Coefficients					
μ_B	[-]	0.35	[Table 5.9], [Table 5.10]	0.35	[Table 5.9], [Table 5.10]
f_L	[-]	0.91	[Airbus 2005c]	0.91	[Airbus 2005d]

Note: The coefficients with respect to the asymmetric flight conditions are (partially) speed dependent. To get an idea regarding the magnitude and partition, see Figure 2.11 to Figure 2.14 and Figure 2.15 to Figure 2.17.

8.4 Flap Dependent Coefficients

Additional coefficients, which depend on the flap angle, are listed in Table 8.6.

Table 8.6 Flap dependent coefficients

	A320			A340		
	[°]	value	source	[°]	value	source
$C_{D0,gear}$						
Confi 1+F	10	0.0152	(8.1)	17	0.0241	(8.2)
Confi 2	15	0.0145	""	22	0.0231	""
Confi 3	20	0.0136	""	26	0.0221	""
$C_{D0,f}$						
Confi 1+F	10	0.00307	(2.91)	17	0.00261	(2.91)
Confi 2	15	0.00395	""	22	0.00521	""
Confi 3	20	0.00482	""	26	0.00894	""
$C_{L0,f}$						
Confi 1+F	10	0.462	(2.78)	17	0.578	(2.78)
Confi 2	15	0.681	""	22	0.733	""
Confi 3	20	0.894	""	26	0.838	""

The correlation between the flaps and the coefficients $C_{D0,f}$ and $C_{L0,f}$ is graphically visualized with Figure 8.3 and Figure 8.4 for the respective A/C model.

The statistical average values from Figure 2.7 are transferred to Excel to extract polynomial functions depending on the flap angle δ_f (see Figure 8.2). The resulting functions are provided with (8.1) and (8.2).

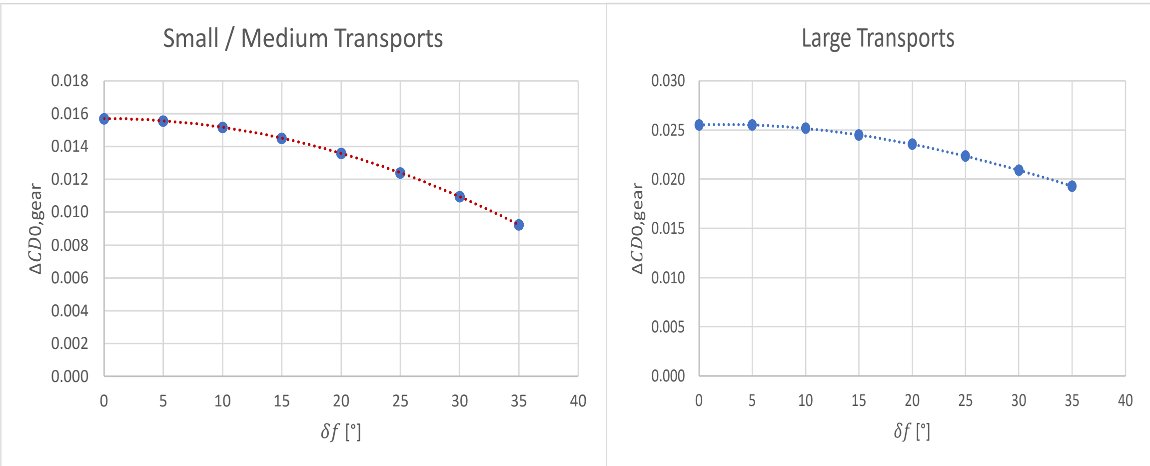

Figure 8.2 Landing gear drag coefficient (Excel)

Large Transports:

$$\Delta CD0_{gear} = 4 \cdot 10^{-8}\ \delta_f^3 - 7.485 \cdot 10^{-6}\ \delta_f^2 + 3.542 \cdot 10^{-5}\ \delta_f + 2.551 \cdot 10^{-2} \tag{8.1}$$

Medium/Small Transport:

$$\Delta CD0_{gear} = -1.8 \cdot 10^{-6} \cdot \delta_f^2 - 3.48 \cdot 10^{-5} \cdot \delta_f^1 + 1.57 \cdot 10^{-2} \tag{8.2}$$

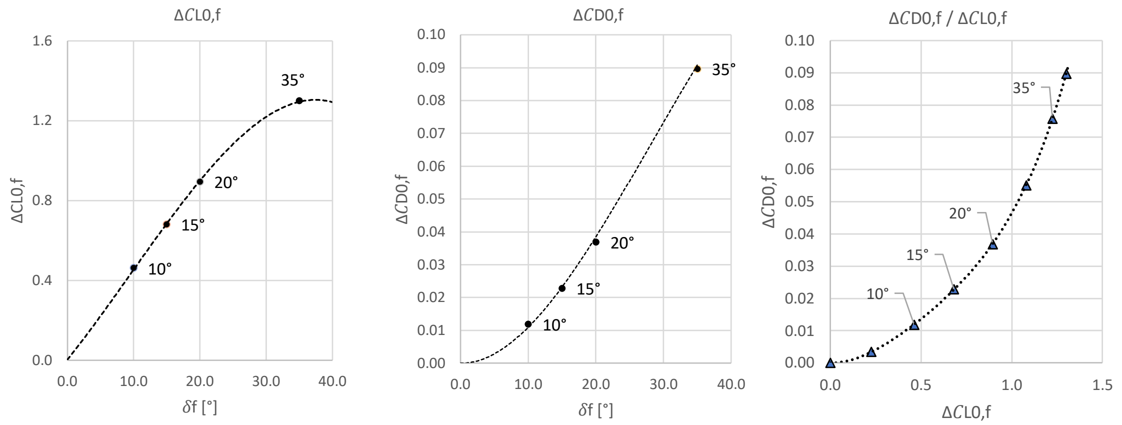

Figure 8.3 Flap increments (A320)

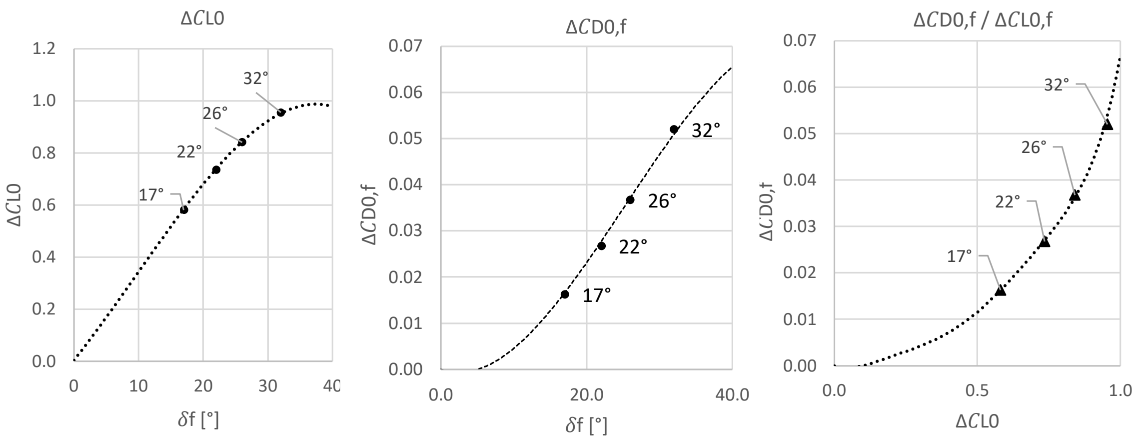

Figure 8.4 Flap increments (A340)

Note: The illustrated drag coefficient increment $C_{D0,f}$ includes the (additional) induced drag resulting from the flaps according to (8.3) with factor k_{TO} from (2.96).

$$C_{Df,induced} = k_{TO} \cdot \Delta C_{L0,f}^2 \tag{8.3}$$

8.5 Lift Slope Coefficient

With respect to the performance calculation, mean values regarding the Lift curve slope coefficients $C_{L,alpha}$ (clean) and $C'_{L,alpha}$ (extended flaps) were applied based on the curves in Figure 8.5. The computations are on the grounds of (2.28) and (2.90). The results are presented in Table 8.5.

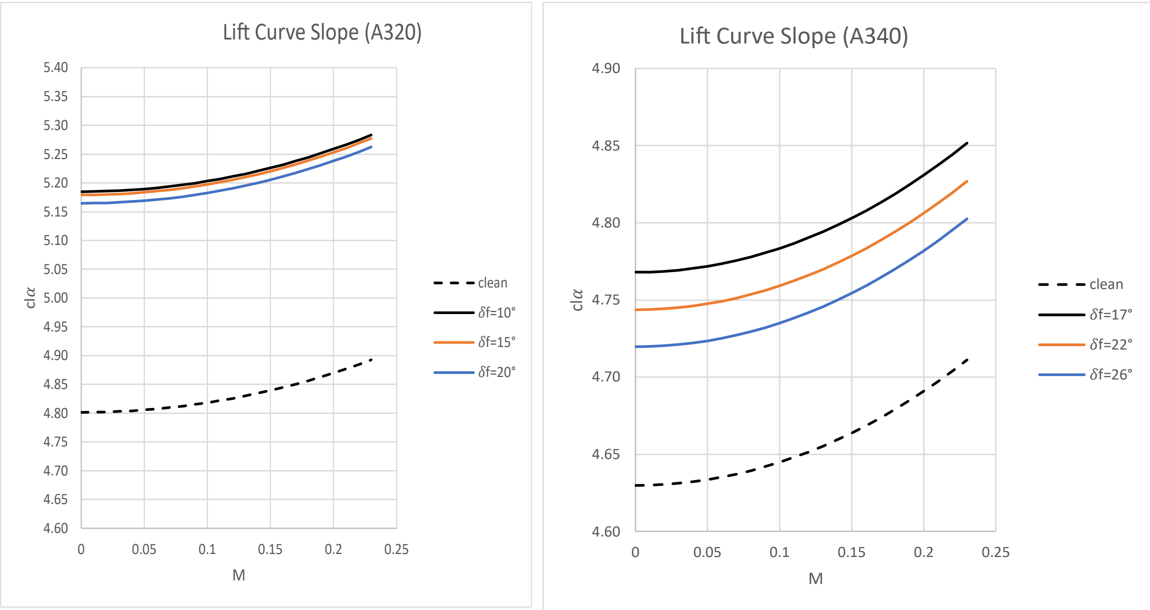

Figure 8.5 Lift curve slope coefficients “clean” and with extended flaps

8.6 Engine Parameter

Table 8.7 Engine parameter

Sign	Unit	A320 Value	A320 Source	A340 Value	A340 Source
N	[-]	2		4	
d_i	[m]	1.74	[Airbus 2005c]	1.84	[Airbus 2005d]
v_{REL}	[-]	0.92	[Torenbeek 1982]	0.92	[Torenbeek 1982]
T_{idle}	[kN]	6	(2.107)	10	(2.107)
T_0	[kN]	117.9	[Wikipedia 2021b]	138.8	[Wikipedia 2021b]
λ_{BPR}	[-]	6	[Wikipedia 2021b]	6.5	[Wikipedia 2021b]
d_a	[m]	2.43	[Airbus 2005c]	2.3	[Airbus 2005d]
d_{fan}	"	1.84	[Wikipedia 2021b]	1.74	[Wikipedia 2021b]
di	"	1.6	[Airbus 2005c]	1.69	(2.50)
A_N	[m2]	2.43	(2.63)	2.3	(2.63)

8.7 Maximum Lift Coefficient

The maximum lift coefficient $C_{L,max}$ is derived directly from the stall speeds $v_{s,1g}$ from (Airbus 2005a) and (Airbus 2005b) in the specific flap positions based on (2.72). Respective values are summarized in Table 8.8 and Table 8.9.

Table 8.8 $C_{L,max}$, A320 (m=78 t)

Confi	F+1	2	3	Full
$v_{s,1g}$	136	129	127.5	122.5
$C_{L,max}$	2.08	2.32	2.37	2.57

Table 8.9 $C_{L,max}$, A340 (m=271 t)

Confi	F+1	2	3	Full
$v_{s,1g}$	142	136.5	134.5	131.5
$C_{L,max}$	2.24	2.42	2.47	2.61

9 Simulation Results

Table 9.1 summarizes the analytical equations on which the results are based.

Table 9.1 Analytical equations

		Equation
BFL	Torenbeek	(6.4)
	Torenbeek, corrected	(6.24)
	Kundu (factor 0.5 / 0.75)	(6.37), (6.38)
	Kundu (factor 0.5 / 0.57)	(6.37), (6.39)
TOD1.15	Multiple Sources	(5.7)
TOFL	Kroo	(7.11), (7.12)
	Loftin (kTO = 2.34)	(7.10)
	Loftin (*y* = *m x* + *b*)	(7.18)

In the following subchapters outputs are presented in which different parameters are varied, such as:

- height and flap configuration (Chapter 9.1)
- thrust to weight ratio and wing loading (Chapter 9.2)

Furthermore a distance breakdown for the numerical soulutions is provided in Subchapter 9.3

The maximum discrepancies of the analytical solutions are indicated in Chapter 9.4.

Outcomes in Chapter 9.1 to Chapter 9.3 where the analytical solutions differ by greater (or equal) 10% are marked accordingly in red, a deviation less (or equal) 5% are highlighted in green.

For all results is valid that:

- $vw = 0\ kt$,
- $\text{slope} = 0\%$.

9.1 Height Variation

9.1.1 Two-Engine Jet

In Table 9.2. Table 9.3, Table 9.4, the results are presented with the "default" parameters ($T_0 = 117.9$ kN, $m = 78$ t) and altitude variation from 0 to 2000 ft with three different flap settings.

Table 9.2 A320 (*H* = 0 ft)

		Confi 1+F			Confi 2			Confi 3		
		s [m]	Δ [m]	Δ [%]	s [m]	Δ [m]	Δ [%]	s [m]	Δ [m]	Δ [%]
BFL	Numerical	2445			2265			2240		
	Analytical Torenbeek	2253	-192	-7.9%	2074	-191	-8.4%	2026	-214	-9.6%
	Torenbeek, corrected	2366	-79	-3.2%	2178	-87	-3.9%	2127	-113	-5.0%
	Analytical Kundu	2333	-112	-4.6%	2091	-174	-7.7%	2047	-193	-8.6%
TOD1.15	Numerical	2221			2008			1967		
TOFL	Numerical	2445			2265			2240		
	Analytical Kroo	2690	245	10.0%	2408	143	6.3%	2358	118	5.3%
	Analytical Loftin (k_{TO} = 2.34)	2322	-123	-5.0%	2082	-183	-8.1%	2038	-202	-9.0%
	Analytical Loftin (y = m x + b)	2405	-40	1.6%	2212	-53	2.3%	2177	-63	2.8%

Table 9.3 A320 (*H* = 1000 ft)

		Confi 1+F			Confi 2			Confi 3		
		s [m]	Δ [m]	Δ [%]	s [m]	Δ [m]	Δ [%]	s [m]	Δ [m]	Δ [%]
BFL	Numerical	2554			2372			2345		
	Analytical Torenbeek	2317	-237	-9.3%	2132	-240	-10.1%	2083	-262	-11.2%
	Torenbeek, corrected	2433	-121	-4.7%	2239	-133	-5.6%	2187	-158	-6.7%
	Analytical Kundu	2441	-113	-4.4%	2189	-183	-7.7%	2142	-203	-8.6%
TOD1.15	Numerical	2310			2088			2045		
TOFL	Numerical	2554			2372			2345		
	Analytical Kroo	2779	225	8.8%	2486	114	4.8%	2434	89	3.8%
	Analytical Loftin (k_{TO} = 2.34)	2430	-124	-4.9%	2178	-194	-8.2%	2132	-213	-9.1%
	Analytical Loftin (y = m x + b)	2491	-63	2.5%	2290	-82	3.5%	2253	-92	3.9%

Table 9.4 A320 (*H* = 2000 ft)

		Confi 1+F			Confi 2			Confi 3		
		s [m]	Δ [m]	Δ [%]	s [m]	Δ [m]	Δ [%]	s [m]	Δ [m]	Δ [%]
BFL	Numerical	2677			2495			2466		
	Analytical Torenbeek	2383	-294	-11.0%	2192	-303	-12.1%	2142	-324	-13.1%
	Torenbeek, corrected	2502	-175	-6.5%	2302	-193	-7.8%	2249	-217	-8.8%
	Analytical Kundu	2556	-121	-4.5%	2291	-204	-8.2%	2243	-223	-9.0%
TOD1.15	Numerical	2407			2174			2129		
TOFL	Numerical	2677			2495			2466		
	Analytical Kroo	2873	196	7.3%	2568	73	2.9%	2513	47	1.9%
	Analytical Loftin (k_{TO} = 2.34)	2544	-133	-5.0%	2281	-214	-8.6%	2232	-234	-9.5%
	Analytical Loftin (y = m x + b)	2583	-94	3.5%	2372	-123	4.9%	2333	-133	5.4%

9.1.2 Four-Engine Jet

In Table 9.5, Table 9.6 and Table 9.7, the results are presented with the "default" parameters ($T_0 = 138.8$ kN, $m = 271$ t) and altitude variation from 0 to 2000 ft with three different flap settings.

Table 9.5 A340 (H = 0 ft)

		Confi 1+F			Confi 2			Confi 3		
		s [m]	Δ [m]	Δ [%]	s [m]	Δ [m]	Δ [%]	s [m]	Δ [m]	Δ [%]
BFL	Numerical	3255			3042			3032		
	Analytical Torenbeek	3331	76	2.3%	3151	109	3.6%	3123	91	3.0%
	Torenbeek, corrected	3498	243	7.5%	3309	267	8.8%	3279	247	8.2%
	Analytical Kundu (factor 0.75)	2500	-755	-23.2%	2314	-728	-23.9%	2267	-765	-25.2%
	Kundu (factor 0.57)	3289	34	1.0%	3045	3	0.1%	2983	-49	-1.6%
TOD1.15	Numerical	3413			3162			3139		
TOFL	Numerical	3413			3162			3139		
	Analytical Kroo	3771	358	10.5%	3470	308	9.8%	3395	256	8.2%
	Analytical Loftin (k_{TO} = 2.34)	3732	319	9.3%	3454	292	9.3%	3385	246	7.8%
	Analytical Loftin ($y = m\,x + b$)	3535	122	3.6%	3313	151	4.8%	3257	118	3.8%

Table 9.6 A340 (H = 1000 ft)

		Confi 1+F			Confi 2			Confi 3		
		s [m]	Δ [m]	Δ [%]	s [m]	Δ [m]	Δ [%]	s [m]	Δ [m]	Δ [%]
BFL	Numerical	3412			3190			3181		
	Analytical Torenbeek	3424	12	0.4%	3239	49	1.5%	3210	29	0.9%
	Torenbeek, corrected	3595	183	5.4%	3401	211	6.6%	3371	190	6.0%
	Analytical Kundu (factor 0.75)	2574	-838	-24.6%	2383	-807	-25.3%	2335	-846	-26.6%
	Kundu (factor 0.57)	3387	-25	-0.7%	3135	-55	-1.7%	3072	-109	-3.4%
TOD1.15	Numerical	3565			3302			3279		
TOFL	Numerical	3565			3302			3279		
	Analytical Kroo	3903	338	9.5%	3591	289	8.8%	3513	234	7.1%
	Analytical Loftin (k_{TO} = 2.34)	3905	340	9.5%	3615	313	9.5%	3542	263	8.0%
	Analytical Loftin ($y = m\,x + b$)	3674	109	3.1%	3441	139	4.2%	3383	104	3.2%

Table 9.7 A340 (H = 2000 ft)

		Confi 1+F			Confi 2			Confi 3		
		s [m]	Δ [m]	Δ [%]	s [m]	Δ [m]	Δ [%]	s [m]	Δ [m]	Δ [%]
BFL	Numerical	3587			3358			3349		
	Analytical Torenbeek	3521	-66	-1.8%	3331	-27	-0.8%	3301	-48	-1.4%
	Torenbeek, corrected	3697	110	3.1%	3498	140	4.2%	3466	117	3.5%
	Analytical Kundu (factor 0.75)	2652	-935	-26.1%	2454	-904	-26.9%	2405	-944	-28.2%
	Kundu (factor 0.57)	3489	-98	-2.7%	3229	-129	-3.8%	3164	-185	-5.5%
TOD1.15	Numerical	3731			3456			3432		
TOFL	Numerical	3731			3456			3432		
	Analytical Kroo	4042	311	8.3%	3717	261	7.6%	3637	205	6.0%
	Analytical Loftin (k_{TO} = 2.34)	4089	358	9.6%	3785	329	9.5%	3708	276	8.0%
	Analytical Loftin ($y = m\,x + b$)	3821	90	2.4%	3577	121	3.5%	3516	84	2.4%

9.2 Thrust to Weight Ratio Variation

9.2.1 Two-Engine Jet

Table 9.8 and Table 9.9 show the output for a two-engine jet with a varying T/W ratio.

Table 9.8 BFL: A320, variable thrust/weight (confi 1+F, H = 0 ft)

		Numerical			Torenbeek			Torenbeek, corrected			Kundu		
	T [kN] →	**111.2**	**117.9**	**133.5**	**111.2**	**117.9**	**133.5**	**111.2**	**117.9**	**133.5**	**111.2**	**117.9**	**133.5**
m/S_w [kg/m²] ↓	m [t]	BFL [m]			BFL [m]			BFL [m]			BFL [m]		
571	**70**	2122	2019	1842	1973	1873	1684	2072	1967	1768	1992	1879	1659
587	**72**	2233	2118	1924	2071	1965	1764	2175	2063	1852	2107	1988	1755
604	**74**	2351	2221	2008	2172	2059	1846	2281	2162	1938	2226	2100	1854
620	**76**	2477	2330	2095	2275	2155	1929	2389	2263	2025	2348	2215	1956
636	**78**	2616	2445	2185	2380	2253	2014	2499	2366	2115	2473	2333	2060
													Δ
571	**70**				-7.02%	-7.23%	-8.58%	-2.37%	-2.59%	-4.01%	-6.13%	-6.93%	-9.93%
587	**72**				-7.25%	-7.22%	-8.32%	-2.62%	-2.58%	-3.73%	-5.64%	-6.14%	-8.78%
604	**74**				-7.61%	-7.29%	-8.07%	-2.99%	-2.66%	-3.47%	-5.32%	-5.45%	-7.67%
620	**76**				-8.16%	-7.51%	-7.92%	-3.56%	-2.89%	-3.32%	-5.21%	-4.94%	-6.63%
636	**78**				-9.02%	-7.85%	-7.83%	-4.47%	-3.25%	-3.22%	-5.47%	-4.58%	-5.72%

Table 9.9 BFL: A320, variable thrust/weight, continued

		Numerical			Kroo			Loftin (k_{TO}=2.34)			Loftin ($y = m\,x + b$)		
	T [kN] →	**111.2**	**117.9**	**133.5**	**111.2**	**117.9**	**133.5**	**111.2**	**117.9**	**133.5**	**111.2**	**117.9**	**133.5**
m/S_w [kg/m²] ↓	m [t]	BFL [m]			BFL [m]			BFL [m]			BFL [m]		
571	**70**	2122	2019	1842	2275	2148	1906	1983	1870	1651	2133	2042	1867
587	**72**	2233	2118	1924	2412	2275	2015	2098	1978	1747	2225	2129	1944
604	**74**	2351	2221	2008	2554	2408	2130	2216	2090	1846	2320	2219	2023
620	**76**	2477	2330	2095	2703	2546	2249	2337	2204	1947	2417	2310	2104
636	**78**	2616	2445	2185	2858	2690	2372	2462	2322	2051	2517	2405	2187
571	**70**				7.21%	6.39%	3.47%	-6.55%	-7.38%	-10.37%	0.52%	1.14%	1.36%
587	**72**				8.02%	7.41%	4.73%	-6.05%	-6.61%	-9.20%	-0.36%	0.52%	1.04%
604	**74**				8.63%	8.42%	6.08%	-5.74%	-5.90%	-8.07%	-1.32%	-0.09%	0.75%
620	**76**				9.12%	9.27%	7.35%	-5.65%	-5.41%	-7.06%	-2.42%	-0.86%	0.43%
636	**78**				9.25%	10.02%	8.56%	-5.89%	-5.03%	-6.13%	-3.78%	-1.64%	0.09%

9.2.2 Four-Engine Jet

Since for a four-engine Jet the TOD1.15 = TOFL. The results for the analytical BFL and TOFL had to be seperated in Table 9.10, Table 9.11 and Table 9.12.

Table 9.10 BFL: A340, variable *T/W* (confi 1+F, *H* = 0 ft)

		Numerical			Torenbeek			Torenbeek, corrected		
	T [kN] →	**138.8**	**144.6**	**151.3**	**138.8**	**144.6**	**151.3**	**138.8**	**144.6**	**151.3**
m/S_w [kg/m²] ↓	*m* [t] ↓	BFL [m]			BFL [m]			BFL [m]		
689	**250**	2761	2647	2533	2832	2703	2570	2974	2838	2699
716	**260**	2986	2855	2725	3063	2921	2775	3216	3067	2914
744	**270**	3230	3077	2929	3306	3150	2988	3471	3308	3137
771	**280**	3496	3317	3145	3560	3389	3212	3738	3558	3373
799	**290**	3793	3577	3377	3826	3638	3445	4017	3820	3617
		Δ								
689	**250**				2.57%	2.12%	1.46%	7.70%	7.22%	6.53%
716	**260**				2.58%	2.31%	1.83%	7.71%	7.43%	6.93%
744	**270**				2.35%	2.37%	2.01%	7.47%	7.49%	7.12%
771	**280**				1.83%	2.17%	2.13%	6.92%	7.28%	7.24%
799	**290**				0.87%	1.71%	2.01%	5.91%	6.79%	7.11%

Table 9.11 BFL: A340, variable *T/W* (confi 1+F, *H* = 0 ft), continued

		Numerical			Kundu (factor 0.75)			Kundu (factor 0.57)		
	T [kN] →	**138.8**	**144.6**	**151.3**	**138.8**	**144.6**	**151.3**	**138.8**	**144.6**	**151.3**
m/S_w [kg/m²] ↓	*m* [t] ↓	BFL [m]			BFL [m]			BFL [m]		
689	**250**	2761	2647	2533	2127	2042	1952	2799	2687	2568
716	**260**	2986	2855	2725	2301	2209	2111	3028	2906	2777
744	**270**	3230	3077	2929	2481	2382	2276	3265	3134	2995
771	**280**	3496	3317	3145	2669	2562	2448	3511	3370	3221
799	**290**	3793	3577	3377	2863	2748	2626	3767	3615	3455
		Δ								
689	**250**				-22.96%	-22.86%	-22.94%	1.38%	1.51%	1.38%
716	**260**				-22.94%	-22.63%	-22.53%	1.41%	1.79%	1.91%
744	**270**				-23.19%	-22.59%	-22.29%	1.08%	1.85%	2.25%
771	**280**				-23.66%	-22.76%	-22.16%	0.43%	1.60%	2.42%
799	**290**				-24.52%	-23.18%	-22.24%	-0.69%	1.06%	2.31%

Table 9.12 TOFL: A340, variable *T/W* (confi 1+F, *H* = 0 ft)

		Numerical			Kroo			Loftin (k_{TO}=2.34)			Loftin ($y = m\,x + b$)		
	T [kN] →	**138.8**	**144.6**	**151.3**	**138.8**	**144.6**	**151.3**	**138.8**	**144.6**	**151.3**	**138.8**	**144.6**	**151.3**
m/S_w [kg/m²] ↓	*m* [t] ↓	TOFL [m]			TOFL [m]			TOFL [m]			TOFL [m]		
689	**250**	2954	2849	2740	3151	3018	2879	3176	3049	2914	3090	2987	2879
716	**260**	3167	3052	2932	3437	3290	3136	3435	3297	3151	3297	3187	3070
744	**270**	3390	3263	3131	3739	3578	3409	3705	3556	3399	3513	3394	3268
771	**280**	3621	3482	3338	4060	3883	3698	3984	3824	3655	3737	3609	3473
799	**290**	3862	3708	3551	4400	4206	4003	4274	4102	3921	3970	3832	3687
		Δ											
689	**250**				6.67%	5.93%	5.07%	7.52%	7.02%	6.35%	4.60%	4.84%	5.07%
716	**260**				8.53%	7.80%	6.96%	8.46%	8.03%	7.47%	4.10%	4.42%	4.71%
744	**270**				10.29%	9.65%	8.88%	9.29%	8.98%	8.56%	3.63%	4.01%	4.38%
771	**280**				12.12%	11.52%	10.78%	10.02%	9.82%	9.50%	3.20%	3.65%	4.04%
799	**290**				13.93%	13.43%	12.73%	10.67%	10.63%	10.42%	2.80%	3.34%	3.83%

9.3 Distance Breakdown (BFL)

9.3.1 Two-Engine Jet

Table 9.13 shows the individual distance components that make up the BFL for the two-engine jet.

Table 9.13 BFL: A320, Distance breakdown (confi 1+F, *H* = 0 ft)

	confi 1+F		confi 2		confi 3	
	[m]	[ft]	[m]	[ft]	[m]	[ft]
$s_{g,AEO}$	1167	3829	1045	3428	1009	3310
$s_{g,OEI}$	418	1371	336	1102	368	1207
$s_{R,OEI}$	350	1148	331	1086	326	1070
$s_{AIR,OEI}$	510	1673	554	1818	538	1765
s_{Stop}	1278	4193	1221	4006	1232	4042
BFL	2446	8025	2266	7434	2241	7352
$TOD_{1.15}$	2221	7287	2008	6588	1967	6453

Figure 9.1 illustrates the (typical) curves of acceleration-Go-Distance and Acceleration-Stop-Distance (ASD) with varying v1 for a two-engine Jet. The intersection point corresponds to the BFL. Furthermore, it can be seen that the fatorized Takeoff Distance is below the BFL (as expected for a two-engine jet).

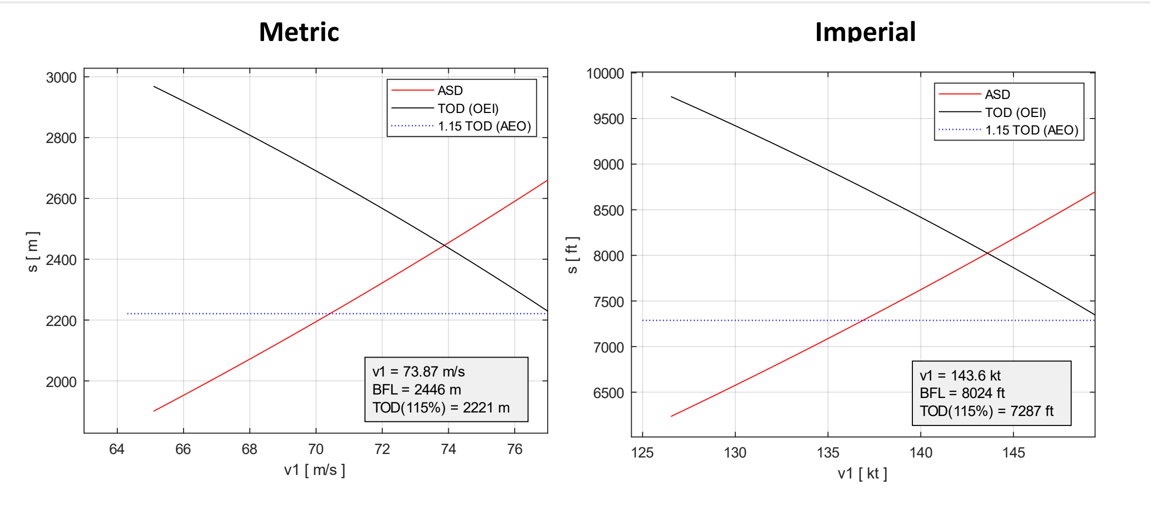

Figure 9.1 BFL, two engines (*m*= 78 t, *T0* = 117.9 kN, confi 1+F, *H* = 0 ft)

9.3.2 Four-Engine Jet

Table 9.14 shows the individual distance components that make up the BFL for the four-engine jet.

Table 9.14 BFL: A340, Distance breakdown (confi 1+F, *H* = 0 ft)

	confi 1+F		confi 2		confi 3	
	[m]	[ft]	[m]	[ft]	[m]	[ft]
$s_{g,AEO}$	1878	6161	1722	5650	1704	5591
$s_{g,OEI}$	622	2041	564	1850	571	1873
$s_{R,OEI}$	256	840	246	807	244	801
$s_{AIR,OEI}$	461	1512	472	1549	475	1558
s_{Stop}	1339	4393	1282	4206	1290	4232
BFL	3216	10551	3004	9856	2995	9826
$TOD_{1.15}$	3337	10948	3089	10135	3067	10062

Figure 9.2 is the result of a simulation of the four-engine jet in configuration 1+F. Compared to Figure 9.1 it can be seen that the factored takeoff distance is in this case (four engines) above the BFL and thus represents the limiting factor with respect to the TOFL. Notice that this applies to all results. Figure 9.1 and Figure 9.2 serve as exemplary visualizations of the subject matter.

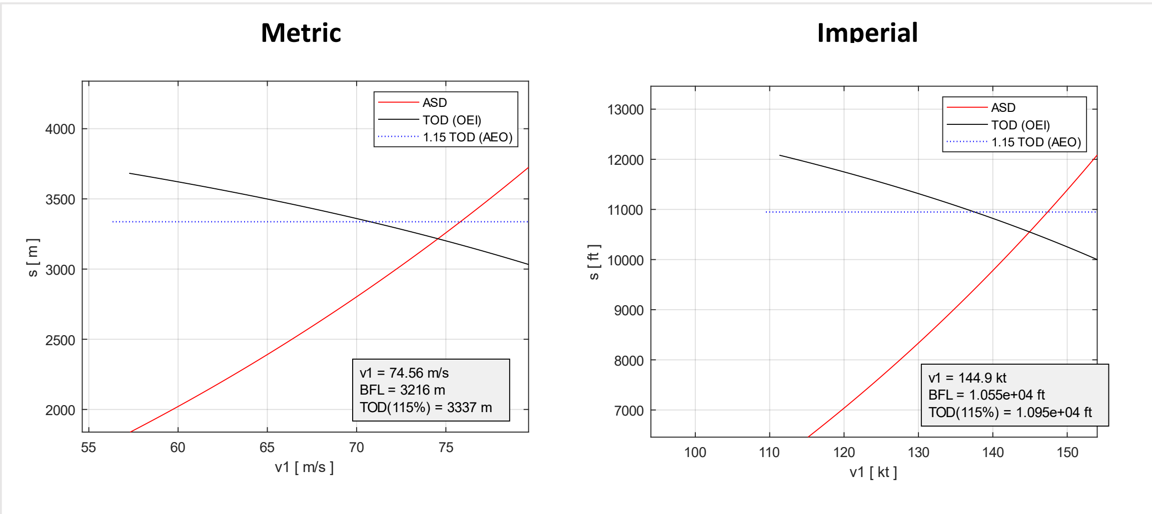

Figure 9.2 BFL, four engines (*m*= 271 t, *T0* = 138.8 kN, confi 1+F, *H* = 0 ft)

9.4 Summary of the Results

Table 9.15, Table 9.16, Table 9.17 display the maximum deviations of the analytical methods results in comparison with the numerical simulation outcomes.

Table 9.15 Δ Min /Max (two engines)

		Δmin	Δmax
BFL	Analytical Torenbeek	7.0%	13.1%
	Torenbeek, corrected (+ 5%)	2.4%	8.8%
	Analytical Kundu	4.4%	9.9%
TOFL	Analytical Kroo	1.9%	10.0%
	Analytical Loftin (k_{TO} = 2.34)	4.9%	10.4%
	Analytical Loftin ($y = m x + b$)	0.1%	5.4%

Table 9.16 Δ Min /Max (four engines)

		Δmin	Δmax
BFL	Analytical Torenbeek	0.4%	3.6%
	Torenbeek, corrected (+ 5%)	3.1%	8.8%
	Analytical Kundu (factor 0.75)	22.2%	28.2%
	Kundu (factor 0.57)	0.1%	5.5%
TOFL	Analytical Kroo	5.1%	13.9%
	Analytical Loftin (k_{TO} = 2.34)	6.4%	10.7%
	Analytical Loftin ($y = m x + b$)	2.4%	5.1%

Table 9.17 Δ Min /Max (total)

		Δmin	Δmax
BFL	Analytical Torenbeek	0.4%	13.1%
	Torenbeek, corrected (+ 5%)	2.4%	8.80%
	Analytical Kundu (factor 0.5 / 0.75)	4.4%	28.2%
	Analytical Kundu (factor 0.5 / 0.57)	0.1%	9.9%
TOFL	Analytical Kroo	1.9%	13.9%
	Analytical Loftin (k_{TO} = 2.34)	4.9%	10.7%
	Analytical Loftin ($y = m x + b$)	0.1%	5.4%

10 Summary

The main intention of the bachelor thesis has been to provide (and test) analytical methods for the calculation of the Takeoff Field Length (TOFL), an essential design parameter in aircraft design. For this purpose, two sample aircraft were investigated (mainly based on Airbus A320 - 200 and A340 - 300). This required the derivation of all relevant performance related aircraft parameters and their dependencies, such as the components of the lift drag coefficient and the drag coefficient in an AEO- or OEI-case. An altitude and speed dependent thrust equation was presented, the influence of asymmetric flight conditions was described and the variation of various parameters with the flap deflection has been discussed.

Moreover, the relationships between the individual speeds ($v_s, v_{s,1g}, v_R, v_2, V_{LOF}, v_3, v_{EF}, v_1$) were highlighted and the conversion between calibrated, true airspeed was derived as a function of the altitude and the Mach number. Furthermore, the most relevant regulations according to CS 25 / FAR 25 were presented with reference to the (takeoff) performance. In compliance with the relevant regulations and with knowledge of all relevant aircraft parameters and speeds, the BFL and $\mathrm{TOD}_{1.15}$ could be established. To achieve this, the sections required were first considered individually. Analytical methods were presented for all components of the takeoff distance (ground roll distance, rotation distance, air distance).

Regarding the ground and stop distance as numerical solution approaches (Euler Method and ODE45 - MATLAB) were introduced. In addition, analytical methods (from Kundu 2010, Torenbeek 1982, Kroo 2001, Loftin 1980) for the calculation of BFL and TOFL were derived and examined. Based on Loftin's approach, a statistical evaluation based on the parameters from Jenkinson 2001 was evaluated and an analytical approach to determine the TOFL was derived from it. Finally, a loop was programmed in MATLAB in which the BFL is numerically simulated and visualized for different engine failure speeds. Furthermore, in each loop the $\mathrm{TOD}_{1.15}$ is solved numerically as well. Eventually, the analytical and numerical results are compared.

Note: The SAE paper mentioned in the problem statement does not provide a concrete analytical BFL approach. The SAE paper describes a method for solving a polynomial function for a polynomial nominator greater two with high computational efficiency. (5.43) provides a very accurate analytical method for determining the ground roll distance (with velocity to the power of two as the highest degree). For wet runways, the velocity v would occur at degrees greater two. This thesis is limited to dry runways. For the purpose of this paper, the SAE paper had no additional benefits; However, the paper gave some hints which led to the basic idea to use Young's thrust model to produce an integral of the form (5.44) and to solve the ground roll distance analytically without average velocity respectively without average thrust.

11 Conclusions and Recommendations

The report demonstrates that for two engines, the Balanced Field Length is the limiting factor, while for four engines, the factored all Engines Takeoff Field Length defines the minimum required Takeoff Field Length.

BFL (Torenbeek)

The equation of **Torenbeek** for the calculation of the BFL provides results, which differ from the numerical solutions from 7% to 13.1% for the two-engine jet and 0.9% to 3.6% for the four-engine Jet. There is no factor that simultaneously improves both outcomes. With an extra markup, the results for the four-engine jet deteriorate, while the results for two engines become more accurate. The intersection point for the best (overall) result is at a 5% markup and gives results, which differ from 2.4% to 8.8% for the tow engine jet and 3.1% to 8.8% for the four-engine jet. Torenbeek applies an average thrust, at the same time, based on statistical evaluations of different aircraft models, an equivalent climb gradient and an average deceleration. According to the evaluation (Figure 7.3), deviations of 13% are to be expected for such a complex process as the BFL / TOFL (depending on the aircraft), therefore, overall, the results seem plausible even without a markup. The Torenbeek approach can only be recommended to a limited extent on the basis of the results, since the method is not intuitive to use and also requires a certain amount of effort. It is recommended (in the early design stage) to switch to the Loftin approach, the approach is "easier" to handle and at the same time gives the more accurate results.

BFL (Kundu)

Kundu performs in the opposite way to Torenbeek. The calculation results for the two-engine jet, for which a BFL calculation is of particular interest, achieves (superior) results (in comparison to the four-engine jet) with deviations of 4.4% to 9%, can thus in principle offer an option for initial design values. With a factor of 0.75 for a four-engine jet, as recommended by Kundu, unacceptably high errors of 22.2% to 28.2% are obtained. If the same factor (0.5) is also used for four engines, the deviations would still be over 15%. A factor of 0.57 achieved tolerable results for a four-engine jet with deviations between 0.1% and 5.5%. The method according to Kundu (which is based on Loftin) offers with the factors 0.5 / 0.57 thus a possible variant in the (early) design process. Apart from that, in the early design phase the necessary polar curve is not yet known, which must be available for the determination of the BFL according to Torenbeek.

TOFL (Kroo)

The approach according to Kroo gives deviations of 1.9% to 13.9% with regard to the calculation of the TOFL, whereby the method gives values that are too high. The approach could therefore in general be an option in the context of aircraft design.

TOFL (Loftin $s_{TOFL} = k_{TO}\,x$)

The procedure based on Loftin produces variations of 6.4% to 10.7% in the calculation of the TOFL, with the approach yielding values that are too low. The deviations thereby appear acceptable in view of the " quick " results.

TOFL (Loftin $s_{TOFL} = m\,x + b$)

The modified Loftin method obtains between 0.1% and 5.4% deviation results for the analytical calculation of TOFL. The equation generated from the statistical evaluation, thus achieves the lowest discrepancies to the numerical results.

However, it must be noted that some assumptions (simplification) were also made within the framework of the numerical calculations, such as the relation between rotation speed and safety speed, the rotation time, the asymmetric flight conditions, and specific geometric parameters, that were not publicly available (VTP, flap chord, drag polars). Besides, subsections were solved only analytically (Rotation Distance, Air Distance). Overall, however, it can be assumed that the numerical results provide realistic results. This is confirmed by looking at the available runways regarding the FCOMs of the presented aircraft models.

Overall, on the basis of the results, it must be recommended to use the modified approach according to Loftin, which already provides decent initial values using the most important aircraft parameters (*T/W, m/S, CLmax*) within the framework of a design process with a manageable amount of effort. However, it must also be realized that during the statistical evaluation it became apparent that "general" equations can never exactly represent all aircraft types. The evaluation according to Figure 7.2 generated a coefficient of determination (R^2) of 0.8553 with maximal deviation from -293 m (10%) to + 393 m (21.5%). Therefore, there should be at least a rudimentary idea of the approximate outcomes to be expected in order to estimate the validity of the results. It is advisable to orientate on aircraft that have a similar geometry, thrust/weight ratio, wing loading as well as similar / same high lift devices, in order to be able to estimate the expected deviations in a reasonable range.

References

AIRBUS, 2002. *Getting to Grips with Aircraft Performance. A320*. Blagnac, France.
Available from: https://bit.ly/32qvdX8
Archived at: https://perma.cc/JR78-L4SX

AIRBUS, 2005a. *Flight Crew Operating Manual (FCOM): A318/A320/A321*. Blagnac, France.
Available from: https://bit.ly/3qWwLlU (Closed Access)

AIRBUS, 2005b. *Flight Crew Operating Manual (FCOM): A340*. Blagnac, France.
Available from: https://bit.ly/30XZH26 (Closed Access)

AIRBUS, 2005c. *A/C Characteristics Airport & Maintenance Planning A320*. Blagnac, France.
Available from: https://bit.ly/3r2teSY
Archived at: https://perma.cc/Z6VC-TCZD

AIRBUS, 2005d. *A/C Characteristics Airport & Maintenance Planning A340*. Blagnac, France.
Available from: https://bit.ly/3DKNpZk
Archived at: https://perma.cc/2YX8-C4NB

AIRBUS, 2005e. *PERFORMANCE TRAINING MANUAL A318/A319/A320/A321*. Blagnac, France.
Available from: https://bit.ly/3Hh8SeO
Archived at: https://perma.cc/8QUB-2TPJ

AIR TEAM IMAGES, 2010. CFM56 engine.
Available from: https://bit.ly/3FIByLT
Archived at: https://perma.cc/J428-4BQT

BALZER, Sebastian, et al., 2021. *A Focus on the Takeoff Rotation*. In: The Airbus Safety magazine. Blagnac, France: Airbus, January 2021.
Available from: https://bit.ly/3xrk4kd
Archived at: https://perma.cc/YW95-LEBL

BARTEL, Matthias, YOUNG, Trevor, 2008. *Paper: Simplified Thrust and Fuel Consumption Models for Modern Two-Shaft Turbofan Engines*. In: AIAA ATIO Conference, and CEIAT International Conference on Innovation and Integration in Aerospace Sciences No7, Belfast: AIAA.
Available from: https://bit.ly/3cFTDOa (Closed Access)
Available from: https://doi.org/10.2514/1.35589 (Closed Access)

DEMTRÖDER, Wolfgang, 1994. *Experimentalphysik*. Kaiserslautern, Germany: SpringeSpektrum.

DUBS, Fritz, 1987. *Aerodynamik der reinen Unterschallströmung*. Basel, Switzerland: Birkhäuser.

EHRIG, Florian, 2012. *Balanced Field Length Calculation for a Learjet 35A/36A with Under-Wing Stores on a Wet Runway*. Bachelor Thesis. Hamburg, Germany: Department of Automotive and Aeronautical Engineering, HAW Hamburg.
Available from: https://bit.ly/3l9hvhE
Archived at: https://perma.cc/XC9G-X28S

FEDERAL AVIATION ADMINISTRATION: *Federal Aviation Regulations*, Part 25, Transport Category Airplanes

FRENSLICH, Arthur, 2021. *Aerodynamik, Teil 3, Physikalische Grundlagen, Widerstände*. Mannersdorf, Austria.
Available from: https://bit.ly/3PQKhRU
Archived at: https://perma.cc/5U2E-PTFA

GUDMUNDSSON, Snorri, 2014. *General aviation aircraft design: Applied methods and procedures*, Oxford, UK: Elsevier Science.
Available from: https://doi.org/10.1016/C2011-0-06824-2 (Closed Access)

GOUDREAULT, Vincent, 2013. *Algorithmic Approach for Algebraic Derivation of Time and Distance to Speed during Variable Acceleration*. In: SAE 2013 AeroTech Congress & Exhibition.
Available from: https://doi.org/10.4271/2013-01-2324 (Closed Access)

HOWE, Denis, 2000. *Aircraft Conceptual Design Synthesis*. London, UK: Professional Engineering Publishing.

INTERNATIONAL AIRPORT REVIEW, 2018. *The world's top 10 highest airports*.
Available from: https://bit.ly/3DLsQM5
Archived at: https://perma.cc/QBX8-3E4G

JOINT AVIATION AUTHORITIES: *Joint Aviation Requirements, CS -25, Large Aeroplanes*

JENKINSON, Lloyd, RHODES, Darren, SIMPKIN, Paul, 2001. *Civil Jet Aircraft Design*. London, UK: Butterworth-Heinemann.

KLUßMANN, Niels, MALIK, Arnim, 2007. *Lexikon der Luftfahrt*. Düsseldorf, Germany: Springer.

KÜMMEL, Wolfgang, 2007. *Technische Strömungsmechanik*. Wiesbaden, Germany: Teubner.

KUNDU, Ajoy.Kumar, 2010. *Aircraft Design*, New York, USA: Cambridge University Press.
Available from: https://bit.ly/3kK5Sxl

KROO, Ilan, 2001. *Aircraft Design: Synthesis and Analysis*, Stanford, USA: Desktop Aeronautics.
Available from: https://bit.ly/3zByKQS

LOFTIN, Laurence K., 1980. *Subsonic Aircraft: Evolution and the Matching of Size to Performance*. In: NASA Reference Publication 1060.
Available from: https://ntrs.nasa.gov/citations/19800020744

LUFTHANSA 2021a. *Airbus A320-200*.
Available from: https://www.lufthansa.com/de/de/320
Archived at: https://perma.cc/YPN9-VCMK

LUFTHANSA 2021b. *Airbus A340-300*.
Available from: https://www.lufthansa.com/de/de/34p
Archived at: https://perma.cc/8NT3-C4AV

MCCORMICK, Barnes W., 1979. *Aerodynamics, Aeronautics and Flight Mechanics*. NewYorl, USA: Wiley.

McCLAMROCH, N. Harris., 2011. *Steady Aircraft Flight and Performance*. New Jersey, USA: Princeton University Press.

MERZIGER, Gerhard, MÜHLBACH, Günter., WILLE, Detlef., WIRTH, Thomas, 2010. *Formeln + Hilfen Höhere Mathematik*. Barsinghausen, Germany: Binomi Verlag.

NICOLAI, Leland Malcolm, CARICHNER, Grant, 2010. *Fundamentals of Aircraft and Airship Design*, Reston, Virginia, USA: American Institute of Aeronautics and Astronautics.
Available from: https://doi.org/10.2514/4.867538 (Closed Access)

NITA, Mihaela, SCHOLZ, Dieter, 2012. *Estimating the Oswald Factor From Basic Aircraft Geometrical Parameters*. Conference Article. In: Deutscher Luft- und Raumfahrtkongress 2012. Berlin, Germany.
Available from: https://nbn-resolving.org/urn:nbn:de:101:1-201212176728
Archived at: https://perma.cc/HU2R-D7RK

OBERT, Ed, 2009. *Aerodynamic Design of Transport Aircraft*. Amsterdam, Netherlands: Faculty of Aerospace Engineering, Delft University of Technology, IOS Press.
Available from: https://ebooks.iospress.nl/ISBN/978-1-58603-970-7 (Closed Access)
Available from: https://doi.org/10.3233/978-1-58603-970-7-i (Closed Access)

PAAPE, Dennis, 2011. *Integration und Auslegungsmethoden einer Datenbank in ein Programm zum Flugzeugentwurf*. Diplomarbeit. Hamburg, Germany: Department of Automotive and Aeronautical Engineering, HAW Hamburg.
Available from: https://bit.ly/3z6PTBy
Archived at: https://perma.cc/38RY-FKGL

PAPULA, Lothar, 2015. *Mathematik für Ingenieure und Naturwissenschaftler, Band 2*. Wiesbaden, Germany: Springer Verlag.
Available from: https://doi.org/10.1007/978-3-658-07790-7 (Closed Access)

RAYMER, Daniel.P., 1989. *Aircraft Design: A Conceptual Approach*, AIAA Education Series, Washington D.C., USA: AIAA.

RAYMER, Daniel P., 2012. *Aircraft Design: A Conceptual Approach*, AIAA Education Series, Washington D.C, USA: AIAA.

SCHEIDERER, Joachim, 2008. *Angewandte Flugleistung: Eine Einführung in die Operationelle Flugleistung vom Start bis zur Landung*. Berlin, Heidelberg, Germany: Springer.
Available from: https://doi.org/10.1007/978-3-540-72724-8 (Closed Access)

SCHOLZ, Dieter, 1997. *Entwicklung eines CAE-Werkzeuges zum Entwurf von Flugsteuerungs- und Hydrauliksysteme*. Dissertation. Hamburg, Germany: Technischen Universität Hamburg, TUHH.
Available from: https://tore.tuhh.de/handle/11420/1222
Available from: https://doi.org/10.15480/882.1220

SCHOLZ, Dieter, 1998. *Berechnung der Rollstrecke beim Start Konventioneller Flugzeuge*. Hamburg, Germany: Department of Automotive and Aeronautical Engineering, HAW Hamburg.
Available from: https://bit.ly/3xfNSjJ
Archived at: https://perma.cc/2X7C-25ER

SCHOLZ, Dieter, 1999. *Tafelbilder zur Vorlesung Flugmechanik*. Hamburg, Germany: Department of Automotive and Aeronautical Engineering, HAW Hamburg.
Available from: https://bit.ly/3O76xFq
Archived at: https://perma.cc/9XPX-VL9X

SCHOLZ, Dieter, 2015. *Aircraft Design Lecture Notes*. Hamburg, Germany: Department of Automotive and Aeronautical Engineering, HAW Hamburg.
Available from: http://HOOU.ProfScholz.de

SCHOLZ, Dieter, 2017. *Drag Estimation*. Hamburg, Germany: Department of Automotive and Aeronautical Engineering, HAW Hamburg.
Available from: https://bit.ly/3DNalXY
Archived at: https://perma.cc/G9GE-D4WY

Niederkleine, Marco, Schliemann, Karsten, 1999. *Erstellung einer Datenbasis mit Entwurfsdaten für Passagierflugzeuge*. Theoretische Arbeit. Hamburg, Germany: Department of Automotive and Aeronautical Engineering, HAW Hamburg.
Available from: http://library.profscholz.de
Archived at: https://perma.cc/8Y3B-NCYF

SMARTCOCKPIT, 2021. *Avoiding Tail Strike*. Airbus
Available from: https://bit.ly/3lcAVlW (Closed Access)

SUN, Junzi, HOEKSTRA, Jacco, ELLERBROEK, Joost, 2020. *Estimating Aircraft Drag Polar Using Open Fflight Surveillance Data and a Stochastic Total Energy Model*. Delft, Netherlands: Delft University of Technology.
Available from: https://doi.org/10.1016/j.trc.2020.01.026
Archived at: https://perma.cc/6QR4-C8MS

TORENBEEK, Egbert, 1982. *Synthesis of Subsonic Airplane Design*, Delft, Netherlands: Delft University Press.
Available from: https://bit.ly/3HqrF7B
Archived at: https://perma.cc/K8A2-M7MT

TORENBEEK, Egbert, 1972. *An Analytical Expression for the Balanced Field Length*. In: AGARD Lecture Series No. 56

WIKIPEDIA, 2021a. *Minimum control speeds*. San Francisco, USA: Wikipedia.
Available from: https://en.wikipedia.org/wiki/Minimum_control_speeds
Archived at: https://perma.cc/8P3U-LV2Y

WIKIPEDIA, 2021b. *CFM56*. San Francisco, USA: Wikipedia.
Available from: https://de.wikipedia.org/wiki/CFM_International_CFM56
Archived at: https://perma.cc/6GPK-EKSY

WIKIPEDIA, 2021c. *Airbus A320-Fam*ily. San Francisco, USA: Wikipedia.
Available from: https://de.wikipedia.org/wiki/Airbus-A320-Familie
Archived at: https://perma.cc/A53H-H9VG

WIKIPEDIA, 2021d. *Airbus A340-Family*. San Francisco, USA: Wikipedia.
Available from: https://de.wikipedia.org/wiki/Airbus_A340
Archived at: https://perma.cc/5ADF-LNS8

YOUNG, Trevor, 2001. *Flight Mechanics Lecture Notes*. Limerick, Ireland: Department of Mechanical and Aeronautical Engineering, University of Limerick.
Available from: https://bit.ly/3Of6aci (Closed Access)

YOUNG, Trevor, 2013. *Flight Mechanics Lecture Notes*. Limerick, Ireland: Department of Mechanical and Aeronautical Engineering, University of Limerick.

YOUNG, Trevor, 2018. *Performance of the Jet Transport Airplane - Analysis Methods, Flight Operations, and Regulations*. Limerick, Ireland: John Wiley & Sons,

All online resources have been accessed on 2022-05-31 or later.